SCORPIONATE SUPPORTED AND UNSUPPORTED CARBONYL AND ETHYLENE COMPLEXES OF GROUP 11 METALS

by

MAURO FIANCHINI

Presented to the Faculty of the Graduate School of

The University of Texas at Arlington in Partial Fulfillment

of the Requirements

for the Degree of

DOCTOR OF PHILOSOPHY

THE UNIVERSITY OF TEXAS AT ARLINGTON

December 2009

"Look within. Within is the fountain of good,
and it will ever bubble up,
if thou wilt ever dig."

Marcus Aurelius,
Roman Emperor
121 – 180 A.D.

ACKNOWLEDGMENTS

This thesis, its realization and all the massive work that has been done are dedicated to the Fianchini family, Tiziano, Ivana and Massimo, and in memory of Mario Antonio and Vesna Fianchini and Delvisio and Adele Cambi for all their love and support throughout my life. After all these years I realize their teachings were always aimed to make me see and respect the goodness in life, situations and people. These teachings, together with my strong belief that no barrier is hard enough for anyone who truly wishes to crash it against odds and unfavorable circumstances, have been the “driving force” who brought me to the end of this experience.

I would like to thank my “old” Italian friends Riccardo, Dalila, Chiara, Fausto and Rita Capesciotti for the wonderful years we spent back in Italy among motorbike rides, adventurous trips and most pleasant dinners and parties.

I would like to thank Walter Morales, Monica Hernandez, Lear Dobbins-Moreno, Dr. Jose Gracia and Raquel Robles, Dr. Eugenio and Dr. Norma Tacconi, Conner MacDonnell, Elizabeth Snow, Hunter and Chase James, Michael Conerty, Rebecca Snow, Ryan Conerty, Brawder Tatum, Debbie Tatum, Josh and Sarah Tatum, Ricardo Toledo, Maria Rosales, Angelica Perea, Jose Gallegos, Martin Perez, Carlos Zafra, Steve Kunkel, Amy Kunkel, Alan Davis, Robert Hayes, Tom Doundolakis, Zak Nixon, Andra Carter, Tran Tran Thi Ngoc, Aaron Drew, Blake Arthur, Vanessa Brown, Sandra Spencer, Justin Furchner, Chi Chen, Leticia Laredo, Dr. Reddy Vanga, Hare Timmaji, Dr. Abhishek Yadav, Sabuj Mukherjee, Dr. Shreeyukta Singh, Dr. Xiaodi “Cindy” Kou, Laura Maroun, Chad Varnell, Dr. Ardavan Motahari, Reece Challinor and Jessica Rodriguez for their sincere friendship, their support, their vitality and for all the awesome time we spent together. This time will not be forgotten and it has never been long enough.

For what concerns the academics, I would like to thank Prof. H.V. Rasika Dias for his advice and for collecting and solving the X-Ray crystal structures presented in this thesis as well as the members of my Ph.D. committee, Prof. Fred MacDonnell, Prof. Christopher O'Brien, Prof. Dennis Marynick, Prof. Kevin Schug and Prof. Daniel Armstrong. Particularly, I want to thank Prof. Christopher O'Brien for the challenging and passionate diatribes about "calculated vs experimental chemistry", Dr. Jose Gracia for the useful comments on the calculations, Prof. Gamini Rajapakse for his teachings on cyclic voltammetry and electrochemical impedance, Aruna Wijeratne and Prof. Kevin Schug for running the ESI-MASS experiment on [Cu(ttt-cdt)][SbF_6] and interpreting the results, Dr. Hui Dai for improving the synthesis of [$Au(C_7H_{10})_3$][SbF_6] as well as collecting the NMR spectra, Charles Savage and Dr. Brian Edwards for their competence and their constant support in solving problems in NMR and RAMAN spectroscopy, Jim Garner and Jill Howard for their hard work in the stockroom and Ruth Handley, Debbie Cooke, Autumn Huddleston and Yvonne Russell for the help they constantly provided to solve administrative issues.

My acknowledgements go also to Dr. Brad Boring, Dr. Brent Waguespack, Dr. Leon Doneski, Patricia Patenaude, Joan Hook and Dr. Daniel Dunn for creating an awesome and yet very professional environment that strongly contributed to my excellent working experience at Alcon Laboratories, Inc. in Fort Worth. NSF, Welch's Foundation and UTA are greatly acknowledged for providing the funds to support our research.

I think it is more than fair to dedicate the final acknowledgement to Chemistry, among the sciences the most deceiving, but, with no doubt, a constant inspiration to higher horizons.

November 11, 2009

ABSTRACT

SCORPIONATE SUPPORTED AND UNSUPPORTED CARBONYL AND ETHYLENE COMPLEXES OF GROUP 11 METALS

Mauro Fianchini, PhD

The University of Texas at Arlington, 2009

Supervising Professor: Prof. H.V. Rasika Dias

Carbon monoxide (CO) and small olefins represent perhaps the simplest, but most important ligand systems in coordination/organometallic chemistry. Simple carbonyl and ethylene compounds have started to appear in the field since the early nineteen century. Due to their peculiar electronic properties, strong bonds to late transition metal cations such as Cu^{I}, Ag^{I}, and Au^{I} are generally discouraged. However, intermediates involving M-CO or M-olefin (where M = Cu^{I}, Ag^{I}, Au^{I}) have been claimed to be key-steps in reactions and industrial processes involving coinage metals. Unfortunately, experimental data on coinage metal complexes with CO and olefins are scarce due to the difficulty of isolating such adducts. In this work several novel metal carbonyl and olefin compounds will be presented, which make a precious addition to the coinage metal chemical 'landscape'. Their syntheses will be presented and their principal characteristics discussed on the basis of spectroscopic data and metric parameters derived from X-ray diffraction; furthermore, their electronic structures, obtained by density functional theory (DFT), will be studied in detail.

TABLE OF CONTENTS

LIST OF ILLUSTRATIONS

Figure Page

LIST OF TABLES

CHAPTER 1

INTRODUCTION

1.1 Coinage metals

The chemical symbols of copper, Cu, silver, Ag, and gold, Au, originate from the Latin names *cuprum*, *argentum* and *aurum*. The first name relates to the the isle of Ciprum, from which the Romans initially extracted the metal. Copper, silver and gold are probably the first three metals discovered in history. They are commonly called *coinage* metals, which recalls their use as forging metals for coins (their use was already present in Egypt in 3400 B.C.)[1]. Gold has been used as an ornamental metal since the Stone Age; it was the immediate reflection of the power of kings (Tutankhamen's sarcophagus contained no less than 112 kg of gold!) and the cause of the rise and fall of empires (the Mayan and Aztec empires' legendary treasures were at the base of the Spanish conquer, for example). Copper has been used since 5000 B.C[1].

After 3000 B.C., ancient civilizations in the Mediterranean Sea and Middle East learned how to produce bronze using copper/tin alloys. This period is known to historians as the "Bronze age". The use of silver as coinage metal is probably contemporary with gold[1]. All three elements are present in the Earth's crust in the native state. The relative abundances are comparable to Ni, Pd, and Pt, with Cu at 68 ppm, Ag 0.08 ppm, and Au 0.004 ppm, respectively. Principal minerals containing copper are chalcopyrite, $CuFeS_2$, galena, Cu_2S, cuprite, Cu_2O, and malachite, $Cu_2CO_3(OH)_2$. Silver is present in nature as argentite, Ag_2S, as well as metallic silver. Gold is present as metallic gold or often associated with tellurides, quartz, or pyrite.

Before 1830, almost all the gold circulating in the world was coming from the ancient South American civilizations[1]. The production increased tenfold after the discovery of mines in Siberia and after the famous “Gold Rushes” of 1849 in California, 1851 in New Wales, 1884 in Transvaal and 1896 in Klondike[1].

All the chemical properties of the coinage metals can be directly correlated with their electronic configuration $d^{10}s^{1}$. They are great conductors of electricity, with maximum values for silver. They are tender, ductile, and malleable. Gold is the most electronegative of all metals, with an electronegativity of 2.4 on the Pauling scale, equal to that of selenium[1].

Electron affinity is very high for coinage metals (87 $kJmol^{-1}$ for Cu, 97 $kJmol^{-1}$ for Ag and 193 $kJmol^{-1}$ for Au). The formation of CsAu is a typical result of this high electron affinity of gold. This compound is supposed to have partial ionic behavior, evidenced by the fact that it melts more like a salt than a proper alloy. This aspect, together with the formation of a stable solvate of Au^{-} in liquid ammonia, can suggest a strong analogy between gold and the halogens[1].

Pyykko and coworkers linked all these interesting properties to the relativistic effects.[2-21] It is well known now that group 11 is the “maximum of the relativistic effects”. Valence electrons move generally slower compared to the speed of light; however for heavier atoms, the electrons in inner K- and L-shells approach the speed of light. This leads to a sensible increment in their masses, thus leading further to shrinkage of the spatial radius of the shell and, to some extents of the outer shells as well. Furthermore, since the relativistic perturbation acts near the nucleus, where valence electrons also have a non-zero part of their density (especially s electrons), relativistic contraction affects the valence orbitals as well (*direct relativistic effect*). It follows that, since the nucleus becomes more screened, orbitals with higher angular momenta undergo a quite large expansion (*indirect relativistic effect*). Spin-orbit coupling is another consequence of

the relativistic effects. All these effects roughly increase with the square of Z, the nuclear charge (in group 11, Cu < Ag < Au).

The analogy between alkali and coinage metals, legitimated by their respective electronic configurations $d^{10}s^1$ and p^6s^1, is however only possible on the basis of the stoichiometry of their compounds in formal oxidation +1, for the other properties are very different. Coinage metals are harder, denser and less reactive, they show higher melting points and they form compounds with more covalent character. They have higher first ionization energies (745,3 $kJmol^{-1}$ for Cu, 730.8 $kJmol^{-1}$ for Ag and 889.9 $kJmol^{-1}$ for Au) and lower second and third ionization energies (1957.3 and 3577.6 $kJmol^{-1}$ for Cu, 2072.6 and 3359.4 $kJmol^{-1}$ for Ag and 1973.3 and 2895 $kJmol^{-1}$ for Au) in comparison to alkali metals[1]. The ionic radii are smaller for group 11 than for group 1. This difference in properties can be attributed to the poor shielding effect of the d electronic cloud on the electron in the s orbital with respect to the p cloud. In addition, a d closed shell is much less stable than a p closed shell, making it easier for group 11 to have oxidation states beyond +1. The covalent radii follow the trend Cu < Ag > Au (with gold's radius being smaller than silver's). This trend can be explained by relativistic and lanthanide-contraction effects that reach their apex in gold chemistry.

In their +1 oxidation states, all three cations are diamagnetic with a configuration $^1S_0$, and their compounds are generally colorless (unless strong LMCT and MLCT are present). Cu^I is normally very unstable in water and tends to disproportionate into Cu^0 and Cu^{II}, mostly due to the high hydration heat of the +2 cation. For silver, the oxidation state +1 is the most common. Au^I is very unstable in water and promptly disproportionates into Au^0 and Au^{III}[22].

All three cations can be stabilized, however, using a wide range of hard and soft N-, S-, P-, As-donor monodentate, chelate, and tripodal ligands. Especially good soft π-acceptors such as phosphines can be very effective in stabilizing Au^I. Dinuclear phosphine complexes with

gold, like $[Au_2(dppm)_2]_2^+$, exhibit strong luminescence due to close contact of Au···Au units. Pyrazolate trimers exhibit strong luminescence depending on solvent, temperature and excitation wavelength.

Ag^I has very low affinity for oxygen donors, although complexes of silver with DMSO, carboxylate ions and crown ethers are known. Dias et al reported the synthesis and the characterization of very stable complexes of silver with THF and ethylene oxide[23]. Cu^I forms interesting complexes with oxygen donors. Copper(I) trifluoromethanesulfonate, obtained as benzene adduct $[Cu(O_3SCF_3)]_2.C_6H_6$ can be prepared as a white crystalline solid by treating Cu_2O with methanesulfonic anhydride in benzene. Generally, Cu^I prefers tetra-coordination while its heavier congeners Ag^I and Au^I prefer tri- or linear coordination. This behavior can be a direct consequence of the relativistic contraction on the 5s and 6s orbital: the contraction in copper is less important than in silver or gold and, the spherical 4s orbital being more available, there is no real preferred spatial arrangement for the ligands. Conversely, especially in gold, the 6s is highly contracted and the 5d orbitals are more expanded, leading to an increased preference for directional bonds.

Metal halides are very important for this group. The structure of copper halide can be very complicated since they can be mononuclear, binuclear with halide bridges, polynuclear, or infinite chains. Silver halides are generally poorly soluble in water and organic solvents, and this characteristic can be effectively used to provide a strong thermodynamic force in metathesis reactions by precipitation of AgX. AgX treated with an excess of X^- ions provides AX_2^- complexes (with relative stability $Cl^- < Br^- < I^-$). Silver halide and thiosulphate are commonly used in the process of the photography. Gold(I) compounds with sulfur donor ligands are known to be active in the treatment of rheumatoid arthritis (Auranofin and Myocrisin). The sulfur donor in this type of compounds is displaced by SH-proteins[22].

Oxidation states beyond +1 are also very common for these three elements. For example, Cu^{II} is a good oxidizing agent with very rich background in aqueous chemistry. All these salts are generally green or blue and show paramagnetic activity with antiferromagnetic exchange. Cu^{II} centers are well-known to transport oxygen, stabilize superoxo, peroxo, and μ-oxo; and catalyze a variety of different oxidations in both biological (ex. Superoxide dismutase, Cytochrome c Oxidase, Hemocyanins) and non-biological systems (ex. Wacker process).

Gold(III) salts are the starting materials for the preparation of a variety of gold(I) compounds. Metallic gold can be dissolved in a strong oxidant such as "aqua regia" to give tetrachloroauric acid, $HAuCl_4.3H_2O$. This compound can be treated with $OSCl_2$ to give the deep red dimer Au_2Cl_6. Each gold atom is in a square planar environment with two bridging chlorides. Au_2Cl_6 is a compound with a great synthetic importance since it can be reduced by carbon monoxide, olefins, and sulfides to give the corresponding $Cl\text{-}Au^{I}\text{-}L$ compounds[22].

1.2 Carbon monoxide in chemistry

Carbon monoxide is the simplest oxocarbon known. Though it is virtually undetectable (lacks odor, taste, and color) to humans, it is toxic[24]. Ancient Greeks and Romans used carbon monoxide for the smelting of iron and other metallic ores as well as for executions. It was identified by the English chemist William Cumberland Cruikshank in the year 1800. Carbon monoxide is a minor constituent of the atmosphere, mainly produced by volcanic activity or natural fires, but also anthropogenic factors such as inefficient burning of fossil fuels (i.e. internal combustion engines). Carbon monoxide does not survive long in the atmosphere since it oxidizes readily to carbon dioxide. It is a very important reagent in chemistry as evidenced by the numerous production approaches, including combustion of excess of carbon at high temperatures, "water-gas shift" reaction, and reduction of metal oxide ores with carbon[22]. In the

chemical industry carbon monoxide is combined with alkenes and hydrogen gas to form aldehydes (hydroformylation), and it is hydrogenated to form methanol. Using CO hydroformylation in combination with C-C bond formation, it is possible to produce liquid hydrocarbon fuels (Fischer-Tropch process)[25, 26]. Moreover carbon monoxide can be reacted over a rodhium catalyst to produce acetic acid (Monsanto process, Fig. 1.1), which produces most of the acetic acid that is commercially available. Metallic nickel is corroded at room temperature by carbon monoxide. The process releases $Ni(CO)_4$, a volatile and extremely toxic compound. It decomposes back to Ni^0 and CO upon heating, affording extremely pure nickel samples (Mond process)[27].

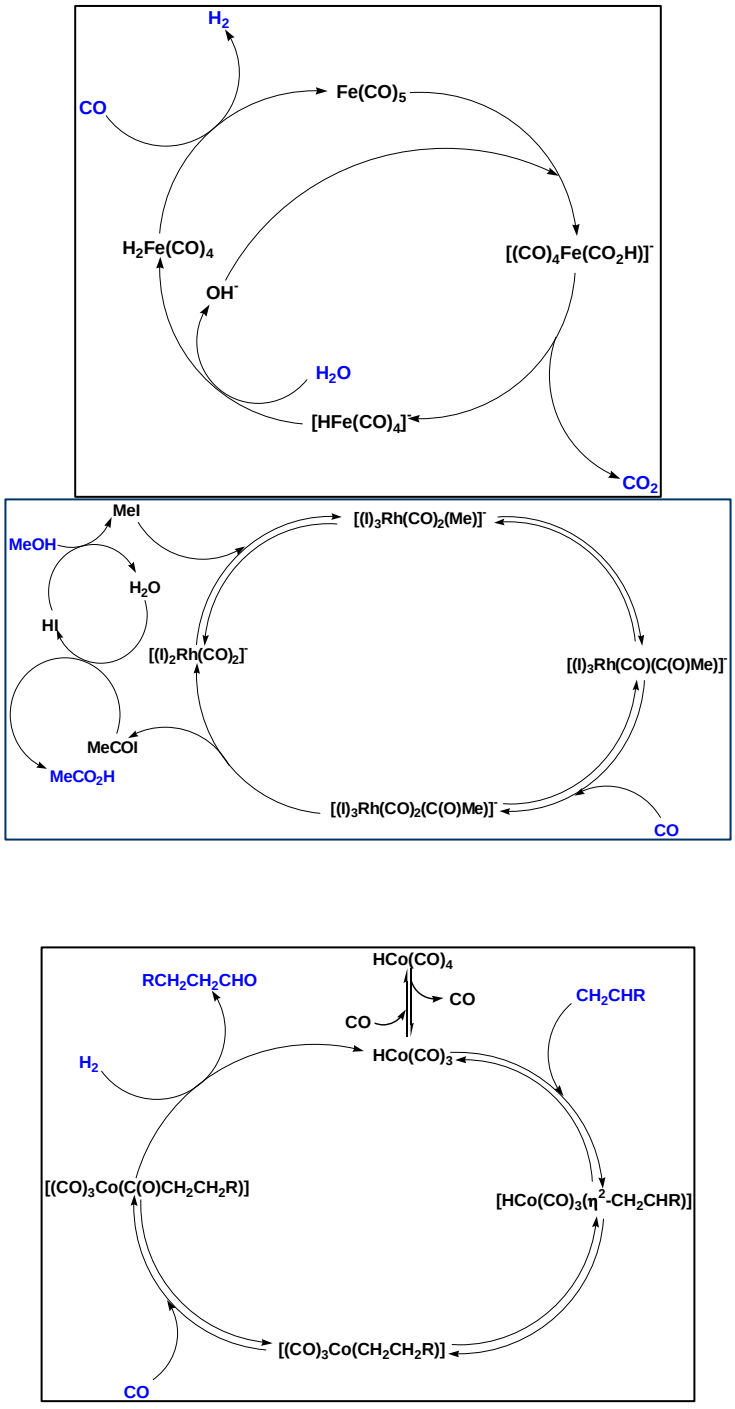

Figure 1.1. Catalytic cycles involving carbon monoxide. From top to bottom: "water-gas shift", Monsanto, hydroformilation

Carbon monoxide is very toxic[28]: it binds to hemoglobin in the blood to give a complex called carboxyhemoglobin, which incapacitates the circulatory system ability to deliver oxygen (anoxemia). Carbon monoxide compromises other important molecules such as myoglobin and mitochondrial cytochrome oxidase, and repeated exposure damages the heart and central nervous system. Mammals produce carbon monoxide naturally, which plays a vitla role in metabolism (breakdown of heme) and as signaling molecule responsible for vasodilation[29]. Moreover, it modulates the neuro, circulatory, immune, respiratory, reproductive, and gastrointestinal systems. CO is also under intense study in several research laboratories for some of its properties, which can potentially prevent severe pathologies, like transplant rejection, atherosclerosis, or autoimmunity[29].

1.2.1. "Classical" versus "non-classical" carbonyls.

Carbon monoxide is a very poor Lewis base and a very good Lewis acid. It coordinates metals in lower oxidation states, is generally electron-rich or "soft", and is generally capable of good to excellent π-back-bonding (ex. Rh^{I}, Ir^{I}, Pt^{0}). Although the oxygen atom is more electronegative than the carbon atom (therefore a more substantial quantity of electron charge should be assigned to the oxygen as demonstrated by NBO charges calculated at B3PW91/6-311+G(d) level, say, 0.47 for C atom and -0.47 for O atom), carbon monoxide exclusively coordinates metal acceptors through the carbon atom. This is because the "highest occupied molecular orbital', HOMO, lies almost exclusively on the carbon atom (Fig. 1.2, left). When a metal binds CO, its HOMO interacts with an empty orbital of appropriate symmetry (nominally d_{z^2} or $d_{x^2-y^2}$) in the metal (Lewis acid behavior) to give what is normally called σ-donation or σ-bonding (*sigma* because, like a conventional *sigma* bond in organic chemistry, the bond lies in the region connecting the metal and the carbon atoms). CO can also accept electron density

(Lewis acid behavior) from a filled orbital of the metal of appropriate symmetry (nominally d_{xy}) into the "lowest unoccupied molecular orbital", LUMO, π^* (Fig. 1.2, right). This interaction is called π-back-donation or π-back-bonding (*pi* because, like a conventional *pi* bond in organic chemistry, the interaction is formed by orbitals indirectly pointing at each other). This synergic interaction is at the base of the Chatt-Dewar-Duncanson model for carbon monoxide[25, 30].

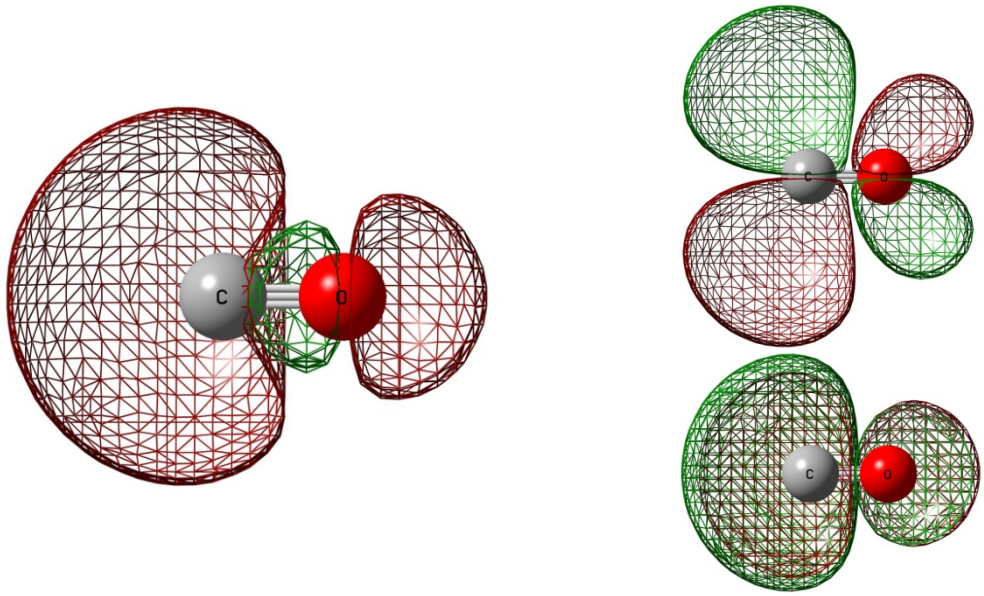

Figure 1.2. Carbon monoxide KS HOMO (Σ_g, - 0.38599 hartrees), left, and LUMO (Π, -0.03963 hartrees), right, calculated at B3PW91/6-311+G(d), 0.02 hartrees isovalue

The first metal complex featuring a coordinated carbon monoxide molecule, cis-$PtCl_2(CO)_2$, was discovered in 1870[31] and soon after the first homoleptic metal carbonyl compound, $Ni(CO)_4$ was reported by Mond in 1890[31]. $Ni(CO)_4$ is so volatile that it was a common saying among scientists that Mond "gave wings" to nickel.

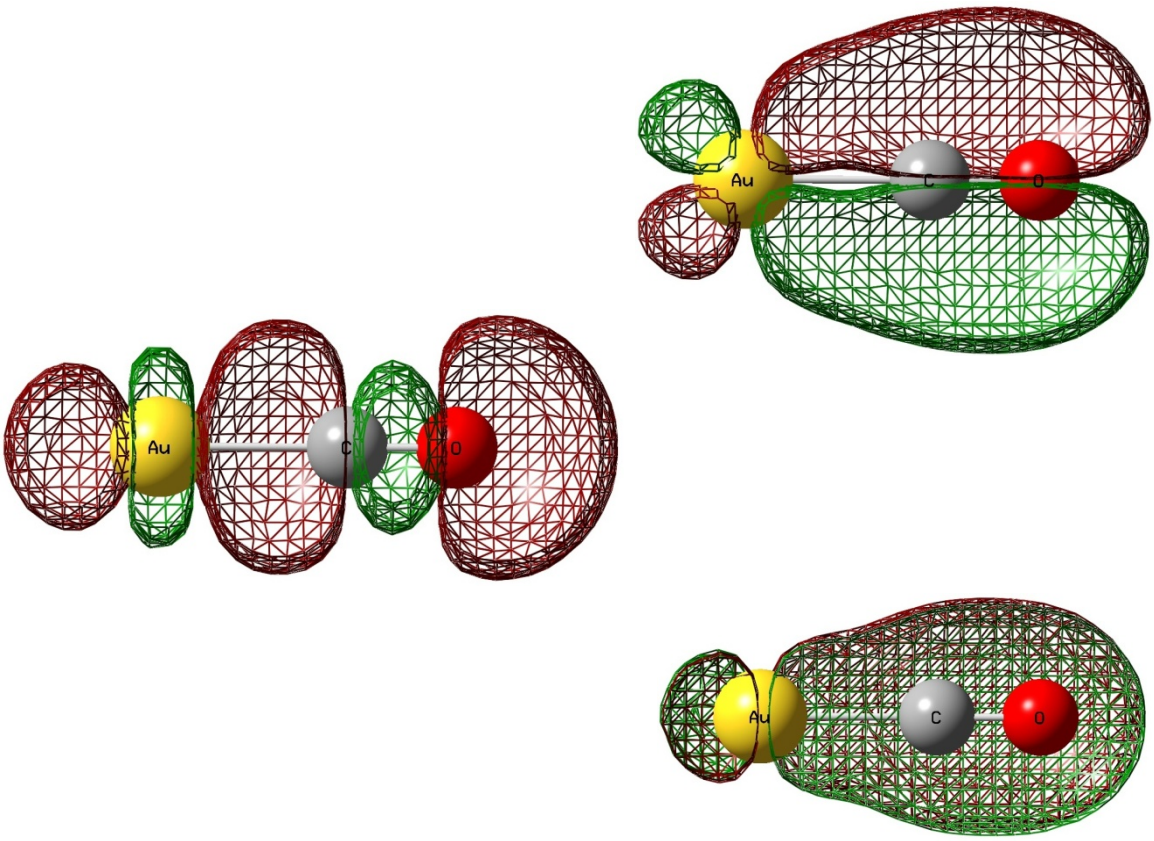

Figure 1.3. Qualitative diagram of KS orbitals of possible σ-donation (Σ_g, - 0.76735 hartrees), left, and π-back-donation (Π_t - 0.73384 hartrees), right, between Au^+ and CO, (calculated at B3PW91/ 6-311+G(d), 0.02 hartrees isovalue)

Although both compounds can be defined as "metal carbonyls", their coordinated CO moieties show totally different chemical and spectroscopic behavior. The first striking difference resides in their ν(CO) stretching bands: a value of 2058 cm^{-1} is reported for $Ni(CO)_4$ while 2175 cm^{-1} is reported for $PtCl_2(CO)_2$, with 2143 cm^{-1} being the stretching frequency of carbon monoxide in the gas phase. Since the frequency can be correlated with the force constant and the reduced mass for a vibrating system ($\nu=(2\pi)^{-1}(F/m)^{1/2}$, if harmonic model is considered), it is

not hard to see that for compounds such as $Ni(CO)_4$ the C-O bond seems to weaken upon coordination, while for compounds like $PtCl_2(CO)_2$ it seems to strengthen.

The nature of this dual behavior has been at the base of a heated diatribe for the last 10-15 years and gave rise to the coining the definition of "classical" and "non-classical" terms. A classical carbonyl is a carbon monoxide complex whereupon coordination:

- ✓ as ν(CO) stretching frequency decreases (< 2143 cm^{-1}), the triple bond weakens;
- ✓ CO bond distance notably lengthens within a $\pm 3\sigma$ level of confidence if compared to 1.1282 Å, the bond distance for free CO;
- ✓ M-C bond distance decreases (M-C bond strengthens) thanks to improved π-back-bonding when more electron density is present on the metal.

Classical carbonyl characteristic are associated with electron-rich metal centers that are capable of good to very good π-back bonding (Rh^{I}, Ir^{I}, Ni^{0}, Co^{-}, Fe^{2-}, Mn^{3-}). It is logical to postulate that addition of σ-donor ligands to such metal centers (say, increasing their electron density and thus the availability of π-back bonding) further weakens the C-O bond (shorter CO distance, lower ν(CO) stretching frequency) and strengthens the M-C bond, while the introduction of π-back bonding competitors (other carbon monoxide moieties, olefins…) strengthens the C-O bond (shorter CO distance, lower ν(CO) stretching frequency), weakening the M-C bond. We could say with reasonable confidence that the degree of π-back-bonding is proportionally affecting the properties of the coordinated monoxide in a classical carbonyl.

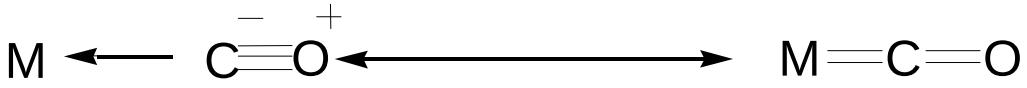

Figure 1.4. Resonance forms for coordinated carbon monoxide; left, form 1, "non-classical carbonyl, right, form 2, "classical" carbonyl

Different story can be told for the other class, the non-classical carbonyls. This term was coined by Strauss, Frenking et al. and accounts for the strange behavior that coordinated CO seems to have in carbonyls of group 10 (especially true for d^8 configurations), 11 and 12 metals[31, 32]. These carbonyls show very high ν(CO) stretching frequencies (> 2143 cm^{-1}) and shorter CO bond distances than free carbon monoxide for mainly two reasons[31, 32].

Some have explained this behavior considering that the 5σ of the CO has a slight anti-bonding nature. Thus, when CO is coordinated to metals, the lone pair is shared and this removal of anti-bonding electron density leads to an increment of the the C-O bond order. Conversely Goldman and Krogh-Jespersen showed the reason behind the strengthening of CO bond is attributed to electrostatic effects[33]. They started from the assumption that structure **1** should be favored when the carbon is in the presence of an electrostatic charge near the carbon (Fig. 1.5).

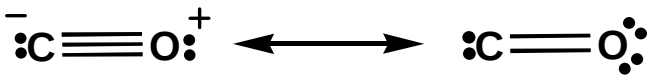

Figure 1.5. Lewis structures for carbon monoxide; structure 1 (left) and structure 2 (right)

Then, calculated sets of organic and organometallic adducts of carbon monoxide at MP2/6-311G* and MP2/LAN2DZ/6-31G* levels demonstrated that the electron donation from the 5σ orbital has not intrinsic effect on the force constant[33].

Whatever reason lays behind this first effect, chemists seem to agree on the fact that there is another important effect playing a major role: “non-classical” carbonyls possess very low π-back-bonding from the metal or at least not enough to overcome the afore-mentioned effects, lengthen the C-O bond distance and lower ν(CO) stretching frequency below 2143 cm^{-1}. Lupinetti, Strauss and Frenking used Moeller-Plesset theory truncated at the second level

(MP2) to study the interaction of linear $[M(CO)_2]^+$ fragments (where M is a d^{10} configuration, Rh^-, Pd^0, Cu^+, Ag^+, Au^+, Zn^{2+}, Cd^{2+}, Hg^{2+}) with two apical fluorides (σ-donor only ligand). The result of the study highlights two main trends. Rh^- and Pd^0 react to the perturbation as "classical" carbonyls would do, reducing M-C bond and increasing C-O bond. The behavior of Zn^{2+}, Cd^{2+}, and Hg^{2+} is different: they tend to increase M-C bond while slightly increasing the C-O bond as well. Cu^+ and Au^+ behave classically, like Rh^- and Pd^0, while Ag^+ tends to behave non-classically, like Zn^{2+}, Cd^{2+}, and Hg^{2+}. In the second group the π-back-bonding is not totally excluded from the description of the bond interactions, but it cannot overcome other polarization/electrostatic effects. The reason underlying the different behavior of Ag^I has been attributed to greater σ repulsion between the d^{10} filled shell and the HOMO of the ligand.

Carbonyl complexes of copper, silver and gold are of significant historical, scientific and technological importance. They are intermediates playing an important role in industrial processes such as the oxidation of carbon monoxide. Several non-classical M-CO species (M = Pd^{II}, Cu^I, Ag^I, Au^I, Hg^{II}) have been observed spectroscopically. However adducts characterized using X-ray crystallography are extremely rare, with a few excellent examples including mono-carbonyl adducts $(CO)CuAlCl_4$ and $(CO)CuGaCl_4$ (both show $\nu(CO) = 2156\ cm^{-1}$)[34] reported by Martin and co-workers; $[Ag(CO)][B(OTeF_5)_4]$ ($\nu(CO) = 2204\ cm^{-1}$) reported by Strauss and co-workers[35], $[HB(3,5\text{-}(CF_3)_2Pz)_3]Ag(CO)$ ($\nu(CO) = 2178\ cm^{-1}$) and $[HB(3,5\text{-}(CF_3)_2Pz)_3]Au(CO)$ ($\nu(CO) = 2144\ cm^{-1}$) reported by Dias and co-workers[36, 37]; di-carbonyl adducts, $[Cu(CO)_2](1\text{-}Bn\text{-}CB_{11}F_{11})$ ($\nu(CO) = 2166, 2184\ cm^{-1}$)[38] and $[Ag(CO)_2][B(OTeF_5)_4]$ ($\nu(CO) = 2198\ cm^{-1}$)[35], and tetra-carbonyl adducts, $[Cu(CO)_4][1\text{-}Et\text{-}CB_{11}F_{11}]$ ($\nu(CO) = 2184\ cm^{-1}$)[38], described by Strauss and co-workers[31]. Aubke et all reported the synthesis and the characterization of the "non-classical" $[Au(CO)_2][Sb_2F_{11}]$[39], $[Pd(CO)_4][Sb_2F_{11}]$[40] and $[Hg(CO)_2][Sb_2F_{11}]$[41-43]. Most of these "non-classical" compounds are homoleptic because they feature carbon monoxide as the only

coordinated ligand. Some of them have been isolated in super-acidic media because they are so labile that even weakly-coordinating solvents could displace the coordinated carbon monoxide. Typically, non-classical carbonyls show higher ν(CO) than that of the free CO (2143 cm^{-1}) and shorter C-O bond distances. It is worth re-mentioning that this interesting behavior can be explained as a sum of σ-interaction and polarization/electrostatic effects in concomitance with very little, if any, π-back-bonding.

Isolable "classical" copper carbonyls like $[HB(Pz)_3]CuCO$ (ν(CO) = 2083 cm^{-1}) or $[HB(3,5\text{-}(CF_3)_2Pz)_3]Cu(CO)$ (ν(CO) = 2137 cm^{-1}) are relatively common, but, as we will see in chapter 4, to my knowledge, no "classical" carbonyls of Ag^I and Au^I have been reported in the literature to date. Even though the direct goal of this thesis is not to discuss the homoleptic carbonyls of group 11 in depth (they have been the focus of a plethora of very interesting and detailed experimental, theoretical, and computational studies)[44-48], they come in handy for preliminary evaluation of the performance of the hybrid functional B3PW91, used throughout this work in conjunction with Figgen's Pseudopotential MDF and large correlation-consistent basis sets (such as aug-cc-pvDZ-PP or aug-cc-pvTZ-PP), in reproducing equilibrium geometries, spectroscopic properties (vibrations and NMR shielding tensors), and in evaluating thermodynamic measurables (like enthalpy or Gibbs free energy of reaction). To my knowledge, this combination theory/ECP/basis set has not been used thus far, even though several other DFT and post-HF methods have been extensively used. Particularly important is the fact that bond dissociation energies (BDEs) have been found experimentally by mass experiment and extrapolated to 0 K for the reaction $[M(CO)_n]^+ \rightarrow [M(CO)_{n-1}]^+ + CO$ (n= 4, 3, 2, 1 and M = Cu and Ag) in a seminal paper by Armentrout and co-workers[49]. The availability of these dissociation energies is not that common for the relative ethylene $M(C_2H_4)_n^+$, thus making a direct comparison of theory versus experiment for that class of compounds quite difficult.

Table 1.1. Experimental values of D_0 in comparison with calculated values in this and related works

Reaction	Experimental, KJ/mol (Kcal/mol)[49]	Calculated (this work) Kcal/mol	Calculated Kcal/mol
$[Cu(CO)_4]^+ \rightarrow [Cu(CO)_3]^+ + CO$	53±3 (12.7±0.7)	14.0	-
$[Cu(CO)_3]^+ \rightarrow [Cu(CO)_2]^+ + CO$	75±4 (17.9±1.0)	18.3	-
$[Cu(CO)_2]^+ \rightarrow [Cu(CO)]^+ + CO$	172±3 (41.1±0.7)	38.8	(32.5)[50]
$[Cu(CO)]^+ \rightarrow [Cu]^+ + CO$	149±7 (35.6±1.7)	39.8	(32.0)[50]
$[Ag(CO)_4]^+ \rightarrow [Ag(CO)_3]^+ + CO$	45 (+18-4) (10.8+4.3-1.0) 64±12 (15.3±2.9)	7.3	-
$[Ag(CO)_3]^+ \rightarrow [Ag(CO)_2]^+ + CO$	55±8 (13.1±1.9) 54±10 (12.9±2.4)	10.2	11.9[48]
$[Ag(CO)_2]^+ \rightarrow [Ag(CO)]^+ + CO$	109±4 (26.1±1.0)	28.6	25.1[48] (18.0)[50]
$[Ag(CO)]^+ \rightarrow [Ag]^+ + CO$	89±5 (21.3±1.2)	25.4	20.2[48] (18.2)[50]

Calculated data are generally in good agreement with the experimental ones (Tab. 1.1). Our DFT accounts for a maximum positive error of + 3.5 kcal/mol and a negative of – 4.2 kcal with an overall MAD of 2.7 kcal/mol. These are very good results considering that no correction for basis set superimposition errors (BSSE) has been applied and no single point calculation at higher level of theory has been carried out (especially post-HF methods).

The tris(pyrazolyl)borate ligand system has been successfully used to stabilize coinage metal carbonyls (chapter 4). These monoanionic boron-based ligands can effectively enforce a tetrahedral symmetry on d^{10} metals leaving a vacant position for coordination of neutral molecules. The first fully characterized Cu^{I}-CO adduct was supported by the tripodal $HBPz_3^-$. Fluorinated tris(pyrazolyl)borate led to the isolation and characterization of rare Ag^{I}-CO and Au^{I}-

CO, such as $[HB(3,5\text{-}(CF_3)_2Pz)_3]CuCO$, $[HB(3,5\text{-}(CF_3)_2Pz)_3]AgCO$, $[HB(3,5\text{-}(CF_3)_2Pz)_3]AuCO$, and $[CH_3B(3\text{-}(C_2F_5)Pz)_3]AgCO$.

1.3 Olefins in chemistry

Alkenes or olefins are chemical compounds that contain one or more carbon-carbon double bond. They have the general formula C_nH_{2n}, with ethylene being the lightest of the series. The double bond is stronger than a single covalent bond (173 kcal/mol for C=C in ethylene vs. 90 kcal/mol for C—C in ethane)[51] and is also shorter. Rotation about the carbon-carbon double bond is blocked because it would break the π bond (~ 65 kcal/mol)[51, 52]. The angle C=C-R may vary depending on the functional groups attached to the sp^2 carbons. For instance, the C=C-C bond angle in norbornene, another alkene presented in this thesis, is 106.5° (107.5° calculated at B3PW91/6-311++G(d,p) l evel). Industrially, alkenes are synthesized through petroleum cracking (involving high temperatures and heterogeneous catalysts) and successive fractional distillation. Other ways to produce alkenes are the catalytic dehydrogenation of alkanes (loss of hydrogen at high temperatures), β- or α-elimination of alkyl halides, alcohols, and similar compounds, dehydration of alcohols, coupling of carbonyl compounds followed by reduction (McMurry reaction, Barton-Kellogg reaction), olefin metathesis, coupling reactions (most notably those catalyzed by palladium compounds, such as the Stille, Heck, Suzuki and Negishi reactions), hydrogenation in the presence of Lindlar's catalyst, hydroboration followed by hydrolysis, reduction of the alkyne by sodium metal in liquid ammonia, carbometalation of alkynes, rearrangement of other alkenes, and finally pericyclic reactions (“ene” reaction, Cope rearrangement and Diels-Alder reaction)[53]. Another important reaction for alkene synthesis is the Wittig olefination, which employs a phosphorus ylide $Ph_3P{=}CHR$ to produce an alkene and $Ph_3P{=}O$. Recently a protocol was published to make the reaction catalytic using a sterically cyclic phosphinoxide.[54]

The majority of the alkene reactions involve the cleavage of this π bond: catalytic addition of hydrogen to produce the related alkane (on platinum, nickel or palladium), electrophilic addition, electrophilic halogenation, hydrohalogenation, oxidation in presence of oxygen, catalytic oxidation with oxygen or percarboxylic acids to yield epoxides, breaking of the double bond with ozone in ozonolysis and polymerizations. (ex. Ziegler-Natta) are popular among the vast amount of reactions.

The first transition metal featuring the M-Olefin bond, synthesized in 1827, was the so called Zeise's Salt, $K[PtCl_3(C_2H_4)].H_2O$. Pt^{2+} acts like a Lewis acid catalyzing the dehydration of a molecule of ethanol forming Pt^{2+}-C_2H_4 bond. The real structure was only elucidated in the fifties, and it consists of a molecule of ethylene laying perpendicular to the plane formed by the platinum ion and the three chlorides.[55-57] Olefins can easily coordinate transition metals using the π orbital, and unlike carbon monoxide, they are better Lewis bases. They can behave like Lewis acids as well, accepting electron density from a metal atom orbital of opportune symmetry into their empty π^* (Fig. 1.6). As for carbon monoxide, the Chatt-Dewar-Duncanson model is still a reasonable description of the bond between olefins and transition metals. The coordinated olefin, however, shows a completely different spectroscopic behavior from carbon monoxide. While CO, upon coordination with metals, shows either increasing ("non-classical") or decreasing ("classical") ν(CO) stretching frequency, the olefins always show a decrease of the ν(C=C) frequency (1623 cm^{-1} for unbound ethylene in gas phase). This is a very important observation that leads to the belief that the presence of the metal always weakens the C=C bond distance. In other words, both M $\leftarrow$ L σ-donation and M $\rightarrow$ L π-back-donation synergistically act to weaken the double bond either by removing electron density from a filled bonding orbital (π, the former) or by enforcing electron density in an empty anti-bonding orbital (π^*, the latter) (Fig. 1.7).

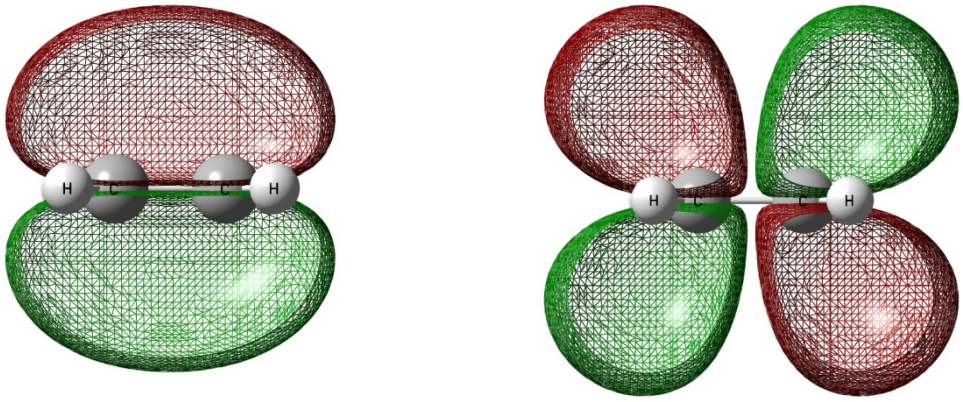

Figure 1.6. Ethylene KS HOMO (B_{3u}, - 0.28305 hartrees), left, and LUMO (B_{2g}, -0.00847 hartrees), right, calculated at B3PW91/6-311++G(d,p), 0.02 hartrees isovalue.

The C=C bond distance in Zeise's salt is slightly elongated from the unbound ethylene, signaling that the coordination to the metal weakens the C=C bond.

As for the case of carbon monoxide, two resonance forms can be drawn for the M-C_2H_4 structure: the first one is normally referred to as the π-complex (Figure 1.8, left), a structure where the interaction between metal and olefin is mostly due to an electrostatic polarization of the π cloud of the olefin. The second one is called metallacyclopropane (Figure 1.8, right), for it recalls the structure of the cyclopropane where one CH_2 unit has been substituted by a metal atom. It is logical to assume that the metallacyclopropane structure will contribute more to the real structure in metal complexes where the metal is a very good π-back-donor, able to deplete charge in the inter-nuclear region of the interaction to redistribute it along the M-C axes, or where the olefin has a particularly low-lying LUMO (as in the case of fluorinated olefins, for example). It logically follows that the M-C and C-C bond orders for a metallacyclopropane

structure approximate **1**, while they are 0 < M-C < 1 and 1< C-C < 2 respectively for the π-complex structure (the C=C bond order is around 2 for a non-complexed olefin)[22, 25, 30].

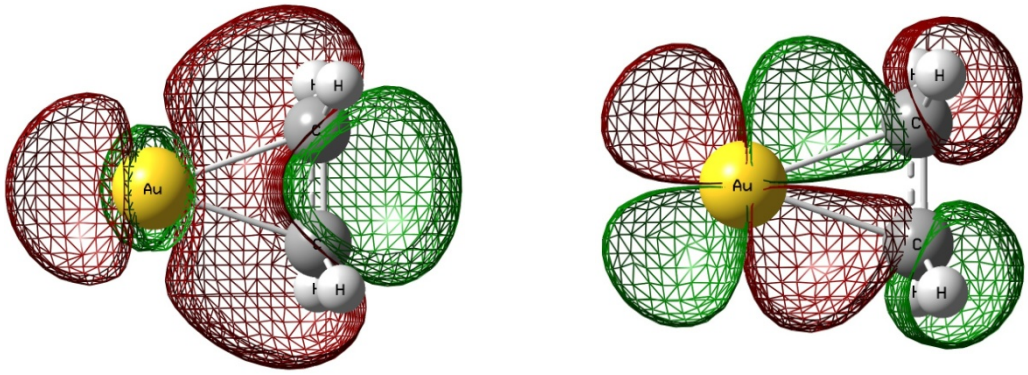

Figure 1.7. Qualitative diagram of KS orbitals of possible σ-donation (A_1, - 0.60505 hartrees), left, and π-back-donation (B_2, - 0.58220 hartrees), right, between Au^+ and C_2H_4 (calculated at B3PW91/ 6-311++G(d,p), 0.02 hartrees isovalue)

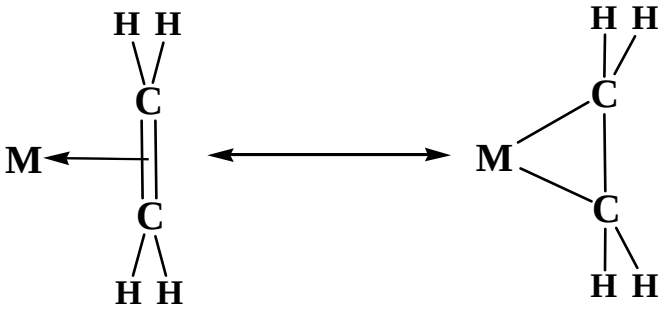

Figure 1.8. π-complex (left) versus metallacyclopropane resonance structure (right)

CHAPTER 2

HOMOLEPTIC M-OLEFIN COMPLEXES

In this chapter the principal homoleptic compounds featuring a coinage metal and olefins will be extensively discussed. The word “homoleptic” derives from ancient greek *homos* and *leptos*, meaning “same connection”. In other words, olefins are the only ligands surrounding the metal center. Such adducts are extremely rare in chemistry, which is particularly true for group 11. The compounds will be discussed and compared based on their metric parameters (when available) and spectroscopic data. A particular emphasis will be given to the description of the bond in these rare adducts in an attempt to classify and rationalize their peculiar chemistry.

2.1 Homoleptic olefin complexes of “Coinage” metals

Simple olefins are widely used in coordination chemistry. As previously stated, olefins can be both Lewis bases and Lewis acids, and their interaction is qualitatively well described by the Chatt-Dewar-Duncanson model. My study of the simple homoleptic olefin systems with coinage metals started in a somewhat serendipitous way. I was interested in synthesizing and studying the properties of $ClAu(C_2H_4)$, which I intended to use as synthetic starting material for gold derivatives. Similar compounds with heavier olefins have already been characterized and reported by Calderazzo and co-workers. Homoleptic copper-olefin adducts have been reported in the pioneering work of Kochi and co-workers.[58, 59] Homoleptic silver-norbornene adducts have been reported by Nelson and co-workers[60] and Solodar and co-workers[61]. When a suspension/solution of AuCl in dichloromethane is saturated with ethylene, the metal compound

becomes somewhat more soluble and the solution turns a deep yellow color. Such a solution left in a NMR tube for several days gives yellow needle-like crystals and a consistent amount of decomposition product. The crystals are very reactive and they decompose quickly when exposed to the air. Although a complete and precise X-ray analysis has been unsuccessful, we managed to obtain a partially refined diagram showing the presence of a 1:1 mixture of Au^{I} and Au^{III} in the crystal. Three ethylene moieties are surrounding a gold cation in a "spoke-wheel" arrangement, and the formally cationic moiety is stabilized by $AuCl_4^-$ anion. This was very surprising considering that Au^{I} prefers di-coordinate over tri-coordinate or tetra-coordinate coordination environments (preference for directional bonds is a direct consequence of the relativistic effects). The decomposition plays a major role in the formation of this compound. It is well-known that Au^{I} dismutes easily in the presence of moisture into Au^0 and Au^{III}. Au^{III} is easily reduced to $[Au(C_2H_4)_3]^+$ in the presence of ethylene. Another reason could be the presence of impurities of $AuCl_3$ dimer in the mixture since AuCl is obtained directly from it by warming it up to 160℃.

Such spoke-wheel tris-ethylene compounds have been known since 1970 for metal atoms of group 10. Wilke et al. reported a very interesting $[Ni(C_2H_4)_3]$ compound.[62, 63] The assumption that the ethylene moieties are in a spoke-wheel, rather than up-right (or barrel) conformation, was confirmed experimentally by Wilke and co-workers and theoretically by Schaefer in 1979 (using HF calculations)[64]. In the late seventies, Stone and co-workers reported the synthesis of the related Pd^0 and Pt^0 adducts. $[Pt(C_2H_4)_3]$ is the only compound of this class for which metric parameters are available. Stone and co-workers also reported the synthesis and the characterization of Pd^0 and Pt^0 adducts with heavier olefins like norbornene, $[Pd(C_7H_{10})_3]$[65, 66] and $[Pt(C_7H_{10})_3]$[65, 66].

I decided to carry on a more systematic investigation, both theoretical and experimental of $[M(Olefin)_n]^+$ in group 11 (Tab. 2.1). Krossing et al. reported the use of a bulky non-coordinating anion in the isolation of $[Ag(C_2H_4)_3][Al\{OC(CF_3)_3\}_4]$[67] in 2003 and of $[Cu(C_2H_4)_3][Al\{OC(CF_3)_3\}_4]$[68] in 2007. As for the previous compounds, this one as well shows the characteristic spoke-wheel arrangement around the metal cation. Monolefins have been extensively studied computationally[45, 69-103], but, to my knowledge, they have not been isolated and fully characterized yet, probably because of the high degree of coordinative unsaturation at the metal centre. Complexes like $[M(C_2H_4)_2]^+$ (M = Cu, Ag and Au) exist in the "staggered", D_{2d}, and "eclipsed", D_{2h}, conformations.[71, 83, 87-89, 92, 103-107] While the first one has been confirmed to be a true minimum by Hessian analysis, the second has a negative frequency about the local C_2 axis of the ethylene and thus is a first order saddle point. $[M(C_2H_4)_3]^+$ structures exist only in a planar D_{3h} symmetry, commonly called "spoke-wheel" arrangement.[67, 68, 71, 87, 88, 103, 108, 109] 2 C_{2v} structures were found (one up-side down ethylene plus two in plane and vice versa) and characterized as first order saddle points by Hessian analysis. The barrel conformation, D_{3h}, where the ethylene moieties are upside-down with respect to the σ_h plane for the "spoke-wheel", is a 3rd order saddle point on the PES with 3 imaginary frequencies (3rd order saddle points have very low interest, at least from an experimental point of view). $[M(C_2H_4)_4]^+$ are currently under investigation at the same level of theory and are not included in the present thesis. $[M(C_7H_{10})]^+$ is calculated using C_s symmetry, while only a C_2 conformation was found to be a real minimum for $[M(C_7H_{10})_2]^+$ compounds. This conformation resembles the D_{2d} conformation for $[M(C_2H_4)_2]^+$, and it possibly allows the maximum M→L π-back-bonding, since two different orthogonal orbitals are involved in it (ex. d_{xy} and d_{yz}). The eclipsed (both methylenes are in the same σ_v plane and pointing at each other) and the staggered (both methylenes are in the same

σ_v plane, but on opposite sides with respect to the metal) conformations are found to be 1st order saddle point and, consequently, disregarded.

$[M(C_7H_{10})_3]^+$ structures present two minima on the PES, one being a C_3 structure with all the methylene units pointing up (in substantial agreement with the X-ray structures), and the other one belonging to C_1 point group symmetry with two methylene units up and one down.

Table 2.1. Calculated versus X-Ray parameters obtained for $[M(olefin)_n]^+$

Compound	Point group (in calculations)	M-C bond distance (average, Å)		C-C bond distance (average, Å)	
		Experimental Min-Max, Average	Calculated	Experimental Average	Calculated
C_2H_4	D_{2h}	-	-	1.313(1)	1.328
$Cu(C_2H_4)^+$	C_{2v}	-	2.057	-	1.375
$Cu(C_2H_4)_2^+$	D_{2d}	-	2.106	-	1.361
$Cu(C_2H_4)_3^+$	D_{3h}	2.150(7)-2.190(7), 2.174(7)	2.172	1.368(11)	1.361
$Ag(C_2H_4)^+$	C_{2v}	-	2.318	-	1.366
$Ag(C_2H_4)_2^+$	D_{2d}	-	2.325	-	1.359
$Ag(C_2H_4)_3^+$	D_{3h}	2.393(9)-2.418(8), 2.401(9)	2.382	1.315(15)	1.357
$Au(C_2H_4)^+$	C_{2v}	-	2.162	-	1.402
$Au(C_2H_4)_2^+$	D_{2d}	-	2.236	-	1.375
$Au(C_2H_4)_3^+$	D_{3h}	2.263(4)-2.272(4), 2.268(4)	2.283	1.364(7)	1.377
C_7H_{10}	C_s	-	-	1.334(1)	1.338
$Cu(C_7H_{10})^+$	C_s	-	2.067	-	1.395
$Cu(C_7H_{10})_2^+$	C_2	-	2.121	-	1.376
$Cu(C_7H_{10})_3^+$	C_3	2.197(4)–2.199(4) 2.198(4)	2.215	1.378(6)	1.373
$Ag(C_7H_{10})^+$	C_s	-	2.327	-	1.387

Table 3.1 - continued

$Ag(C_7H_{10})_2^+$	C_2	-	2.343	-	1.374
$Ag(C_7H_{10})_3^+$	C_3	2.397(3)–2.420(3) 2.409(3)	2.429	1.369(4)	1.369
$Au(C_7H_{10})^+$	C_s	-	2.189		1.423
$Au(C_7H_{10})_2^+$	C_2	-	2.262		1.389
$Au(C_7H_{10})_3^+$	C_3	2.281(3)–2.302(4) 2.292(4)	2.319	1.378(5)	1.390

$[Au(C_7H_{10})_3]^+$ behaves under C_s point group symmetry. As I mentioned earlier, thermodynamic experimental measurements are not available for the M-olefin bond. Experimental values are known for silver complexes reactions (see Tab. 2.2 below). Our calculations seem to be in very good agreement with the experimental values, especially when considering the level of theory at which they have been performed. Better values were obtained by Gordon and co-workers—though using post-HF methods that are more precise in evaluating exchange-correlation energy—but also several order of magnitude slower than DFT.[87] Generally, norbornene seems to bind stronger than ethylene to coinage metal. This is probably due to the fact that both M←L σ-bonding and M→L π-back-bonding work synergistically to weaken the C=C bond and consequently to relieve the strain energy around the double bond. While the formation of $[M(Olefin)]^+$ and $[M(Olefin)_2]^+$ from M^+/Olefin and $[M(Olefin)]^+$/Olefin respectively is always exergonic ($\Delta G < 0$), the formation of the $[M(Olefin)_3]^+$ from $[M(Olefin)_2]^+$/Olefin is exergonic in the case of the ethylene complexes. Preliminary calculations show that ΔG is slightly endergonic for the norbornene complexes. A plausible explanation is the increased steric bulkyness when passing from ethylene to norbornene. ΔG decreases along the group for $[M(C_2H_4)]^+$, with - 4.5 kcal/mol for copper, - 1.5 kcal/mol for silver and - 1.1 kcal/mol for gold.

Table 2.2. Calculated versus experimental D_0 for $[M(L)_n]^+$ (M = Cu, Ag, Au and L = C_2H_4)

Reaction (298.25 K and 1 atm)	ΔD_0
$Cu^+ + L \rightarrow Cu(L)^+$	- 50.8 **(- 42.0 ± 3.2)**[107]
$Cu(L)^+ + L \rightarrow Cu(L)_2^+$	- 40.1 **(- 41.5 ± 3.0)**[107]
$Cu(L)_2^+ + L \rightarrow Cu(L)_3^+$	- 14.9
$Ag^+ + L \rightarrow Ag(L)^+$	- 36.9 **(- 32.3 ± 3.0)**[89]
$Ag(L)^+ + L \rightarrow Ag(L)_2^+$	- 31.8 **(- 30.2 ± 1.4)**[89]
$Ag(L)_2^+ + L \rightarrow Ag(L)_3^+$	- 12.1 **(- 13.6 ± 0.7)**[89]
$Au^+ + L \rightarrow Au(L)^+$	- 65.2
$Au(L)^+ + L \rightarrow Au(L)_2^+$	- 47.1
$Au(L)_2^+ + L \rightarrow Au(L)_3^+$	- 12.0

As I mentioned above, $[Cu(C_2H_4)_3][Al\{OC(CF_3)_3\}_4]$ and $[Ag(C_2H_4)_3][Al\{OC(CF_3)_3\}_4]$ have been isolated using the bulky fluorinated anion $[Al\{OC(CF_3)_3\}_4]^-$. Due to the sometimes problematic syntheses of these bulky fluorinated anion, we opted for something easier to manipulate and readily available, namely the SbF_6^- anion. When commercially available $AgSbF_6$ is dissolved in dichloromethane saturated with ethylene, it intakes up to three equivalents of

ethylene to promptly give $[Ag(C_2H_4)_3][SbF_6]$ (Fig. 2.1 and 2.2). In the same way, $AgSbF_6$ reacts with a dichloromethane solution of norbornene (3 equivalents or excess) to give $[Ag(C_7H_{10})_3][SbF_6]$. The norbornene adduct is relatively stable compared to ethylene and it does not decompose under vacuum. Ag^I adducts can be used to synthesize the corrisponding Cu^I and Au^I adducts in metathesis reactions that have a strong driving force in the precipitation of AgCl or AgBr. $[Cu(C_2H_4)_3][SbF_6]$, $[Ag(C_2H_4)_3][SbF_6]$ and $[Au(C_2H_4)_3][SbF_6]$ are very reactive in the air, and they tend to decompose, releasing the coordinated gas and leaving green precipitate in the case of copper, “silver mirror”, or metallic gold (Fig. 2.1).

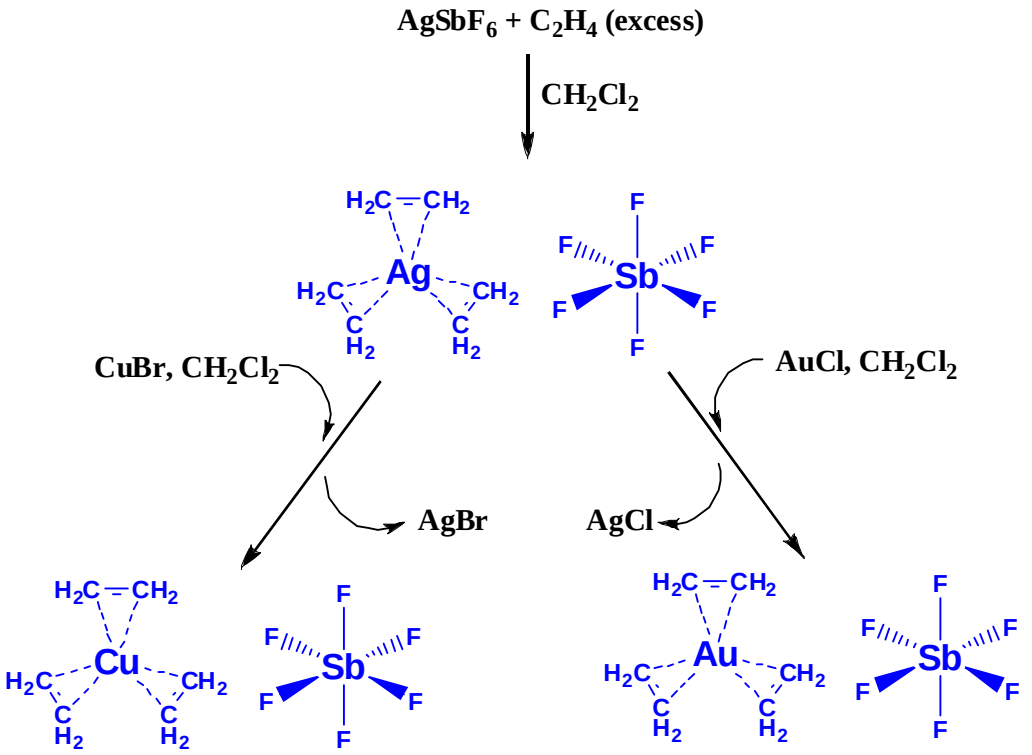

Figure 2.1. Synthetic scheme for $[M(C_2H_4)_3][SbF_6]$ (M = Cu, Ag, Au)

$[Au(norbornene)_3][SbF_6]$ was obtained by treating a dichloromethane solution containing norbornene and $AgSbF_6$ with a mixture of AuCl and norbornene in dichloromethane at -50℃

(Fig. 2.2). [Au(norbornene)$_3$][SbF_6] is a white solid and can be handled in air under ambient light for short periods without any signs of decomposition; however, it is best stored in a -20℃ freezer under nitrogen. [Au(C_7H_{10})$_3$][SbF_6] slowly decomposes (several hours) in CD_2Cl_2 at room temperature as evident from the deposition of pink solids on the walls of the container, but it is more stable at -20℃. The analogous silver ad duct [Ag(C_7H_{10})$_3$][SbF_6] can be synthesized quite easily using commercially available $AgSbF_6$ and norbornene. The copper(I) complex was obtained using a metathesis process involving CuCl and [Ag(C_7H_{10})$_3$][SbF_6]. The treatment of silver(I) complex [Ag(C_7H_{10})$_3$][SbF_6] with AuCl in dichloromethane at room temperature also leads to the [Au(C_7H_{10})$_3$][SbF_6], but the reaction is not very clean. [Ag(C_7H_{10})$_3$][SbF_6] and [Cu(C_7H_{10})$_3$][SbF_6] complexes are also thermally stable white solids and can be handled in air for short periods without decomposition. These six compounds are isoelectronic compounds to [Ni(C_2H_4)$_3$], [Pd(C_2H_4)$_3$], [Pt(C_2H_4)$_3$], [Pd(C_7H_{10})$_3$], and [Pt(C_7H_{10})$_3$], but unlike their counterparts, however, they present much higher thermal stability and can be handled long enough at room temperature (always using light protection and under argon atmosphere, especially for the ethylene adducts) to be fully characterized. X-ray crystallographic analysis of [Ag(C_2H_4)$_3$][SbF_6] shows that the cation and the anion are two separate species in the unit cell. In the case of [Ag(C_2H_4)$_3$][SbF_6], conversely, the anion sits on top of the cation, and the fluorines lie right above the C=C bonds (there is close contact with a hydrogen of one ethylene). The reason for this symmetrical arrangement might be weak electrostatic or dipole-dipole interactions between the fluorines and the coordinated ethylenes, but the system was not modeled computationally owing to the inability of the DFT methods to deal with dispersive forces. An X-ray diffraction of [Cu(C_2H_4)$_3$][SbF_6] could only be obtained in a mesomeric crystal species that was generated by the reaction of CuCl (instead of CuBr) with $AgSbF_6$ in presence of ethylene. Two different species, [Cu(C_2H_4)$_3$][SbF_6] and the trimer {[Cu(C_2H_4)$_2$]$_3$(Cl)[SbF_6]$_2$}, are observed in the crystal

lattice. A chloride anion coordinates three copper ions in a trigonal planar fashion, and two ethylene moieties are coordinated per copper. The coordination motif seen here closely resembles another structure, $[Cu(C_2H_4)_2][ClAlCl_3]$. $[Cu(C_2H_4)_3][SbF_6]$ shows that cation and anion are forming an array with F···Cu distances of about 2.823 Å, which is on the order of the sum of the F-Cu Van der Waals radii (2.87 Å). M-C bond distances are the longest in the silver adduct with an average of 2.401(9) Å, followed by the gold, av. 2.268(4) Å and copper, av. 2.174(7) Å. These distances follow the same trend as the covalent radii of the M^I ions[110]. C=C bond distances are comparable to that of free ethylene for copper and silver adducts and slightly longer for the gold adduct, av. 1.364(7) Å. This is a sign of weakened C=C bond, brought about by a combination of σ-bonding and/or increased π-back-bonding. $[Pd(C_2H_4)_3]$ shows slightly longer C=C bond distance, av. 1.402(7) Å , probably due in this case to more efficient M→L π-back-bonding. X-ray crystallographic analysis of $[M(C_7H_{10})_3][SbF_6]$ (M = Au, Ag, Cu) shows that all three adducts crystallize in the rhombohedral R3 space group, and have similar cell dimensions. They are isomorphous compounds. The metal ion (M) sits on a three-fold rotation axis. It coordinates the exo-faces of the three norbornene molecules in an up-up-up arrangement. Preferred exo-reactivity of the norbornene is well documented and has been attributed to factors such as p-orbital distortions and torsional strain[111, 112]. The three η^2-bonded alkene moieties and the metal ion form an essentially planar spoke-wheel. Stone and co-workers reported an up-up-down conformation for $[Pd(C_7H_{10})_3]$ and $[Pt(C_7H_{10})_3]$ in the solid state. It is interesting to note that calculations in gas phase predict C_1/C_s structures (one norbornene upside-down) to be the global minima, more stable than C_3 structures by 1.9 kcal/mol for silver, and 2.6 kcal/mol for gold. It is not unreasonable to assume that the reduced steric hindrance at the metal center has an important part in this increased stability. However, we were not able to obtain clear data of the existence of the C_1/C_s rotamers, in solid state or in

solution at room temperature. The interconversion $C_1 \rightarrow C_3$ might have a low-laying transition state, thus happening quickly in solution. ^{1}H NMR at low temperature as well as additional calculations might provide useful insight on the fluxional behavior of these molecules, though clear experiments regarding this aspect have yet to be run. In my opinion, solvent effects are also important factors in the selective crystallization of one isomer over the other (considering that the crystals are grown in solvent at -20 ℃). Cu, Ag, and Au ions and alkene moieties show small deviations from the ideal trigonal planar arrangement as evident from the metal ion displacement distances (0.08, 0.06, and 0.10 Å corresponding to the Au^I, Ag^I, and Cu^I adduct, respectively) and alkene moiety dihedral angles (9.6°, 11.2°, and 12.6° corresponding to the Au^I, Ag^I, and Cu^I adduct, respectively) from the plane defined by the three alkene centroids.

The M-C (alkene) distance is longest in the silver adduct, followed by gold and copper. These distances follow the same trend as covalent radii of the M^I ions. The C=C distances show significant lengthening relative to that of the free norbornene (1.334(1) Å), but the three adducts have similar C=C distances within the error limits. There are no close intermolecular M···M or inter/intra-molecular M···F contacts in $[M(C_7H_{10})_3][SbF_6]$ adducts.

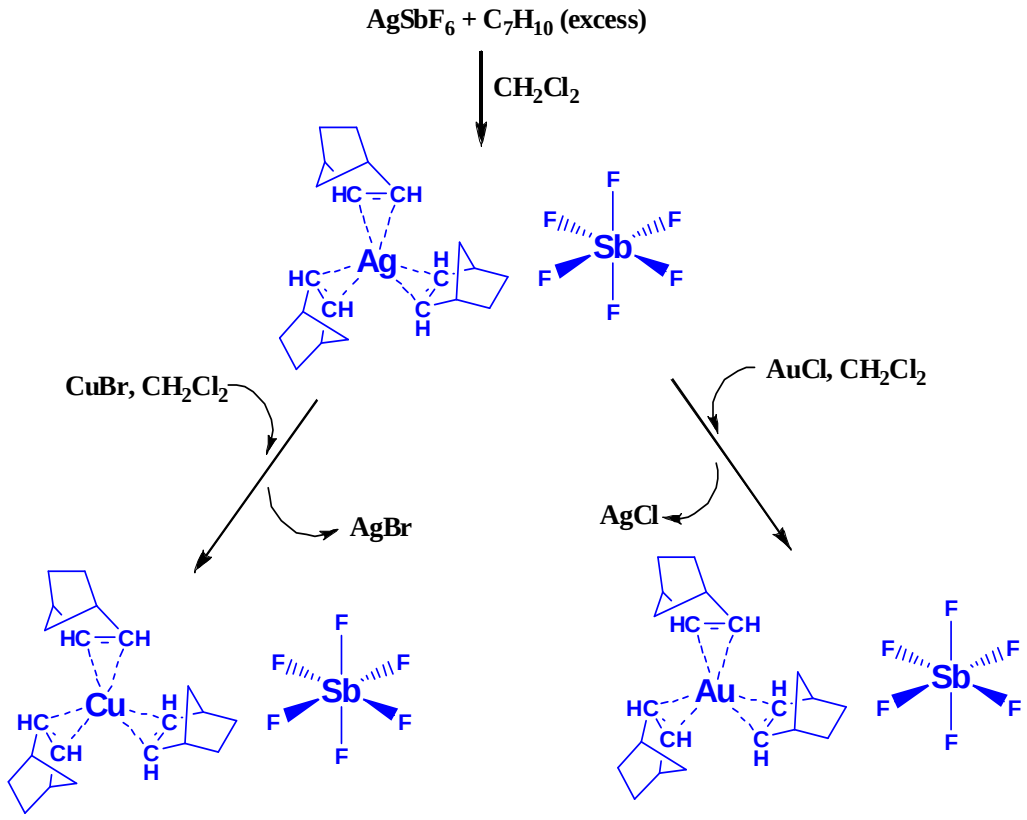

Figure 2.2. Synthetic scheme for $[M(C_7H_{10})_3][SbF_6]$ (M =Cu, Ag, Au)

Although the norbornene adducts seem to be more stable than their ethylene relatives, vibrational spectra (Raman) have been extremely difficult to obtain. The experimental conditions (laser wavelength, intensity, etc.) have been determined for each compound separately, and several crystals sealed under inert atmosphere were analyzed before acquiring spectra of good quality. The crystals of almost all the compounds were very sensitive to the laser, decomposing fast and leaving charred precipitates in their place. The Raman spectrum for $[Au(C_2H_4)_3][SbF_6]$ was obtained in less than 5 seconds before the compound totally decomposed. No spectrum for $[Au(C_7H_{10})_3][SbF_6]$ could be captured after several attempts since the compound seems to decompose very quickly under the laser, but a good estimation of it is offered by our DFT

calculations that place ν(C=C) at 1474 cm^{-1} (average between *A* and *E* modes, $\Delta\nu_{AE}$= ~ 2 cm^{-1}). For all the compounds analyzed, there is no clear resolution between *A* and *E* (*A*$_1$' and *E*' in the case of point group D_{3h}) modes for C=C group vibrations. This has been interpreted as a clear sign of a high degree of symmetry, even in the solid state[67, 113-115]. Raman spectra of $[Cu(C_2H_4)_3][SbF_6]$, $[Ag(C_2H_4)_3][SbF_6]$ and $[Au(C_2H_4)_3][SbF_6]$ show a strong band at 1566 (calculated 1563, $\Delta\nu_{AE}$= ~ 0 cm^{-1}), 1584 (calculated 1572, $\Delta\nu_{AE}$= ~ 1 cm^{-1}), and 1543 cm^{-1} (calculated 1536, $\Delta\nu_{AE}$= ~ 3 cm^{-1}) respectively. These values are respectively - 57 (calculated - 81), - 39 (calculated - 72), and - 80 cm^{-1} (calculated - 108) red-shifted with respect to the ν(C=C) band of free ethylene (1623 cm^{-1}, calculated 1644). Raman spectra of $[Cu(C_7H_{10})_3][SbF_6]$ and $[Ag(C_7H_{10})_3][SbF_6]$ show a strong band at 1491 (calculated 1495, $\Delta\nu_{AE}$= ~ 4 cm^{-1}), and 1507 cm^{-1} (calculated 1504, $\Delta\nu_{AE}$= ~ 0 cm^{-1}) respectively. These values are respectively - 74 (calculated - 101), - 58 (calculated - 92), red-shifted with respect to the ν(C=C) band for non-coordinated norbornene (1565 cm^{-1}, calculated 1596). Wiberg bond orders support vibrational analysis, suggesting a bond order decrement going from C_2H_4 (2.04) > $[Ag(C_2H_4)_3]^+$ (1.82) > $[Cu(C_2H_4)_3]^+$ (1.76) > $[Au(C_2H_4)_3]^+$ (1.64) for the ethylene series. For comparison, the Wiberg bond order for $[Pd(C_2H_4)_3]$ is 1.60. For the compounds in the series, the metallacyclopropane structure (B.O. 1.00) does not contribute significantly to the real structure; however, $[Pd(C_2H_4)_3]$ and $[Au(C_2H_4)_3]^+$ approach it better than $[Ag(C_2H_4)_3]^+$ and $[Cu(C_2H_4)_3]^+$.

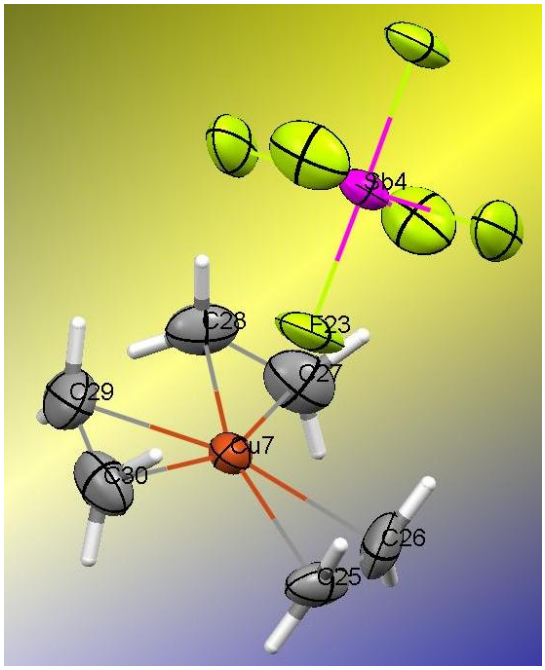

Figure 2.3. ORTEP structure of $[Cu(C_2H_4)_3][SbF_6]$. Thermal ellipsoids have been drawn at 60% probability level. Selected bond lengths (Å) and angles (°): Cu7-C25 2.190(7), Cu7-C26 2.158(7), Cu7-C27 2.150(7), Cu7-C28 2.169(7), Cu7-C29 2.187(7), Cu7-C30 2.189(7), C25-C26 1.370(10), C27-C28 1.374(11), C29-C30 1.361(11), Sb4-F23 1.872(4), C27-Cu7-C28 37.1(3), C29-Cu7-C30 36.2(3), C26-Cu7-C25 36.7(3), Cu7···F23 2.823

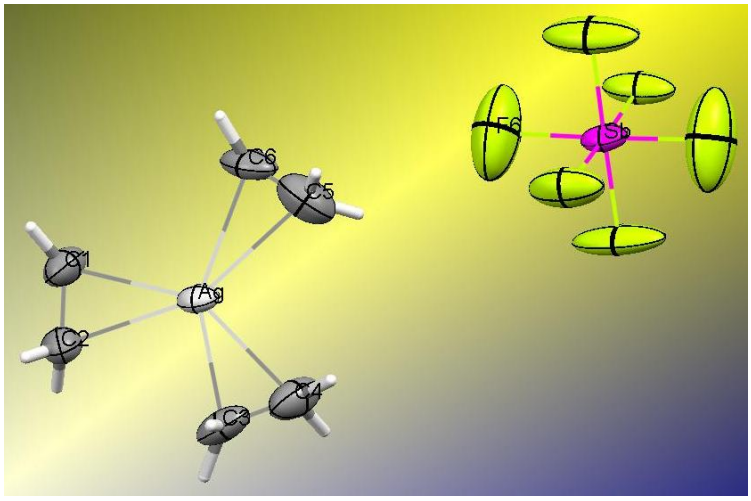

Figure 2.4. ORTEP structure of $[Ag(C_2H_4)_3][SbF_6]$. Thermal ellipsoids have been drawn at 60% probability level. Selected bond lengths (Å) and angles (°): Ag-C1 2.405(9), Ag-C2 2.399(9), Ag-C3 2.393(9), Ag-C4 2.396(9), Ag-C5 2.394(10), Ag-C6 2.418(8), C1-C2 1.339(13), C3-C4 1.286(15), C5-C6 1.319(16), Sb-F6 1.841(9), C2-Ag-C1 32.4(3), C3-Ag-C4 31.2(4), C5-Ag-C6 31.8(3)

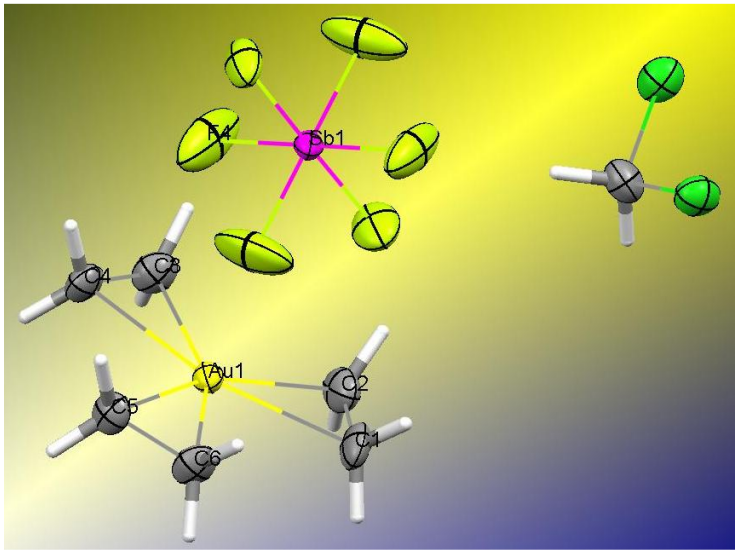

Figure 2.5. ORTEP structure of $[Au(C_2H_4)_3][SbF_6].CH_2Cl_2$. Thermal ellipsoids have been drawn at 60% probability level. Selected bond lengths (Å) and angles (º): Au-C1 2.271(5), Au-C2 2.267(6), Au-C3 2.267(4), Au-C4 2.263(4), Au-C5 2.269(4), Au-C6 2.272(4), C1-C2 1.371(7), C3-C4 1.351(7), C5-C6 1.369(7), Sb-F4 1.860(4), C2-Au-C1 32.16(18), C3-Au-C4 34.71(17), C5-Au-C6 35.10(17)

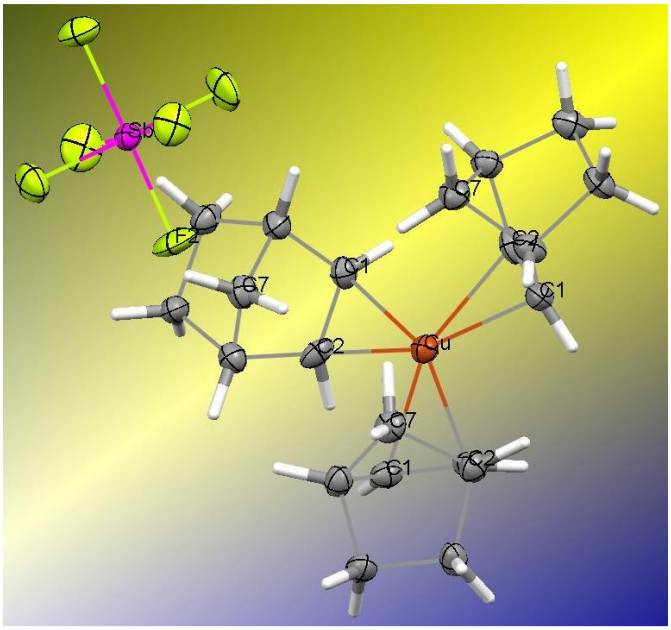

Figure 2.6. ORTEP structure of $[Cu(C_7H_{10})_3][SbF_6]$. Thermal ellipsoids have been drawn at 60% probability level. Selected bond lengths (Å) and angles (º): Cu-C1 2.197(4), Cu-C2 2 .199(4), C1-C2 1.378(6), Sb-F2 1.867(3), C2-Cu-C1 36.53(16), Cu···C7 3.116

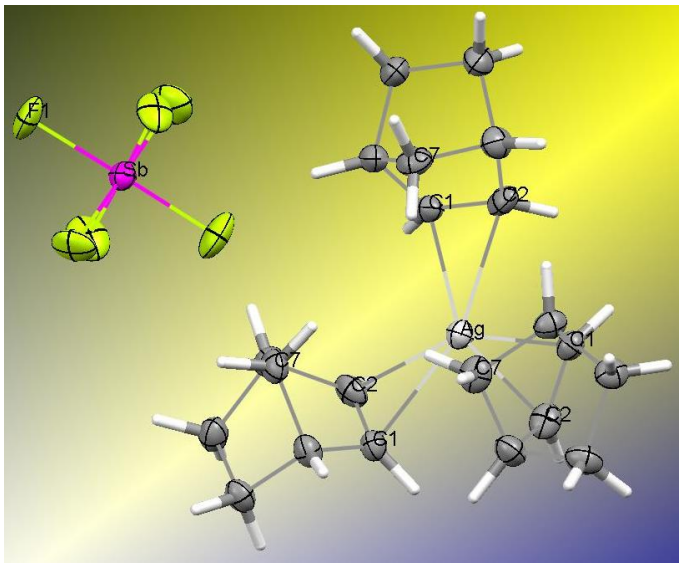

Figure 2.7. ORTEP structure of $[Ag(C_7H_{10})_3][SbF_6]$. Thermal ellipsoids have been drawn at 60% probability level. Selected bond lengths (Å) and angles (º): Ag-C1 2.395(4), Ag-C2 2.414(4), C1-C2 1.356(6), Sb-F1 1.875(2), C2-Ag-C1 32.75(14), Ag···C7 3.245

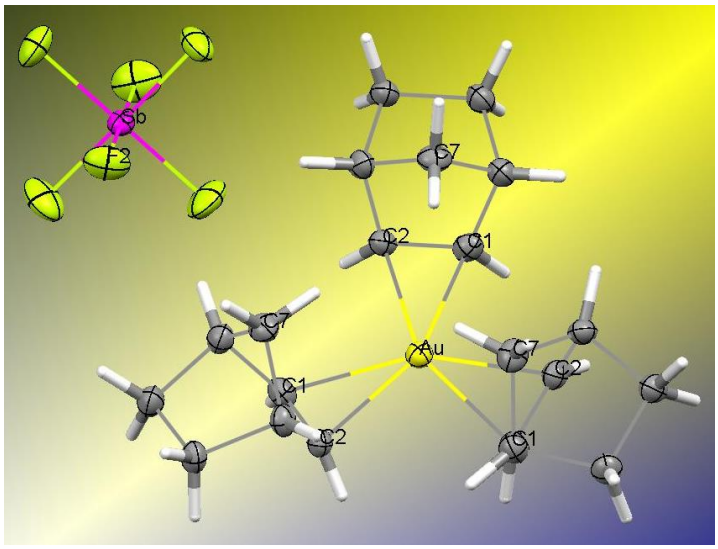

Figure 2.8. ORTEP structure of $[Au(C_7H_{10})_3][SbF_6]$. Thermal ellipsoids have been drawn at 60% probability level. Selected bond lengths (Å) and angles (º): Au-C1 2.302(4), Au-C2 2.281(3), C1-C2 1.378(5), Sb-F2 1.878(2), C2-Au-C1 34.99(13), Au···C7 3.207

Table 2.3. X-ray and spectroscopic parameters for $[M(Olefin)_3][SbF_6]$ (M = Cu, Ag, Au)

Compound	$[Cu(C_2H_4)_3]$ $[SbF_6]$	$[Ag(C_2H_4)_3]$ $[SbF_6]$	$[Au(C_2H_4)_3]$ $[SbF_6]$	$[Cu(C_7H_{10})_3]$ $[SbF_6]$	$[Ag(C_7H_{10})_3]$ $[SbF_6]$	$[Au(C_7H_{10})_3]$ $[SbF_6]$
Molecular formula	$C_6H_{12}CuF_6Sb$	$C_6H_{12}AgF_6Sb$	$C_6H_{12}AuF_6Sb$	$C_{21}H_{30}CuF_6Sb$	$C_{21}H_{30}AgF_6Sb$	$C_{21}H_{30}AuF_6Sb$
FW	383.46	427.78	601.80	581.74	626.07	715.17
Crystal system	Triclinic	Monoclininc	Orthorhombic	Rhombohedral	Rhombohedral	Rhombohedral
Space group	*P-1*	*P 21/n*	*P* 2_1 2_1 2_1	*R*3	*R*3	*R*3
a (Å)	18.1377(9)	8.2670(4)	8.4490(4)	11.3580(3)	11.5119(3)	11.3842(3) Å
b (Å)	20.3187(10)	11.9204(6)	10.9541(5)	11.3580(3)	11.5119(3)	11.3842(3) Å
c (Å)	101.544(2)	11.9555(6)	16.0772(8)	14.0341(7)	14.1244(7)	14.1889(7)
V ($Å^3$)	3064.8(3)	1173.38(10)	1487.96(12)	1567.90(10)	1621.04(10)	1592.52(10)
Z	2	4	4	3	3	3
Temp (K)	100	100	100	100	100	100
R1, wR2 (all data)	0.0559, 0.1058	0.0792, 0.0836	0.0195, 0.0487	0.0276, 0.0731	0.0175, 0.0449	0.0156, 0.0395
M-C (Å).	2.150(7)-2.190(7)	2.393(9)-2.418(8)	2.263(4)-2.272(4)	2.197(4)-2.199(4)	2.397(3)-2.420(3)	2.281(3)-2.302(4)
C=C (Å) av.	1.368(11)	1.315(15)	1.364(7)	1.378(6)	1.369(4)	1.378(5)
C-M-C (deg) av.	36.7(3)	31.8(3)	33.99(17)	36.53(16)	33.02(9)	34.99(13)
^{1}H NMR, δ, C*H* = (ppm)	5.44	5.83	4.94	5.77	6.42	5.53
^{13}C NMR, δ, *C*H= (ppm)	109.6	116.9	92.7	122.1	132.6	112.6
Raman, ν(C=C) cm^{-1}	1566	1584	1543	1491	1507	-

NMR spectra were collected for all six compounds at room temperature in CD_2Cl_2. The shift of the ^{13}C NMR in all six compounds versus the free ligands is particularly interesting, because it has been linked by several groups to the amount of M→L π-back-bonding. As a

consequence of strong π-back-bonding, the carbon shifts from pure sp^2 hybridization (free olefin) to sp^3-like hybridization: the signal moves downfield with respect to the signal of the free olefin. ^{13}C NMR spectra of $[Cu(C_2H_4)_3][SbF_6]$, $[Ag(C_2H_4)_3][SbF_6]$ and $[Au(C_2H_4)_3][SbF_6]$ show singlets at δ 109.6, 116.9, and 92.7 ppm respectively. These values are - 13.8, - 6.5, and - 30.7 ppm shielded with respect to the value of free ethylene (δ 123.4 ppm). ^{13}C NMR spectra of $[Cu(C_7H_{10})_3][SbF_6]$, $[Ag(C_7H_{10})_3][SbF_6]$, and $[Au(C_7H_{10})_3][SbF_6]$ show singlets at δ 122.1, 132.6, and 112.6 ppm, respectively. These values are - 13.8, - 3.3, and - 23.3 ppm shielded with respect to the value of the non-coordinated norbornene (δ 135.9 ppm).

A direct comparison of these NMR data with the vibrational analysis points out that, though these norbornene adducts show less M→L π-back-bonding than the corresponding ethylene complexes (13.4 ppm vs 17.0 ppm of average difference for norbornene vs ethylene in ^{13}C NMR), their C=C bonds are more weakened upon coordination. For a quick comparison with group 10, we can consider the case of $[Pd(C_2H_4)_3]$, $[Pt(C_2H_4)_3]$, and $[Pt(C_7H_{10})_3]$. These complexes show high M→L π-back-bonding, as can be appreciated from their ^{13}C NMR values for the olefinic carbons, 63.5 ppm, 48.4 ppm and 68.0 ppm. Pt^0 is a metal with good π-back-bonding capability, which can be easily seen from the huge shielding shift of the olefinic carbon signal that almost approaches the aliphatic region.

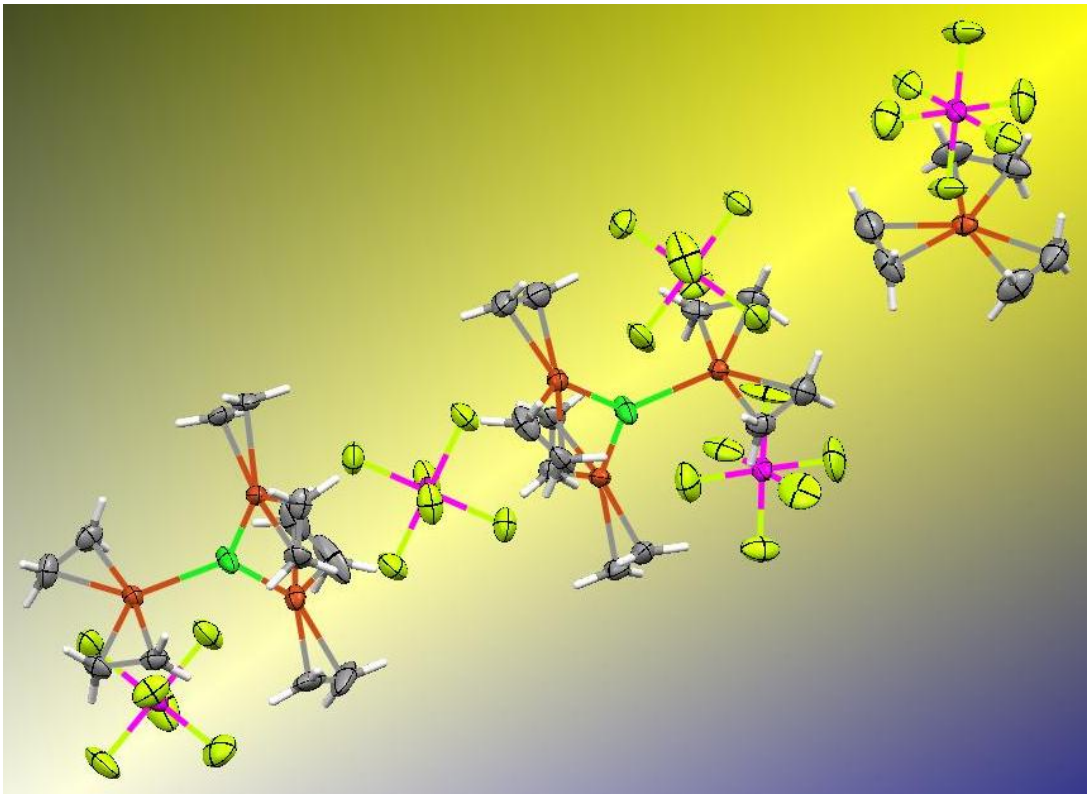

Figure 2.9. ORTEP structure of $[Cu(C_2H_4)_3][SbF_6]$ and $\{[Cu(C_2H_4)_2]_3(Cl)\}[SbF_6]_2$

We also extended the research to other counter-ions. Triflate and hexafluoroantimonate are commonly labeled as weakly-coordinating counter-ions, however, when $[Cu(OTf)]_2.C_6H_6$ is used instead of $CuBr/AgSbF_6$, the reaction does not produce the expected "wheel" compound. It proceeds overnight in an excess of ethylene (frozen at 100K) to give a seemingly colorless solution with little unreacted starting material. X-ray diffraction of one crystal grown at – 20 ℃ in dichloromethane shows a polymeric structure in which only one molecule of ethylene is coordinated per metal center. The copper environment is a distorted tetrahedron environment with three oxygen donors coming from two triflate counter-ions and one ethylene in the primary sphere of coordination. Two Cu-O bond distances are essentially the same, 2.028(2) and 2.0299(18), while the apical Cu-O bond distance is slightly elongated with a value of 2.3125(12)

Å. The C=C bond distance is 1.359(3), only slightly longer than the C=C bond distance of free ethylene, 1.313(1) Å (Fig. 2.10). It is clear from this experiment that triflate is much more nucleophilic than hexafluoroantimonate, and even an excess of ethylene cannot displace it from the metal center. ^{13}C NMR is a good indication of the M→C_2H_4 π-back-bonding. A higher degree of M→C_2H_4 π-back-bonding can be noticed for $[Cu(C_2H_4)(OSO_2CF_3)]_n$ in comparison to $[Cu(C_2H_4)][SbF_6]$ with two peaks at 93.4 ppm and 109.6 ppm respectively (4.72 versus 5.44 ppm in ^1H NMR). Vibrational data could not be collected because of the reactivity of the compound, which promptly loses ethylene, even under a sealed atmosphere, and decomposes.

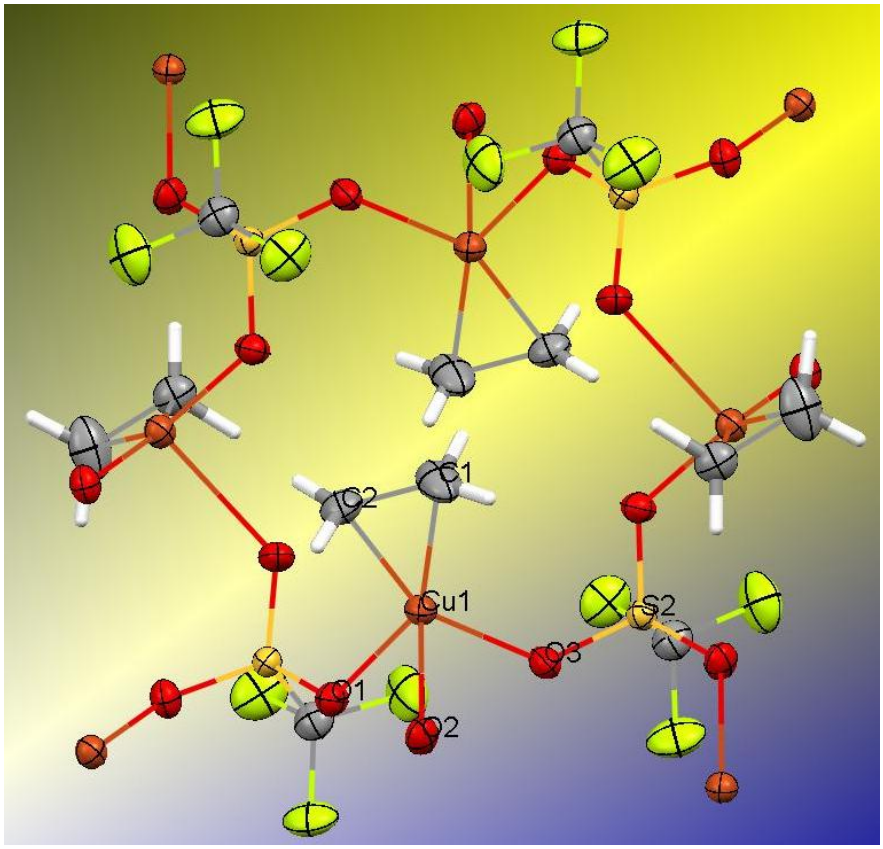

Figure 2.10. ORTEP structure of $[Cu(C_2H_4)(OSO_2CF_3)]_n$. Thermal ellipsoids have been drawn at 60% probability level. Selected bond lengths (Å) and angles (°): Cu1-C1 2.028(2), Cu1-C2 2.0299(18), C1-C2 1.359(3), Cu1-O1 2.0575(13), Cu1-O2 2.3125(12), Cu1-O3 2.0266(12), C2-Cu-C1 39.13(8), O3-S2 1.4566(12)

One of the most interesting features of these $[M(C_2H_4)_3]^+$ complexes is the contact between carbon atoms belonging to different olefin moieties. X-ray crystal structures show that C···C intermolecular contacts are shorter than the sum of Van Der Walls radii for two carbon atoms, 3.40 Å. $[Cu(C_2H_4)_3][SbF_6]$ shows C···C interaction distance of 2.892 Å (~ - 0.50 within Van Der Waals sum), 3.371 Å (~ - 0.03 Å) for $[Ag(C_2H_4)_3][SbF_6]$, and 3.065 Å (~ - 0.34 Å) for $[Au(C_2H_4)_3][SbF_6]$. $[Pt(C_2H_4)_3]$ shows C···C interaction distance of 2.867 Å (~ - 0.53 Å).

These results might be valuable if one considers the analogous example of $[Ni(C_2H_4)_3]$. The x-ray crystal structure for $[Ni(C_2H_4)_3]$ has not yet been reported in the literature yet; however, Herges and Papafilippopoulos calculated the C···C intermolecular distance in this complex to be 2.681 Å, ~ - 0.72 Å within the Van Der Waals sum for carbon atoms.[116] They predicted the possibility of the existence of an "aromatic-to-be" system (these are 6π e^- systems after all) leading to homoconjugation between the three ethylene moieties. In their opinion, E orbital pairs mixing (π and π^* characters) is responsible for this effect.[116] The authors point out that this homoconjugation might be at the base of the planarity of the molecule as well as the peculiar Ni^0 carbon-carbon bond formation (Reppe's reaction). The possibility of $(2_{2\pi}+2_{2\pi}+2_{2\pi})$ cycloaddition to form cyclohexane from ethylene would be a very interesting development for this chemistry.

The contours for A_1' molecular orbitals of $[M(C_2H_4)_3]^+$ (M =Cu, Ag, Au) are shown in Fig. 2.11. The contact between intermolecular carbon atoms is particularly evident from the electron density lying along the C···C contact direction (particularly for the gold complex).

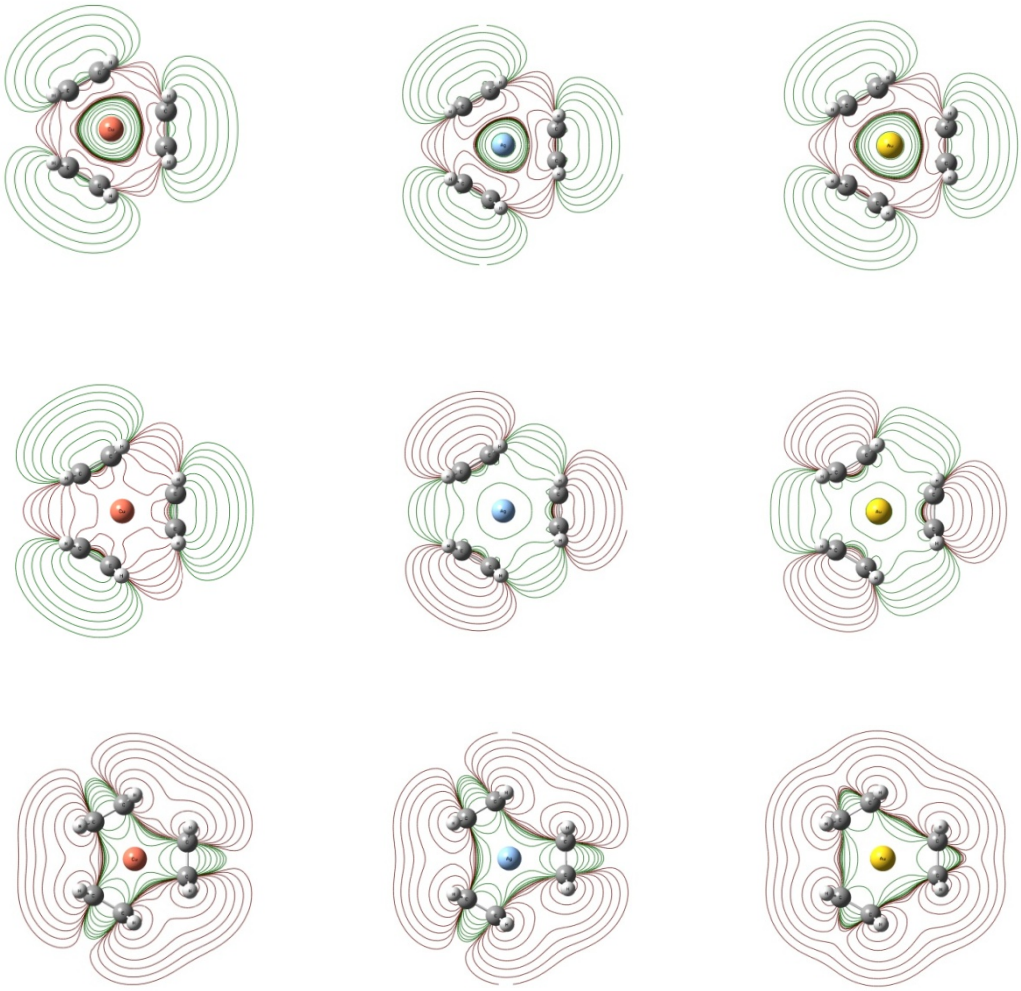

Figure 2.11. KS molecular orbital (A_1' symmetry) contours showing contact between adjacent carbon atoms in $[M(C_2H_4)_3]^+$

2.2 NBO analysis

Natural Bond Orbitals analysis (NBO) carried out on the densities obtained by B3PW91/aug-cc-pVTZ-PP/6-311++G(d,p) calculations provides interesting information on the nature of these bonds. It is useful at this point to introduce some specific nomenclature that will be used throughout the remainder of this thesis pertaining NBO analysis: BD stands for 2-center bonding type orbital, BD* stands for 2-center-anti-bonding type orbital, LP for one-center occupied lone pair, and LP* for one-center unoccupied lone pair. The numbers in brackets indicate the order of the bond or the type of lone-pair under consideration. Excited orbitals (Rydberg) have been excluded.

Localized BD(1) M-C orbitals between the coinage metal atoms and the carbon atoms of the ethylene are not present. This is clear proof of the absence of a net covalent M-ethylene bond. $[Pd(C_2H_4)_3]$ does not show any localized BD(1) M-C orbital either. Five types of main interactions contribute energetically to the delocalization present in these molecules (based on second order perturbation analysis of the Fock Matrix): they are listed below for $[M(C_2H_4)_3]^+$ complexes (Tab. 2.4).

DONOR → ACCEPTOR

(1) BD (2) C-C → LP* (6) M

(2) LP (4 or 5) M → BD* (2) C-C

(3) 4 x BD (1) C-H → BD* (1) C-H (hydrogens in trans)

(4) 4 x BD(1) C-H → LP* (6) M

(5) BD(2) C-C → BD*(2) C-C

The dominating delocalization in these complexes is BD (2) C-C → LP* (6) M, where electron density is given from the olefin to the metal atom. Orbitals of this type represent the

interactions that best describe the idea of L → M σ-donation. The contributions BD(1) C-C → LP* (6) M or CR C → LP* (6) M, where the olefin donates electron density through the C-C single bond or core orbitals of the carbon atoms, are negligible for these complexes. LP*(6) M has prevalently s character with minor d contribution, as might be expected for group 10 M^0 and group 11 M^I atoms (in detail, 99% s 1% d character for Cu^+, 98% s 2% d character for Ag^+, 96% s 4% d character for Au^+, and 97% s 3% d character for Pd, for ethylene complexes and essentially the same for norbornene complexes). The second predominant type of delocalization is LP (4 or 5) M → BD* (2) C-C, where electron density is given back to the olefin. Orbitals of this type represent the interactions that best describe the idea of M → L π-back-donation. LP (4 and 5) M have prevalently d character (in detail, 100% s character for Cu^+, Ag^+, Au^+, and Pd for ethylene complexes and essentially the same for norbornene complexes).

Table 2.4. Principal NBO delocalizations in $[Cu(C_2H_4)_3]^+$, $[Ag(C_2H_4)_3]^+$, $[Au(C_2H_4)_3]^+$, and $[Pd(C_2H_4)_3]$ per ethylene unit (the numbers in brackets represent the ratio between the strongest and the considered delocalization)

Interaction type	E^2 Donor → Acceptor (kcal/mol)			
	$Cu(C_2H_4)_3^+$	$Ag(C_2H_4)_3^+$	$Au(C_2H_4)_3^+$	$Pd(C_2H_4)_3$
BD (2) C-C → LP* (6) M	106.41	79.99	184.04	86.73
LP (4 or 5) M → BD* (2) C-C	12.08 **(8.8)**	11.53 **(6.9)**	25.08 **(7.3)**	38.57 **(2.2)**
4 x BD (1) C-H → BD* (1) C-H (hydrogens in trans)	16.64 **(6.4)**	16.96 **(4.7)**	15.40 **(12.0)**	15.20 **(5.7)**
4 x BD(1) C-H → LP* (6) M	13.00 **(8.2)**	9.20 **(8.7)**	9.8 **(18.8)**	12.36 **(7.0)**
BD(2) C-C → BD*(2) C-C	3.95 **(26.9)**	1.85 **(43.2)**	4.77 **(38.6)**	4.84 **(17.9)**

The first striking difference between group 10 and group 11 d^{10} metals concerns the charge. NBO metal charges systematically decrease upon complexation in Cu^I, Ag^I, and Au^I

(Tab. 2.5). In other words, the olefins make the coinage metals less positive, donating more than receiving electron-density. In the case of Pd^0, however, the metal is actually becoming more positive upon complexation, implying a marked depletion of electron-density. Carbon atoms of the olefin ligands seem to consistently become more negative for all the four metals, along the order $[Pd(C_2H_4)_3] > [Cu(C_2H_4)_3]^+ \sim [Au(C_2H_4)_3]^+ > [Ag(C_2H_4)_3]^+$ (Tab. 2.6). Interestingly olefinic hydrogens lose electron charge upon complexation in the order $[Au(C_2H_4)_3]^+ > [Cu(C_2H_4)_3]^+ \sim [Au(C_2H_4)_3]^+ > [Pd(C_2H_4)_3]$. The strong delocalization BD(1) C-H → LP* (6) M (metal orbital with mainly s character) seems to account for this loss of charge in the protons. For $[Cu(C_2H_4)_3]^+$, this delocalization is energetically so strong to rival LP (4 or 5) M → BD* (2) C-C (ex. π-back-bonding). π^* populations of the ethylene accurately reproduce the trend seen in NMR studies (especially ^{13}C NMR), assigning to $[Pd(C_2H_4)_3]$ the highest population (0.30 e^-), followed by $[Au(C_2H_4)_3]^+$ (0.19 e^-), $[Cu(C_2H_4)_3]^+$ (0.13 e^-), and $[Ag(C_2H_4)_3]^+$ (0.09 e^-). Gold seems to be the metal that best polarizes the π system of the ethylene, depleting 0.25 e^- from 2.00 e^- in the non- coordinated olefin (probably because of its high Lewis acidity). It can be seen from Tab. 2.4 that an interaction like π-back-bonding is almost as important as σ-bonding for $[Pd(C_2H_4)_3]$ (σ/π = 2.2), while for coinage metals the σ-bonding component energetically surpasses the π-back-bonding. Paradoxically, the π-back-bonding component is more important in stabilizing the $[Ag(C_2H_4)_3]^+$ (σ/π = 6.9) than the $[Cu(C_2H_4)_3]^+$ (σ/π = 8.8) and $[Au(C_2H_4)_3]^+$ structure (σ/π = 7.3).

Table 2.5. NBO charges in $[Cu(C_2H_4)_3]^+$, $[Ag(C_2H_4)_3]^+$, $[Au(C_2H_4)_3]^+$ and $[Pd(C_2H_4)_3]$ (per ethylene unit; the numbers in red represent the charges of the non-complexed metal atom)

Compound	Metal charge	Carbon (sp^2)	Hydrogen
C_2H_4	-	- 0.37	+ 0.19
$Pd(C_2H_4)_3$	+ 0.38 **(0.00)**	- 0.48	+ 0.21
$Cu(C_2H_4)_3^+$	+ 0.88 **(1.00)**	- 0.45	+ 0.23
$Ag(C_2H_4)_3^+$	+ 0.83 **(1.00)**	- 0.43	+ 0.23
$Au(C_2H_4)_3^+$	+ 0.84 **(1.00)**	- 0.45	+ 0.24

Table 2.6. NBO populations in $[Cu(C_2H_4)_3]^+$, $[Ag(C_2H_4)_3]^+$, $[Au(C_2H_4)_3]^+$ and $[Pd(C_2H_4)_3]$ (per ethylene unit)

Compound	Metal LP* (6)	Olefin π	Metal LP (4), (5)	Olefin π^*
C_2H_4	-	2.00	-	0.00
$Pd(C_2H_4)_3$	0.32	1.81	2 x 1.66	0.30
$Cu(C_2H_4)_3^+$	0.35	1.83	2 x 1.88	0.13
$Ag(C_2H_4)_3^+$	0.35	1.85	2 x 1.90	0.09
$Au(C_2H_4)_3^+$	0.55	1.75	2 x 1.80	0.19

The most direct and effective proof of the lack of direct M-C covalent interaction as in the metallacyclopropane resonance structure— thus supporting the NBO findings—comes from the

^{13}C NMR spectra of the pairs $[Ag(C_2H_4)_3][SbF_6]$/$[Ag(C_7H_{10})_3][SbF_6]$ and $Pt(C_2H_4)_3$/$Pt(C_7H_{10})_3$. Both nuclei are magnetically active with isotopes having S=1/2 (ex. ^{107}Ag/^{109}Ag, ^{195}Pt), but coupling constants between metal and carbon atoms of the olefins, $^1J_{(M-C)}$, are only seen for platinum compounds (δ 48.4 ppm, $^1J_{(Pt-C)}$ = 113 Hz in the case of $Pt(C_2H_4)_3$, and δ 68 ppm, $^1J_{(Pt-C)}$ = 189 Hz in the case of $Pt(C_7H_{10})_3$). Silver complexes show sharp singlets instead.

In conclusion, I hereby report the synthesis and the complete characterization of six rare tri-olefin adducts of copper, silver, and gold.[103, 110, 117] They are related to $[M(C_2H_4)_3]$ and $[M(C_7H_{10})_3]$ (M = Ni, Pd, Pt). Even though coinage adducts show a lower degree of M→L π-back-bonding than the related adduct in group 10, they are more stable than their congeners and survive easily at room temperature when protected from light and moisture. A combination of vibrational analysis, NMR spectroscopy, X-ray diffraction, and computational data/NBO analysis confirm that the three olefins are held together around the metal and no direct M-C covalent bond is present as it would be if these compounds followed the metallacyclopropane structure. C=C bond seems to be more weakened in norbornene than in ethylene adducts, though the former shows less M→L π-back-bonding (^{13}C NMR shift). None of the ethylene compounds reach the metallacyclopropane ideal structure, but the gold compounds approach it. The C···C intermolecular contact is particularly interesting, and it is a phenomenon that should be further investigated for potential catalytic applications[116, 118].

CHAPTER 3

CARBONYL COMPLEXES SUPPORTED BY OLEFINS

I extensively spoke in chapter 2 of the wheel motif as a recurrent one in coinage metal chemistry when an excess of olefin is present in solution. I decided to extend the investigation to cyclic tri-olefins containing a potentially "wheel-like" environment for the metal. Cyclic tri-olefins such as *trans,trans,trans*-1,5,9-cyclododecatriene (*ttt*-cdt), *cis,trans,trans*-1,5,9-cyclododecatriene (*ttt*-cdt) or *cis,cis,cis*-1,5,9-cyclododecatriene (*ccc*-cdt) are commercially available. They are normally obtained for cyclotrimerization of butadiene on a nickel catalyst. There are studies in the literature that report the synthesis and characterization of several copper compounds with these olefins (ex. [Cu(*ttt*-cdt)][OSO_2CF_3]). Based on thermodynamic NMR studies at low temperature, Bellott and Girolami suggest that tetrahedral environments are greatly favoured either by ctt-cdt or ttt-cdt, whereas it was demonstrated by GGA DFT studies that trigonal planar environments tend to favor ttt-cdt coordination[119]. The HOMO of this ligand is all localized in the middle of the ring and it is not hard to see that it is mostly the result of an in-phase combination of three π systems of the olefins (Fig. 3.1). It seems logical to assume that this situation is particularly suitable to bind relatively small metal ions having an empty atomic orbital of spherical symmetry (4s for Cu^{I} or 6s for Au^{I} for example) ready to accept electron density.

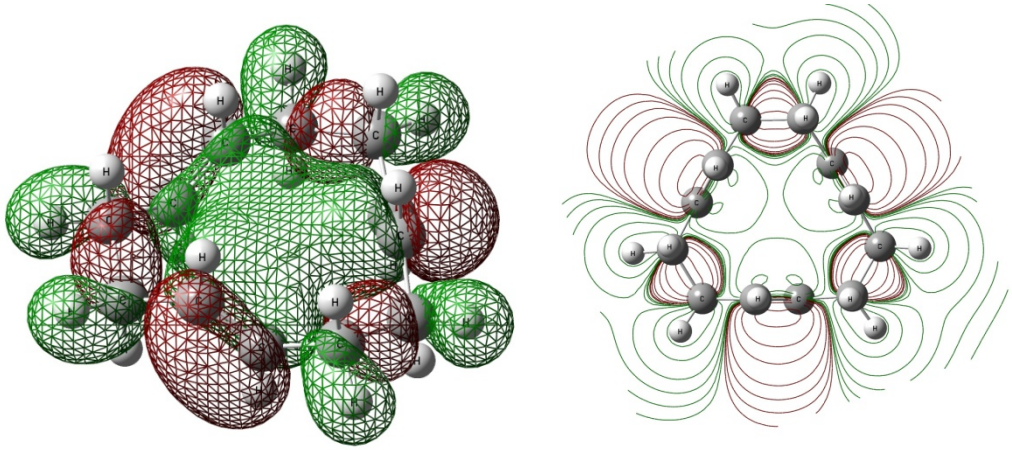

Figure 3.1. KS HOMO of ttt-cdt (0.00331 hartrees), left, and relative contour in xy plane, right

Trans,trans,trans-1,5,9-cyclododecatriene (*ttt*-cdt) reacts promptly with $AgSbF_6$ in dichloromethane. The reaction is immediate and leads to the formation of an insoluble white product. This solid seems to be quite stable in the air, it does not re-dissolve in dichloromethane, but it becomes soluble in acetone. Although a X-ray diffraction was not obtained due to the challenge of obtaining a suitable crystal (the minimal solubility of the compound in non-coordinating solvents is a major problem), a clear assignment of the structure is impossible, the elemental analysis shows a stoichiometric ratio Ag:ligand of 1:1. It is logical to assume a polymeric structure for this compound since similar compounds have already been reported in the literature. This silver compound reacts overnight at room temperature in dichloromethane with CuCl to form a clear solution and a white precipitate of AgCl (Figure 3.2). The product, formed in excellent yield, is [Cu(*ttt*-cdt)][$FSbF_5$]. [Cu(*ttt*-cdt)][$FSbF_5$] shows very remarkable air and thermodynamic stability. As a powder, it can be kept for days without showing signs of decomposition. Its solutions in THF or acetone slowly become green-blue over several hours, probably due to the decomposition of the compound and the concomitant

formation of Cu^{II} ions favoured by non-anhydrous conditions. In comparison, [Ni(*ttt*-cdt)], the isoelectronic relative in group 10, shows high instability and must be synthesized and kept at low temperature to avoid decomposition. [Ni(*ttt*-cdt)] reactivity in solution has gained it the name of "naked nickel" and made it a valuable synthetic intermediate in Ni^0 chemistry.

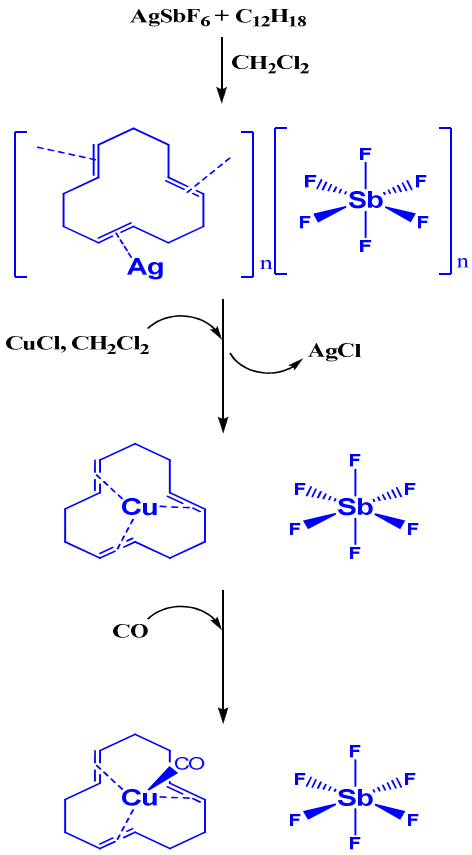

Figure 3.2. General synthetic scheme for $[Cu(ttt\text{-}cdt)]^+$ and $[Cu(ttt\text{-}cdt)(CO)]^+$

The X-ray structure of [Cu(*ttt*-cdt)][$FSbF_5$] shows that Cu^I sits slightly above the cradle created by the 12-membered *ttt*-cdt ring (the copper atom lies 0.272 Å above the plane defined by the three olefin centroids). Copper coordinated to the three olefins essentially forms a trigonal planar (sum of Cu-olefin(midpoint) angles = 354.7°) arrangement that is slightly distorted by a Cu••••F contact at 2.794 Å (cf. sum of vdW radii of Cu and F = 2.87 Å). Geometry

optimization of the model [Cu(*ttt*-cdt)]$^+$ obtained by our DFT calculations (first imposing C_1 and then C_3 symmetry) shows that the copper atom lies right in the middle of the cradle, and the overall point group could be further reduced to D_3 within < 0.01 Å threshold (in other words, adding 3 C_2 axes about the Cu-Centroid$_{(C=C)}$). The small distortion seen in the solid state might be attributed to the presence of the SbF_6^- ion. A most remarkable thing to notice is that the olefin groups form a C_3 propeller type arrangement and, given a restricted C_2 inversion of the C=C bond, the complexed ligand should create a chiral environment. We noticed that the presence of a 50:50 racemate in the crystal resulted in disorder of the *ttt*-cdt moiety (Fig. 3.3). The average Cu-C distance of 2.130(4) Å (range 2.110(4)-2.149(4) Å) is only not slightly different from those observed for $[Cu(C_2H_4)_3]^+$ (av. 2.174 Å) (Fig. 3.4). The X-ray structure of the all *cis*-cdt analog [Cu(*ccc*-cdt)][Al{OC$(CF_3)_3$}$_4$] has been reported, which exhibits a flattened trigonal copper center. The copper atom lies in a more pyramidal environment with respect to [Cu(*ttt*-cdt)][SbF_6], 0.47 Å above the plane defined by the three olefin centroids, and has longer Cu-C bonds (average 2.192(4) Å, range 2.174(4)-2.218(4) Å).

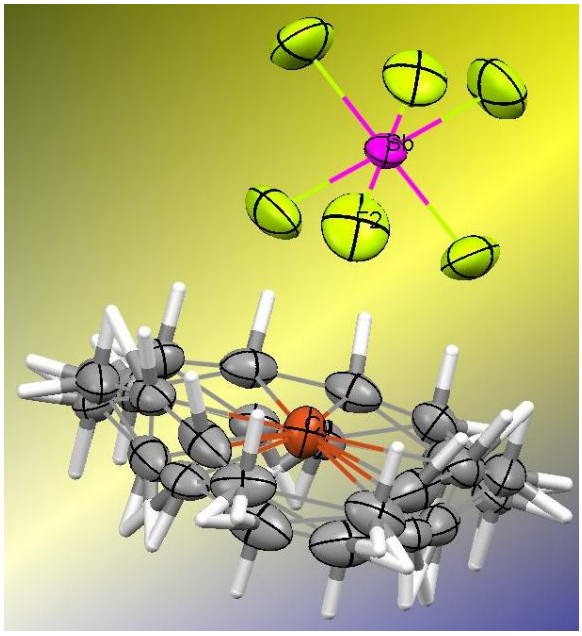

Figure 3.3. ORTEP structure of [Cu(*ttt*-cdt)($FSbF_5$)], shown here with its C_3 disorder

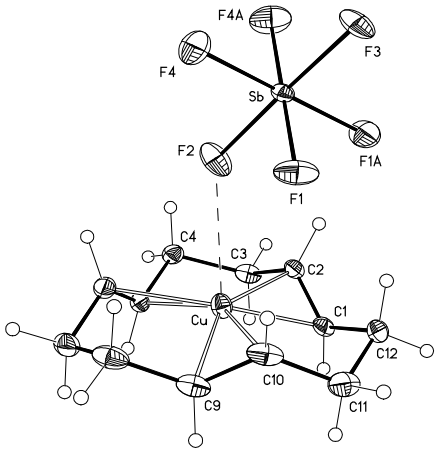

Figure 3.4. Molecular structure of [Cu(*ttt*-cdt)][$FSbF_5$] (thermal ellipsoids at 35% probability, only one of the disordered components of the *ttt*-cdt is shown). Selected bond distances (Å) and angles (º): Cu-C(1) 2.110(4) , Cu-C(2) 2.133(4), Cu-C(5) 2.117(3), Cu-C(6) 2.149(4), Cu-C(9) 2.128(4), Cu-C(10) 2.141(4), C(1)-C(2) 1.355(6), C(5)-C(6) 1.354(5), C(9)-C(10) 1.353(7), Sb-F(4A) 1.8633(14), Sb-F(4) 1.8633(14), Sb-F(3) 1.8640(17), Sb-F(1) 1.8640(13), Sb-F(1A) 1.8640(13), Sb-F(2) 1.8789(18), C(1)-Cu-C(2) 37.25(16), C(9)-Cu-C(10) 36.96(18), C(5)-Cu-C(6) 37.00(14)

The ^{1}H NMR spectrum of [Cu(*ttt*-cdt)][$FSbF_5$] in CD_2Cl_2 at room temperature displays three signals at δ 2.42, 2.60 (aliphatic protons), and 5.87 (olefinic protons). The aliphatic protons appear more as non resolved multiplets than as resolved singlets. NMR calculated with GIAO in gas phase shows three discreet groups of signals at δ 2.6, 2.9, and 6.0, assigned to aliphatic axial, aliphatic equatorial, and olefinic protons, respectively. Corresponding signals of the free ligand *ttt*-cdt appear as two singlets and at upfield positions, δ 2.03 (calculated 2.1) and 5.00 (calculated 5.4), respectively. Anet pointed out that spin-spin coupling should show a complex fine structure that would be very difficult to resolve.[119] The presence of two sets of aliphatic protons is a sign of blocked inversion of aliphatic chains in solution. Dale and Greig pointed out that the exchange of methylene proton positions can only happen after a full ring inversion: they noticed that a full inversion of the ring can only happen if a 180° degrees flip of the three double bonds is followed by a change in sign of the torsional angles of the three CH_2-CH_2 bonds. The inversion is fast on the NMR time-scale at room temperature, and this results in a single peak for the methylene protons. The system reaches coalescence at – 92 ℃, and there is clear splitting into two peaks at -138 ℃. Dale and Greig experimentally found the value of $\Delta G^{\ddagger}$= 9 kcal/mol for this inversion. Anet and Rawdah provided the value of 8.6 ± 0.2 kcal/mol at – 92 ℃ and calculated a value of 9.5 kcal/mol using force-field calculations.[119] As stated before, [Cu(*ttt*-cdt)($FSbF_5$)] shows two signal in the aliphatic region. Most interestingly, ^{1}H NMR spectrum of the analogue [Cu(*ttt*-cdt)][OSO_2CF_3] at room temperature more closely resembles the free ttt-cdt than [Cu(*ttt*-cdt)][$FSbF_5$]. Bellott and Girolami's hypothesis is that the two faces of the olefin become equivalent in solution and the ring flip is made possible by a shift of the triflate anion along the ring and a consequent slippage of the copper ion through the cavity. Assuming that this mechanism is correct, I have to conclude that (1) ring inversion in solution (CH_2Cl_2) at room temperature is frozen for our compound, (2) [Cu(*ttt*-cdt)]$^+$ maintains a local D_3 symmetry even in solution since SbF_6^- is not nucleophilic enough to "fish out" the copper ion from the cradle and promote "slippage-inversion", and (3) since chirality depends upon the relative orientation of the

three double bonds (propeller structure) and the blocked inversion of the ring cannot interconvert the enantiomers into each other, the possibility of isolating an enantiomerically pure product should be far from remote (at least in non-coordinating solvents). [Cu(*ttt*-cdt)][$FSbF_5$] and *ttt*-cdt show no sign of ligand exchange on the NMR time scale at room temperature. The olefinic ^{13}C NMR signal of [Cu(*ttt*-cdt)($FSbF_5$)] indicates an essentially negligible change in shift in comparison to the free ligand: 132.0 ppm (140.5 ppm, calculated average) in the free *ttt*-cdt vs. 131.1 ppm (141.2 ppm, calculated average) in the adduct, or $\Delta\delta(^{13}C) = (\delta(^{13}C)_{complex}-\delta(^{13}C)_{free\ ligand}) = -0.9$ ppm (+ 0.7 ppm, calculated value). Small up-field shifts have been correlated with lack of π-back-donation. [Cu(C_2H_4)$_3$][SbF_6], for instance, shows $\Delta\delta(^{13}C) = -13.8$ ppm, while [Cu(*ccc*-cdt)(FBF_3)] shows $\Delta\delta(^{13}C) = -6.1$ ppm. I strongly suggest that the out of plane twist of the C=C bonds in *ttt*-cdt greatly disfavors the interaction between metal-ligand *E* pairs, orbital combinations that are the ones involved in M→L π-back-bonding. Although Ni^0 is a metal atom capable of good back-donation, Ni(C_2H_4)$_3$ and Ni(*ttt*-cdt) also display the same trend; Ni(*ttt*-cdt) shows a significantly reduced level of π-back-bonding as evident from the ^{13}C NMR spectroscopy $\Delta\delta(^{13}C) = -65.5$ ppm ($\Delta\delta(^{13}C) = -25.0$ for Ni(C_2H_4)$_3$).

ESI-MS experiments on [Cu(*ttt*-cdt)($FSbF_5$)] carried out in CH_2Cl_2 by direct infusion at 100 ℃ showed the presence of mainly 4 species in s olution (both positive and negative modes, all the isotopic distribution accounted): [Cu(*ttt*-cdt)]$^+$ (MP: 225.3, 227.3), SbF_6^- (235.1, 237.1), and two "aggregates" {[Cu(*ttt*-cdt)]$_2$[$FSbF_5$]}$^+$ (MP: 685.1, 686.8, 688.6, 689.6) and [Cu(*ttt*-cdt)($FSbF_5$)$_2$]$^-$ (MP: 694.9, 696.6, 698.4, 700.4). Gas phase collision activated dissociation (CAD) experiments provide the enthalpy of dissociation for {[Cu(*ttt*-cdt)]$_2$[$FSbF_5$]}$^+$ → {[Cu(*ttt*-cdt)][$FSbF_5$]} + [Cu(*ttt*-cdt)]$^+$, CAD V = 0.650 ± 0.005 V, and {[Cu(*ttt*-cdt)][$FSbF_5$]$_2$}$^-$ → {[Cu(*ttt*-cdt)][$FSbF_5$]} + [SbF_6]$^-$, CAD V = 0.500 ± 0.005 V. The use of this technique on [Cu(ttt-cdt)]SbF_6 as substrate could be of fundamental importance in deriving experimental values for the binding enthalpy of small molecules, such as N_2, O_2, CO_2, or N_2O to copper.

The peculiar reactivity shown by this molecule in coordinating one triflate, hexafluoroantimonate or even two SbF_6^- (and, as we will see in the following paragraph, even carbon monoxide) could be explained considering the frontier orbitals, especially HOMO and LUMO. The first fifteen open-shell singlet excited states have been calculated using Time-Dependent DFT (TD) for $[Cu(ttt\text{-}cdt)]^+$ on the geometry calculated at B3PW91 (Tab. 3.1). SbF_6^- absorptions with non-zero oscillator strength fall below 190 nm. UV-Vis spectrum of a solution ~ 0.27 μmol of [Cu(ttt-cdt)][SbF_6] in CH_2Cl_2 was obtained and compared to the calculated results (Fig. 3.5 and 3.6). TD DFT is generally quite fast and reliable, and it produces estimations of the excited states energies (included HOMO-LUMO gap) with a good degree of accuracy (considering the common problem in correlation energy evaluation for the first excited state that afflicts all TD DFT methods). The hybrid functional performs poorly in comparison to the gradient-corrected BLYP, which is well-known to provide results in good agreement with experiments (Tab. 3.1).

Table 3.1. TD DFT calculations showing the HOMO-LUMO gap and the principal absorption

Theory	Excited state and symmetry	Energy	Oscillator strenght
TD B3PW91	- Singlet (E), HOMO-LUMO transition	277 nm	f = 0.0001
	- Singlet (A), Principal transition	214 nm	f = 0.1209
TD BLYP	- Singlet (E), HOMO-LUMO transition	317 nm	f = 0.0005
	- Singlet (A), Principal transition	240 nm	f = 0.0766

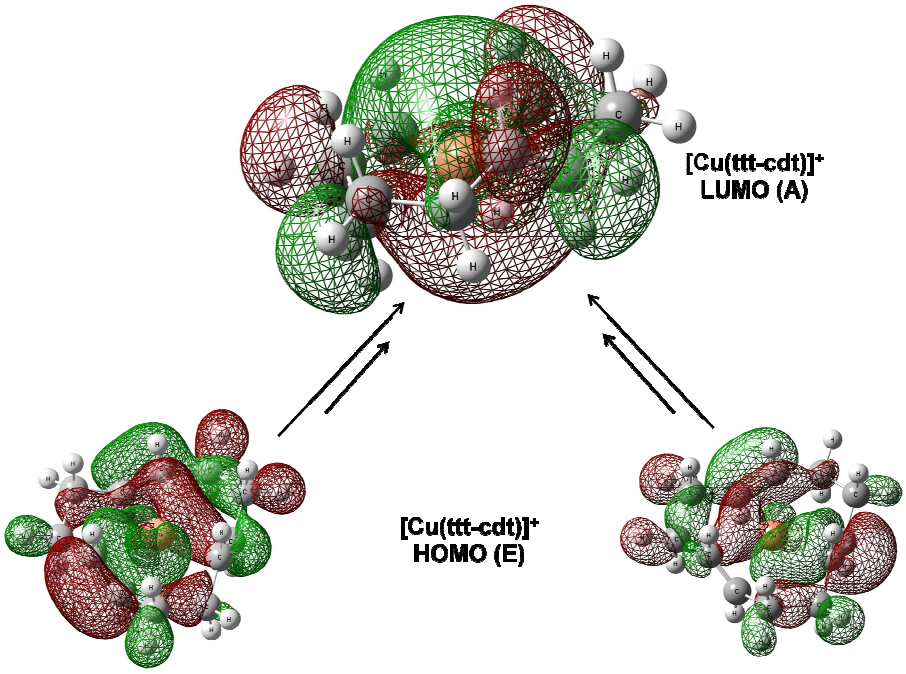

Figure 3.5. KS HOMO-LUMO combination for $[Cu(ttt\text{-}cdt)]^+$

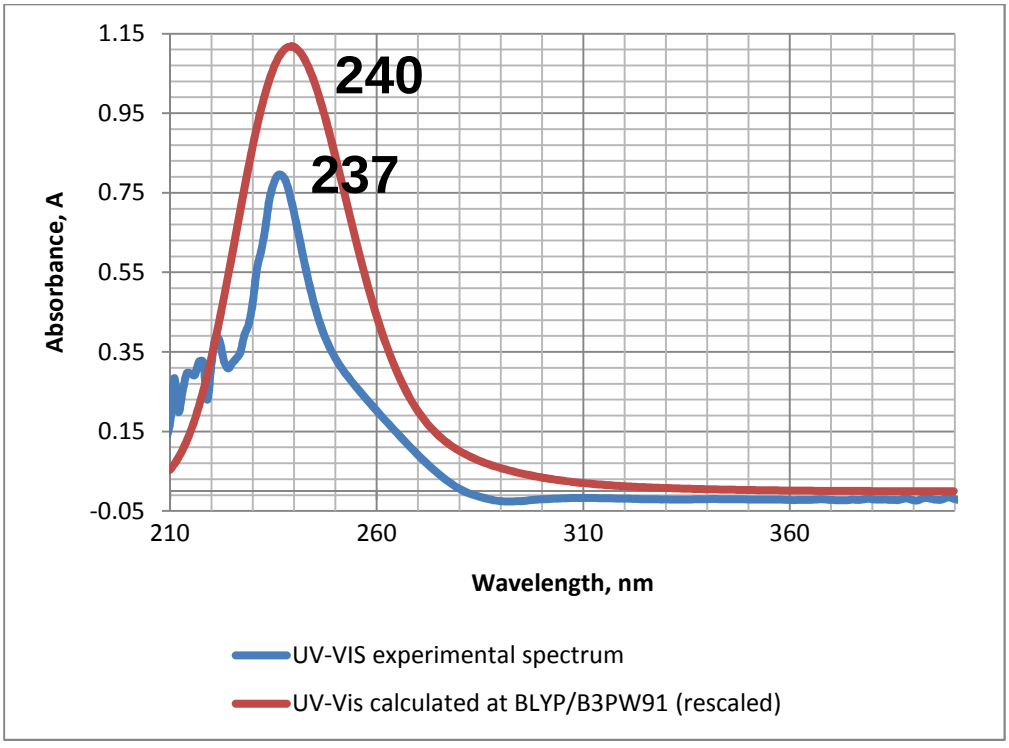

Figure 3.6. UV-Vis spectra for $[Cu(ttt\text{-}cdt)][SbF_6]$ (calculated, in red, and experimental, in blue)

The HOMO of $[Cu(ttt\text{-}cdt)]^+$ is doubly degenerate (E) and closely resembles the HOMO of species such as $[Cu(C_2H_4)_3]^+$ and $[Cu(C_7H_{10})_3]^+$. The LUMO is *A* symmetrical and sits mainly on the inter-nuclear space with two big lobes pointing outside the cradle in opposite directions. It is worthy to point out that the LUMO orbital represents areas of the molecule ready to accept electron density. Although this orbital closely resembles the KS LUMO for the free ligand (the copper atom occupies the nodal interstice at the middle point of the ligand, Fig. 3.7), population analysis identifies some contribution of p_z-type orbital of the copper ion to the molecular orbital (the main contribution is coming from s orbitals of the carbon atoms).

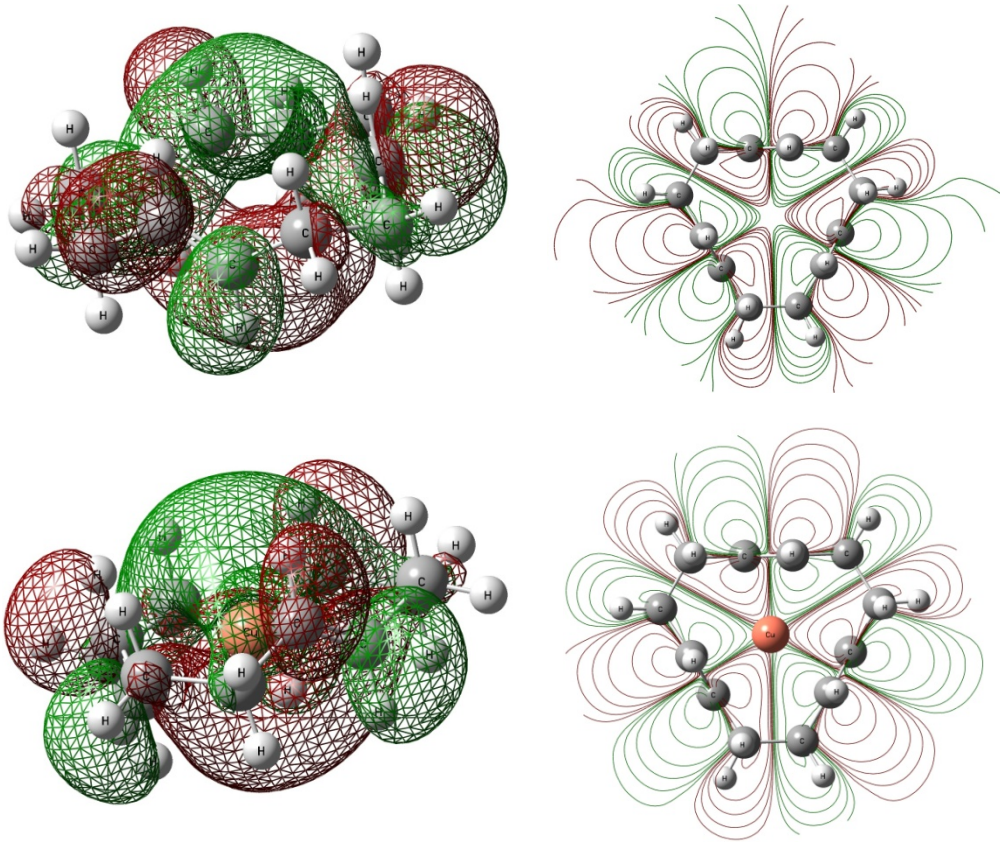

Figure 3.7. KS LUMO for ttt-cdt free ligand (- 0.15961 hartrees), upper left and relative contour in xy plane, upper right. KS LUMO for $[Cu(ttt\text{-}cdt)]^+$ (- 0.20457 hartrees), lower left and relative contour in the xy plane, lower right

Treatment of [Cu(*ttt*-cdt)($FSbF_5$)] with CO (1 atm) led to the carbonyl adduct [Cu(*ttt*-cdt)(CO)][SbF_6] in quantitative yield. Solid samples of this adduct can be handled in air without noticeable decomposition. Freshly prepared solid samples can be dried under reduced pressure for one hour without significant decomposition on Raman and IR base. However, solid samples show massive effervescence upon re-dissolution in dichloromethane. Solutions of [Cu(*ttt*-cdt)(CO)][SbF_6] lose CO upon concentration as well. A sample of carbonyl compound stored at room temperature in a dry-box still retains part of the coordinated carbon monoxide after 30 days. In comparison, [Cu(*ttt*-cdt)][OSO_2CF_3] treated with CO does not show any CO intake. I do believe the triflate ligand binds the copper atom stronger than SbF_6^-, and it is not displaced by carbon monoxide. The difference in coordination between $SO_3CF_3^-$ and SbF_6^- towards Cu^I has also been noted for ethylene chemistry in chapter 2. [Cu(*ttt*-cdt)(CO)][SbF_6] displays a strong absorption band in the IR and Raman at 2160 cm^{-1} that can be assigned to the CO stretch. DFT calculations estimate the ν(CO) at 2155 cm^{-1}, in excellent agreement with the experimental results. This value falls within the non classical region for copper carbonyls considering that the ν(CO) band of free CO appears at 2143 cm^{-1} and the upper limit is represented by the matrix-isolated $[Cu(CO)]^+$ with 2234 cm^{-1} (the value calculated by our DFT is 2260 cm^{-1}). [Cu(*ttt*-cdt)(CO)][SbF_6] shows the highest value that has been reported for a structurally characterized copper(I) mono-carbonyl species ((CO)$CuAlCl_4$ and (CO)$CuGaCl_4$ are the next highest at ν_{CO} = 2156 cm^{-1}). ^{13}C NMR resonance for the quaternary carbon could not be located reliably (probably due to quadrupolar relaxation since the two most abundant isotopes, ^{65}Cu and ^{63}Cu, have a nuclear spin of 3/2), but the GIAO estimation puts it at 185.3 ppm, which is in good agreement with the non-classical nature of [Cu(*ttt*-cdt)(CO)][SbF_6]. While many non-classical carbonyls seen in chapter 2 have been stabilized using heavy fluorinated non-coordinating ligands, in this case we created a non-classical species using a simple electron-rich tri-olefin with high torsional strain. The *trans,trans,trans*-1,5,9-cyclododecatriene is an interesting ligand

since it can support both non-classical and also classical carbonyl adducts. As a matter of fact, the isoelectronic Ni(*ttt*-cdt)(CO) is also known, and it displays a ν(CO) band at 1935 cm^{-1} (matrix isolated Ni-CO shows ν(CO) at 1996 cm^{-1}). Vibrational analysis for [Cu(*ttt*-cdt)($FSbF_5$)] and [Cu(*ttt*-cdt)(CO)][SbF_6] is generally in line with the species seen in chapter 2. There is no clear resolution between A and E vibrational modes for C=C group vibrations. The Raman spectra of free *ttt*-cdt, [Cu(*ttt*-cdt)($FSbF_5$)], and [Cu(*ttt*-cdt)(CO)][SbF_6] show single bands for ν(C=C) at 1671, 1581 and 1601 cm^{-1}, respectively. DFT calculations perfectly reproduce this trend with 1695, 1578 (average, $\Delta_{A\text{-}E}$ ~ 2 cm^{-1}) and 1604 cm^{-1} (average, $\Delta_{A\text{-}E}$ ~ 1 cm^{-1}). The coordination of the olefin to the copper ion detectably weakens the double bond as witnessed in the difference in stretching frequencies, $\Delta\nu$ = - 90 cm^{-1} (an upper limit of - 117 cm^{-1} is calculated by DFT). The small increase of ν(C=C) frequency upon CO coordination, $\Delta\nu$ = 20 cm^{-1} (26 cm^{-1} calculated), points to a weaker contact between the olefin moieties and the copper ion. This is a result of greater pyramidalization at Cu due to CO coordination. Wyberg bond orders substantially agree with the trend in the frequencies, being 1.92, 1.76, and 1.79 the B.O.s for free *ttt*-cdt, [Cu(*ttt*-cdt)($FSbF_5$)] and [Cu(*ttt*-cdt)(CO)][SbF_6] respectively. The solution ^{1}H and ^{13}C NMR data, however, do not show significant changes between [Cu(*ttt*-cdt)($FSbF_5$)] and [Cu(*ttt*-cdt)(CO)][SbF_6].

The X-ray crystal structure of [Cu(*ttt*-cdt)(CO)][SbF_6] is illustrated in Figure 3.8. It consists of discreet $[Cu(ttt\text{-cdt})(CO)]^{+}$ cations and $[SbF_6]^{-}$ anions. The *ttt*-cdt moiety shows similar disorder as observed for [Cu(*ttt*-cdt)(CO)][SbF_6]. The Cu-CO moiety sits on a three-fold rotation axis. The copper center adopts a pseudo tetrahedral geometry (with displacement of Cu from the olefin plane by about 0.836 Å). The Cu-C(olefin) bonds also show a significant lengthening (av. 2.130 Å in [Cu(*ttt*-cdt)($FSbF_5$)] vs. average 2.256 Å in [Cu(*ttt*-cdt)(CO)][SbF_6]). The Cu-CO distance of 1.942(4) Å is the longest observed in a copper mono-carbonyl adduct to our knowledge. My calculations predict a slightly shorter Cu-CO distance of 1.893 Å. For

comparison, the tetrahedral mono-carbonyl adduct $[HB(3,5\text{-}(CF_3)_2Pz)_3]CuCO$ with a fairly high ν(CO) (2137 cm^{-1}) has a Cu-C (CO) distance of 1.808(4) Å. The tetra-carbonyl adduct $[Cu(CO)_4][1\text{-}Et\text{-}CB_{11}F_{11}]$ shows marginally longer Cu-CO bonds (1.961(3)-1.968(3) Å).

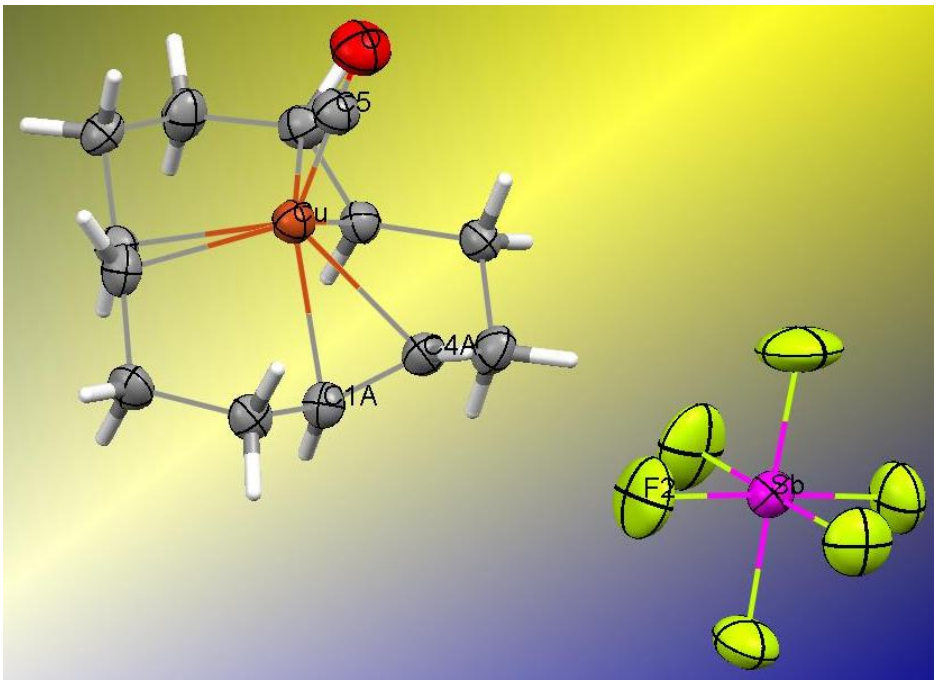

Figure 3.8. ORTEP structure of $[Cu(ttt\text{-}cdt)(CO)][SbF_6]$. Selected bond distances (Å) and angles (º): Cu-C(5) 1.942(4), O-C(5) 1.126(5), Cu-C(1A) 2.267(5), Cu-C(4AB) 2.266(4), C(1A)-C(4AB) 1.361(7); O-C(5)-Cu 180.0(5), C(4A)-Cu-C(1A) 34.96(18)

NBO analysis shows the presence of a polarized covalent bond Cu-CO in $[Cu(CO)]^+$: the orbital is 90% localized on the carbon atom (60% s and 40% p character) and 10% on the copper atom (96% s with minor contributions from p and d). $[Cu(t,t,t\text{-}cdt)(CO)]^+$ shows this orbital as well, implying a Cu-CO covalent interaction. This orbital has predominantly (90%) ligand character localized on the carbon atom (67% s and 33% p character) and 10% on the copper atom (98% s character with minor contributions from p and d). Both $[Cu(t,t,t\text{-}cdt)]^+$ and $[Cu(t,t,t\text{-}cdt)(CO)]^+$ do not show any localized orbitals for Cu···C(olefin) interactions. In this case, the electrostatic nature of the interaction cannot be totally excluded. The NBO charges on

copper of both $[Cu(t,t,t\text{-cdt})]^+$ and $[Cu(t,t,t\text{-cdt})(CO)]^+$ are very close to + 1.00 (charge for the free metal ion), respectively + 0.88 and + 0.82 e^-. The coordination of carbon monoxide alone seems to be responsible for the metal charge lowering by – 0.06 e^- (Tab. 3.2). The second order perturbation analysis points out a strong energetic contribution BD(2) C=C → BD* M-C (and minor contributions from BD(1) C=C and BD(1) C-H). BD* M-C has mostly metal character, being 90 % delocalized over copper (major s orbital contribution). Thus, the presence of the olefin might be the reason of 0.19 e^- population on BD* M-C (for a comparison, $[Cu\text{-}(CO)]^+$ shows essentially no population in that localized orbital) that tends to weaken the bond between metal and carbon monoxide. This behavior will be highlighted again in chapter 4, where the chemistry of tris(pyrazolyl)borates as a weakly coordinating ligand will be discussed. π^* systems of the carbon monoxide in $[Cu(t,t,t\text{-cdt})(CO)]^+$ are more populated than in $[Cu(CO)]^+$, 0.08 e^- vs 0.04 e^- respectively, implying some type of increased M→ttt-cdt π-back-donation when the olefin is also complexed (Tab. 3.3). My conclusion based on experimental and calculated data, is that $[Cu(t,t,t\text{-cdt})(CO)]^+$ should be regarded as being composed by two units, the $[Cu(CO)]^+$ fragment and the olefin supporting it. Another important fact to remark concerns the population on the olefinic π^* system in t,t,t-cdt, $[Cu(t,t,t\text{-cdt})]^+$, and $[Cu(t,t,t\text{-cdt})(CO)]^+$. As it can be seen from the table, the population increases from t,t,t-cdt to $[Cu(t,t,t\text{-cdt})]^+$ (0.05 vs 0.13 e^-) and then decreases from $[Cu(t,t,t\text{-cdt})]^+$ to $[Cu(t,t,t\text{-cdt})(CO)]^+$ (0.13 vs 0.12 e^-). The net change in π^* population between t,t,t-cdt and $[Cu(t,t,t\text{-cdt})]^+$ is 0.08 e^-, while between $[Cu(t,t,t\text{-cdt})]^+$ to $[Cu(t,t,t\text{-cdt})(CO)]^+$ it is 0.07 e^-. Both values are smaller than the value for the π^* population in $[Ag(C_2H_4)_3]^+$ (0.09 e^-). This fact accounts, at least qualitatively, for the small ^{13}C NMR shift seen in $[Cu(t,t,t\text{-cdt})]^+$, - 0.9 ppm, compared to the free ligand. In my opinion, however, the difference in π^* population between $[Cu(t,t,t\text{-cdt})]^+$ and $[Cu(t,t,t\text{-cdt})(CO)]^+$, 0.01 e^-, does not completely justify the shift (+ 26 cm^{-1}) seen in ν(C=C) frequencies between the two complexes. The

explanation might rather be a combined effect of reduced π* (- 0.01 e^-) and increased π populations (+ 0.03 e^-) (both effects work to strengthen the C=C bond).

Table 3.2. NBO charges for $[Cu(ttt\text{-}cdt]^+$ and related compounds

Compound	Metal charge	C (CO)	O (CO)	C (sp^2, av.)	H (sp^2,av.)	C (sp^3, av.)	H (sp^3,av.)
CO	-	+ 0.47	- 0.47	-	-	-	-
ttt-cdt	-	-	-	- 0.18	+ 0.18	- 0.41	+ 0.21
$[Cu(ttt\text{-}cdt)]^+$	+ 0.88	-	-	- 0.25	+ 0.23	- 0.42	+ 0.23
$[Cu(ttt\text{-}cdt)(CO)]^+$	+ 0.82	+ 0.40	- 0.36	- 0.24	+ 0.24	- 0.43	+ 0.23
$[Cu(CO)]^+$	+ 0.91	+ 0.36	- 0.27	-	-	-	-

Table 3.3. NBO population analysis for $[Cu(ttt\text{-}cdt]^+$ and related compounds (in e^-, number in bold red represent $\pi^*_{complex}$-π^*_{ligand})

Compound	BD M-C bonding orbital	BD * M-C anti-bonding orbital	Metal LP (6)	2 x Metal LP (4) and (5)	C lone pair	2 x π* (CO)	Olefin π	Olefin π*
CO	-	-	-	-	2.00	2 x 0.00	-	-
ttt,-cdt	-	-	-	-	-	-	1.96	0.05
$[Cu(ttt\text{-}cdt)]^+$	-	-	0.32	2 x 1.89	-	-	1.86	0.13 **(0.08)**
$[Cu(ttt\text{-}cdt)(CO)]^+$	1.97	0.19	-	2 x 1.93	-	2 x 0.08	1.89	0.12 **(0.07)**
$[Cu(CO)]^+$	1.99	0.00	-	2 x 1.96	-	2 x 0.04	-	-

The Ag^I cation is slightly bigger than the cavity created by ttt-cdt, and it tends to escape to form a pseudo-tetrahedral arrangement, as demonstrated by the gas phase structure calculated by DFT (Fig. 3.9). This phenomenon is probably at the base of the instability of

$[Ag(t,t,t\text{-cdt})]^+$ and the consequent formation of polymeric $[Ag(t,t,t\text{-cdt})]_n^+$. Conversely, Au^I should be more willing to fit in the cradle (Fig. 3.9). B3PW91/aug-cc-pVTZ-PP/6-311++G(d,p) predicts a structure that approaches D_3 symmetry with average Au-C bond distances of 2.204 Å and C=C bond distances of 1.398 Å.

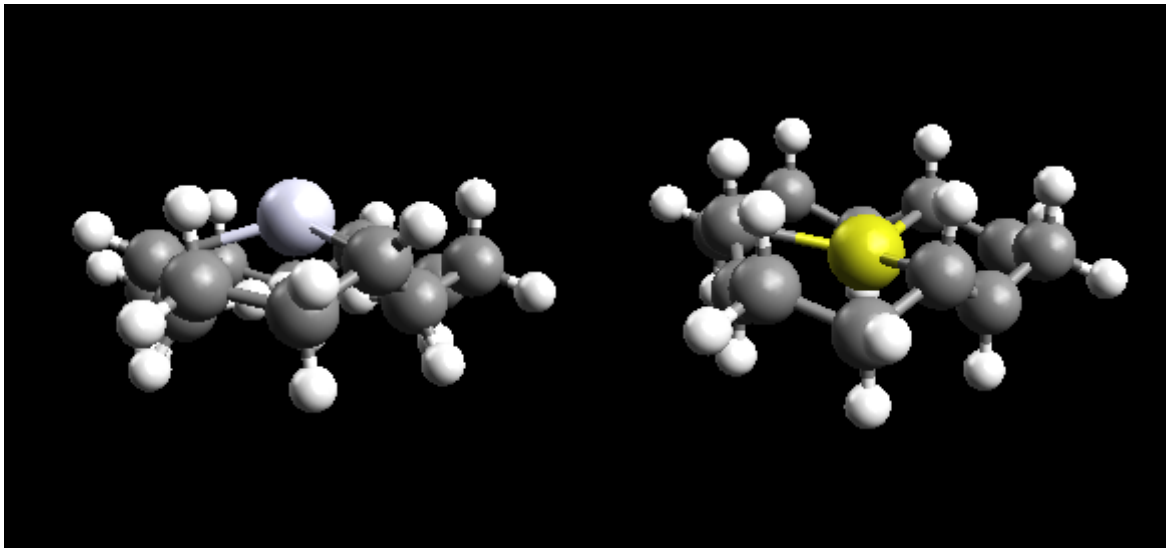

Figure 3.9. Calculated structures: $[Ag(ttt\text{-cdt})]^+$, left, and $[Au(ttt\text{-cdt})]^+$, right

Table 3.4 summarizes the thermochemical analyses calculated at 298.15 K and 1 atm for interaction between Cu^+, Ag^+, and Au^+ and ethylene versus ttt-cdt. It can be easily noticed that only in the case of copper is the interaction with the tridentate olefin more favorable than the interaction with three ethylene molecules. D_0 for the complexation of the tridentate olefin does not follow a monotonous trend along the group and has a minimum in the reaction with silver (ex. D_0 (Cu) – 109.7 kcal/mol > D_0 (Ag) – 64.9 kcal/mol > D_0 (Au) – 64.9 kcal/mol). This is not totally unexpected and a good explanation could be found in the size of the covalent radii of the metals (ex. $Cu^+ < Ag^+ > Au^+$, with Cu^+ being the smallest) compared to the somewhat rigid

cavity created by the ligand. Conversely, ethylene seems to bind stronger than ttt-cdt to Ag^+ and Au^+.

Table 3.4. Calculated D_0 for $[M(L)_n]^+$ (M = Cu, Ag, Au and L = ttt-cdt, C_2H_4)

M^+ + Olefin → $[M(Olefin)]^+$ (gas phase) B3PW91/B3PW91	D_0 (kcal/mol)
$Cu^+ + 3\ C_2H_4 \rightarrow [Cu(C_2H_4)_3]^+$	-105.5
Cu^+ + (t,t,t-cdt) → $[Cu(t,t,t\text{-cdt})]^+$	-109.7
$Ag^+ + 3\ C_2H_4 \rightarrow [Ag(C_2H_4)_3]^+$	-80.5
Ag^+ + (t,t,t-cdt) → $[Ag(t,t,t\text{-cdt})]^+$	-64.9
$Au^+ + 3\ C_2H_4 \rightarrow [Au(C_2H_4)_3]^+$	-124.3
Au^+ + (t,t,t-cdt) → $[Au(t,t,t\text{-cdt})]^+$	-100.0

Thermochemical analysis also grants interesting insight into on the complexation of carbon monoxide with these tri-olefin coinage templates (Tab. 3.4). D_0 follows a different trend with respect to the reaction $M^+ + CO \rightarrow [M\text{-}(CO)]^+$ (M= Cu, Ag, Au): in the former reaction D_0 decreases from copper to silver and increases back from silver to gold ($Ag^+ < Cu^+ < Au^+$). Experimental data are available for the previous reaction showing that D_0 (Ag^+) - 21.4 < D_0 (Cu^+) - 35.6. The trend for ttt-cdt complexed ions is D_0 (Cu^+) < D_0 (Ag^+) < D_0 (Au^+) instead.

DFT estimates negative enthalpies (ΔH_{comp}) for the complexation of carbon monoxide along the entire group, in increasing order Cu^+ (- 7.5 kcal/mol) > Ag^+ (- 14.9 kcal/mol) > Au^+ (- 17.4 kcal/mol) (Tab, 3.5). Interestingly, the reaction with copper is calculated to be endergonic by 1.7 kcal/mol. The transition structure for the complexation of carbon monoxide in the gas phase has been located with a negative frequency of - 63 cm^{-1} (Fig.3.10). The activation energy

for the complexation of carbon monoxide is $\Delta G^{\ddagger}$ = 6.5 kcal/mol, with activation energy for the reverse reaction (loss of carbon monoxide) being $\Delta G^{\ddagger}$ = 4.8 kcal/mol. The barriers of activation are very low, and $[Cu(ttt\text{-}cdt)]^{+}$ intakes and loses fast carbon monoxide in a reaction of equilibrium. This agrees very well with the experimental observations that [Cu(ttt-cdt)(CO)][SbF_6] can be synthesized only in excess of carbon monoxide in solution and loses the coordinated gas when re-dissolved in degassed CH_2Cl_2.

$$[Cu(ttt\text{-}cdt)]^{+} + CO \rightleftharpoons [Cu(ttt\text{-}cdt)(CO)]^{+}$$

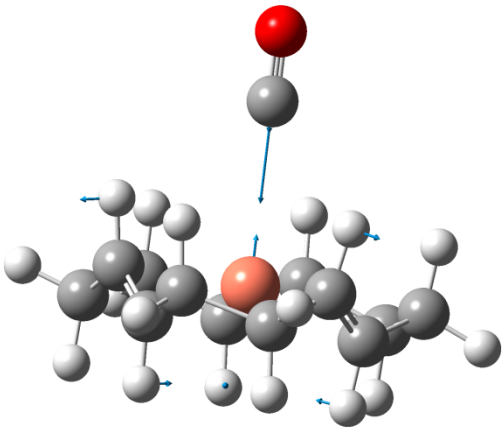

Figure 3.10. Transition state (- 63 cm^{-1}) for the complexation of carbon monoxide on $[Cu(ttt\text{-}cdt)]^{+}$ (displacement verctors are shown above, Cu···C distance = 2.969 Å)

The other two reactions are exergonic. $[Au(ttt\text{-}cdt)]^{+}$ seems to be a very good acceptor for the complexation of carbon monoxide (ΔG = - 10.2 kcal/mol).

Table 3.5. Thermodynamic parameters for complexation of carbon monoxide on $[M(ttt\text{-}cdt)]^+$ template

CO complexation (gas phase) B3PW91/B3PW91	D_0 (kcal/mol)	ΔH_{comp} (298.15 K, 1 atm, kcal/mol)	ΔG_{comp} (298.15 K, 1 atm, kcal/mol)
$[Cu(t,t,t\text{-}cdt)]^+ + CO \rightarrow [Cu(t,t,t\text{-}cdt)(CO)]^+$ $Cu^+ + CO \rightarrow [Cu(CO)]^+$	- 7.4 (- 39.8)	- 7.5	1.7
$[Ag(t,t,t\text{-}cdt)]^+ + CO \rightarrow [Ag(t,t,t\text{-}cdt)(CO)]^+$ $Ag^+ + CO \rightarrow [Ag(CO)]^+$	- 15.0 (- 25.4)	- 14.9	- 6.3
$[Au(t,t,t\text{-}cdt)]^+ + CO \rightarrow [Au(t,t,t\text{-}cdt)(CO)]^+$ $Au^+ + CO \rightarrow [Au(CO)]^+$	- 17.8 (- 50.4)	- 17.4	- 10.2

In conclusion, a Cu^I analogue of "naked" nickel has been isolated and studied. The tridentate olefin trans,trans,trans-cyclododecatriene (ttt-cdt) binds the copper ion generating a remarkably stable complex. The complex shows notably low M→L π-back-bonding and it is mostly stabilized by electrostatic interactions between the tridentate olefin and the copper ion. The LUMO orbital affects the reactivity toward weakly-coordinative anions as well as carbon monoxide. $[Cu(ttt\text{-}cdt)][SbF_6]$ treated with an excess of carbon monoxide in dichloromethane gives a non-classical carbonyl. Its ν(CO) stretching frequency is the highest ever reported for a supported copper carbonyl. NBO analysis supports the presence of Cu^I-CO localized covalent interaction. The carbonyl moiety is very labile in solution, and the compound tends to lose it when dissolved in dichloromethane non-saturated with carbon monoxide. Derivatives of the ttt-cdt with heavier atoms than copper (Ag and Au) should show interesting properties and higher affinity for CO binding.

CHAPTER 4

CARBONYL COMPLEXES SUPPORTED BY SCORPIONATES

In this chapter carbonyl and ethylene compounds of group 11 supported by ancillary ligands of the scorpionate class will be presented and described, and their principal features highlighted. A new trend for carbonyl compounds will be examined, the "classical" one. Once again, the comparison with "non-classical" carbonyls will be made on the basis of stretching frequency and metric parameters. Modeled metric parameters, spectroscopic data, and NBO charges/populations will be introduced to support the conclusions.

3.1 Tris(pyrazolyl)borate family ligands

Ligands of the tris(pyrazolyl)borate family have been well known since 1960. They were first synthesized and reported by Swiatoslaw Trofimenko[120, 121]. These ligands are based on the tetrahedral borate structure, and they are nitrogen based and formally six electron σ-donors (π-component is negligible for these ligands). They have helped to isolate many "firsts" in coordination chemistry, stabilizing several "impossible" bonds including the first Cu^{I}-CO adduct. They are also called "scorpionates" because they act on a metal center mimicking the predatory habits of the scorpion: they can bind a metal with their "clamps" (two pyrazole rings) and then sting (though not necessarily) with their "tail" (the remaining pyrazole ring). Scorpionates have been reported assuming tripodal (κ^3), chelate (κ^2, with one free pyrazole arm), unidentate (κ^1, with two free pyrazole arms), and even counter-ionic (κ^0) coordination fashion. Their fame and wide use in coordination chemistry are due to several interesting and useful characteristics

including easy syntheses, high affinity toward both early and late transition metals, easy modification of in apticity/denticity, and great steric and electronic tunability. Substituents can be changed at will at the 3rd, 4th, and 5th positions of the pyrazole rings to achieve the desired steric/electronic characteristic. All the substituents affect the electron properties of the ligand (especially those in the 5th position), but only the substituents on the 3rd position have a significant impact on the sterics of the metal center (this is particularly valuable in catalysis). Substituents on the 5th position can be used to kinetically protect the reducing B-H functionality in the presence of metals with high oxidative tendency (ex. Ag^{I}, Au^{I}), though a few ligands have appeared in the literature featuring alkyl/aryl groups on the boron atom (boron protected functionality). Nowadays, the tris(pyrazolyl)borato family is so wide that a systematic classification has been necessarily introduced with terms, nomenclature, and concepts introduced from more popular ligands, like phosphines (ex. cone angle). They support several metal mediated activations such as C-H and C-X (X = halogens). Perez and co-workers and Dias and co-workers showed that Cu^{I} and Ag^{I} scorpionates are very effective in catalytic C-H bond activations[122-127], C-Cl bond activation[128, 129], aziridination[130-136], and cyclopropanation with several substrates[137-141].

3.2 Going "classical"

As previously mentioned, cationic carbonyls of group 11 mostly show non-classical behavior, with short C-O bond distances and high ν(CO) stretching frequencies. Some copper carbonyls show classical behavior, at least in the frequency, if opportunely tuned with chelating or tripodal ligands. Lenders and Klaui reported the synthesis of a classical silver carbonyl, $[\{CpCo[P(O)(OEt)_2]_3\}Ag(CO)$.[142] This compound shows a strong absorption at 2125 cm^{-1} in

hexane, however, it has not been fully isolated and characterized.[142] Homoleptic species are extremely unstable, and they can be isolated only in poorly coordinating solvents, if not in super-acidic media. Dias et al. showed the possibility of isolating and stabilizing carbon monoxide adducts of coinage metals using fluorinated tris(pyrazolyl)borates, such as $[HB(3,5\text{-}(CF_3)_2Pz)_3]^-$, in solvents like dichloromethane and hexane. These fluorinated ligands are very poor nucleophiles and act like weakly-coordinating counter-ions. Complexes like $[HB(3,5\text{-}(CF_3)_2Pz)_3]Ag(CO)$ show remarkable thermal stability in solid state, but they tend to lose carbon monoxide only in dilute solutions. $[HB(3,5\text{-}(CF_3)_2Pz)_3]Cu(CO)$[143], $[HB(3,5\text{-}(CF_3)_2Pz)_3]Ag(CO)$[37], and $[HB(3,5\text{-}(CF_3)_2Pz)_3]Au(CO)$[36] has been the only complete triad of carbonyls known along the group in 10 years. Based on $\nu(CO)$ stretching frequency, the copper adduct shows classical behavior (2137 cm^{-1}), while the gold equivalent is borderline at 2144 cm^{-1}, only 1 cm^{-1} higher than that of free carbon monoxide in gas phase. The silver adduct shows a strong band centered at 2178 cm^{-1} in solid state, a value that is indeed in the “non-classical” range. ESP surfaces calculated at B3PW91/aug-cc-pVDZ-PP/6-31+G(d) clearly show the effect of the fluorination (Fig. 4.3). Blue zones represent positive electrostatic potential—in other words areas, where charge is depleted. Warmer colors imply an accumulation of negative charge, or negative potential. A certain stabilization of negative charge is provided by the trifluoromethyl groups on the 5th position of the pyrazole. The ESP surface of $[HB(3,5\text{-}(CF_3)_2Pz)_3]Cu(CO)$ also reveals that the oxygen atom of the carbonyl group is embedded in a more negative potential area than in $[HB(3,5\text{-}(CF_3)_2Pz)_3]Ag(CO)$ and $[HB(3,5\text{-}(CF_3)_2Pz)_3]Au(CO)$.

The work presented in this thesis aims to investigate the property of electron-rich scorpionates, with special attention paid to the bulky electron-rich $[CH_3B(3\text{-}(Mes)Pz)_3]^-$. The mesityl group on the 3rd position should have a marginally higher electron-releasing effect than the hydrogen atom, while maintaining a somewhat rigid protective cavity of almost 6 Å around

the metal ion. This ligand can be prepared in the form of the lithium salt. $CH_3B(OH)_2$ promptly reacts with $LiAlH_4$ in Et_2O to give CH_3BH_3Li. This compound reacts quite fast at high temperature (normally more than 200℃) with a little more than 3 equivalents of (3-(Mes)PzH) to give $[CH_3B(3\text{-}(Mes)Pz)_3]Li(3\text{-}(Mes)PzH)$. The latter is a stable solid, and the extra pyrazole can be removed by heating it up at 210℃ under high vacuum for three days. It, however, reacts with thallium(I) acetate in THF overnight to give $[CH_3B(3\text{-}(Mes)Pz)_3Tl]$ in acceptable yield. Despite their toxicity, thallium salts have several advantages over their alkali metal relatives including improved solubility in organic solvents, high stability, and high capability to be kept pure and dry. $[CH_3B(3\text{-}(Mes)Pz)_3Tl]$ can be washed several times with methanol in order to remove pirazole contamination, giving highly pure starting material.

$[CH_3B(3\text{-}(Mes)Pz)_3Tl]$ reacts with an excess of copper(I) triflate monobenzene complex or silver(I) triflate in dichloromethane saturated with ethylene, to give, upon extraction with n-hexane, $[CH_3B(3\text{-}(Mes)Pz)_3]Cu(\eta^2\text{-}C_2H_4)$ and $[CH_3B(3\text{-}(Mes)Pz)_3]Ag(\eta^2\text{-}C_2H_4)$, respectively, in good yields (Fig. 4.1). $[CH_3B(3\text{-}(Mes)Pz)_3]Cu(CO)$ can be obtained following the same procedure, but saturating the solvent with carbon monoxide instead of ethylene. It is important to notice that $[CH_3B(3\text{-}(Mes)Pz)_3Ag]CO$ cannot be obtained in high yields following the same procedure. However, the ethylene moiety in $[CH_3B(3\text{-}(Mes)Pz)_3Ag](\eta^2\text{-}C_2H_4)$ is quite labile, and it promptly exchanges with extra ethylene in solution. The phenomenon can be monitored on a ^1H NMR timescale. The $Cu^I\text{-}C_2H_4$ bond seems to be less labile, since $[CH_3B(3\text{-}(Mes)Pz)_3]Cu(\eta^2\text{-}C_2H_4)$ does not seem to follow the same behavior as its silver relative. $Ag^I\text{-}C_2H_4$ complexes supported by fluorinated scorpionates are quite labile in solution too. $[CH_3B(3\text{-}(Mes)Pz)_3]Cu(\eta^2\text{-}C_2H_4)$ and $[CH_3B(3\text{-}(Mes)Pz)_3]Ag(\eta^2\text{-}C_2H_4)$ show another interesting effect: the ^1H NMR (also ^{13}CNMR in a minor way) signal for the coordinated ethylene presents a large downfield shift that cannot be accounted for solely by π-back-bonding that the ligand is able to enforce on the

metals. The silver complex shows a singlet at δ 3.40 ppm, which is - 2.00 ppm downshifted with respect to free ethylene in CD_2Cl_2. I noticed that these exaggerated downfield shifts are common in similar complexes featuring two aryl rings "sandwiching" an ethylene moiety (like $[HC\{(CF_3)C(3,5\text{-}(CF_3)_2C_6H_3)N\}_2][Ag(\eta^2\text{-}C_2H_4)]$, ^{1}H NMR for ethylene at 3.78 ppm)[144], but also in organic molecules like annulenes[145-161]. The shift seems to be more intense when the proton is perpendicular to the π-system of the ring. The movement of electrons in the delocalized π-cloud generates a magnetic field whose force lines oppose the NMR field (B_0) for a proton perpendicular to the π-cloud. This effect is called magnetic anisotropy of the aryl ring (every molecule with double or triple bonds carries some degree of magnetic anisotropy)[145-169]. I also synthesized the relative mesityl copper complex to prove that the magnetic anisotropy depends only on the arenes in the ligand and not on the metal. The compound can be synthesized in good yield, and it was characterized by ^{1}H NMR as well as X-ray diffraction (structure not shown in this thesis). It shows a signal for coordinated ethylene at δ 2.71 ppm, - 2.69 ppm downfield from free ethylene in CH_2Cl_2. For comparison, $[CH_3B(3,5\text{-}(Me)_2Pz)_3]Cu(\eta^2\text{-}C_2H_4)$ shows a singlet at δ 4.41 ppm.

$[CH_3B(3\text{-}(Mes)Pz)_3]Ag(\eta^2\text{-}C_2H_4)$ can be used as starting material for other silver complexes. A n-hexane solution of $[CH_3B(3\text{-}(Mes)Pz)_3Ag](\eta^2\text{-}C_2H_4)$ treated with one equivalent of ^{t}BuNC gives $[CH_3B(3\text{-}(Mes)Pz)_3Ag](^t$BuNC) in quantitative yield. Most importantly, I thought that the lability in solution of $[CH_3B(3\text{-}(Mes)Pz)_3]Ag(\eta^2\text{-}C_2H_4)$ could be used to our advantage to synthesize $[CH_3B(3\text{-}(Mes)Pz)_3Ag](CO)$ in a clean way. That is, $[CH_3B(3\text{-}(Mes)Pz)_3Ag](CO)$ can be easily synthesized in quantitative yield by bubbling carbon monoxide for one hour in a n-hexane solution of $[CH_3B(3\text{-}(Mes)Pz)_3]Ag(\eta^2\text{-}C_2H_4)$. The reverse reaction seems to happen somewhat faster (even though precise measurements for experimental kinetic constants are not available), and $[CH_3B(3\text{-}(Mes)Pz)_3Ag](\eta^2\text{-}C_2H_4)$ can be re-obtained in less than five minutes.

Fluorinated silver complexes tested by other members of our group undergo the same reversible transformation in the presence of ethylene or carbon monoxide.

Both $[CH_3B(3\text{-}(Mes)Pz)_3]Cu(CO)$ and $[CH_3B(3\text{-}(Mes)Pz)_3]Ag(CO)$ show high thermal stability and they can be kept in a dry environment sealed in a vial for longer than one year. $[CH_3B(3\text{-}(Mes)Pz)_3Ag](\eta^2\text{-}C_2H_4)$ and $[CH_3B(3\text{-}(Mes)Pz)_3Ag]CO$ lose the coordinated gas, if pumped dry from dilute solution, to presumably form some kind of polymeric silver compound. The reaction is reversible, and when ethylene or carbon monoxide is bubbled into the solution again, the respective adducts can be re-obtained. The process seems to happen without apparent decomposition. $[CH_3B(3\text{-}(Mes)Pz)_3]Au(CO)$ could not be synthesized in a clean way, and all attempts to get a pure powder for analysis or suitable crystals for X-ray diffraction failed. However, I was able to collect a solid state FT-IR spectrum on a sample of crude material.

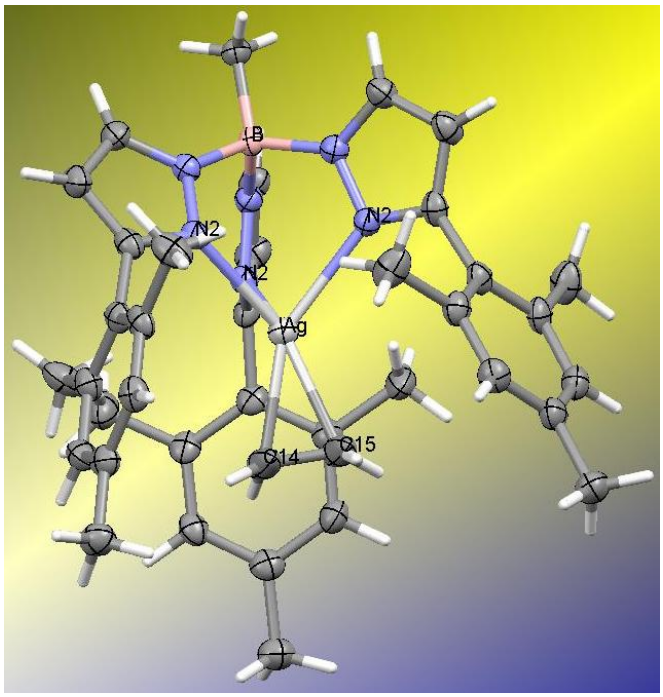

Figure 4.1. ORTEP structure of $[CH_3B(3\text{-}(Mes)Pz)_3]Ag(\eta^2\text{-}C_2H_4)$. Thermal ellipsoids have been drawn at 60% probability level. Selected bond lengths (Å) and angles (°): Ag-C14 2.27(3), Ag-N2 2.3404(14), C14-C15 1.323(13), Ag···B 3.422, C14-Ag-C15 33.8(3)

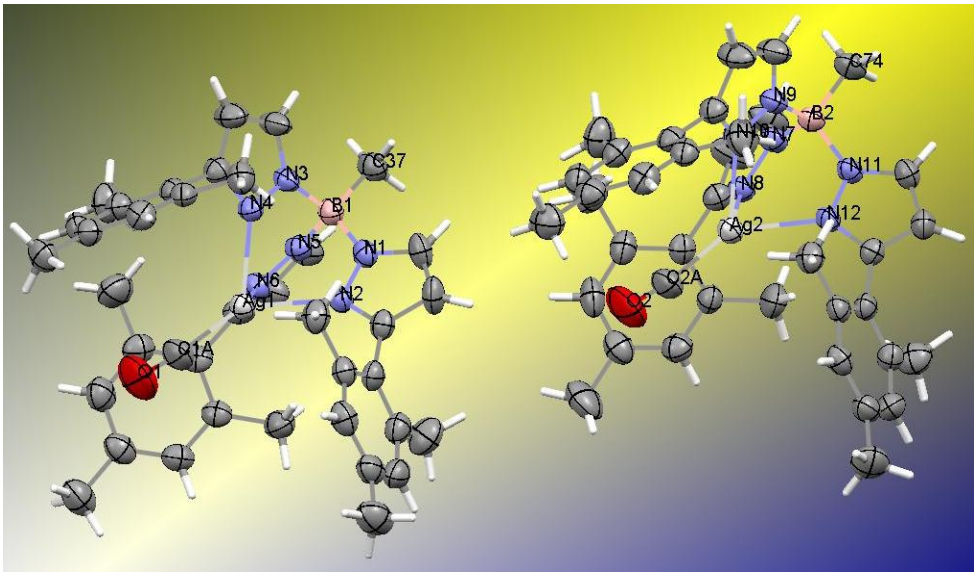

Figure 4.2. ORTEP structure of $[CH_3B(3\text{-}(Mes)Pz)_3]Ag(CO)$. Thermal ellipsoids have been drawn at 60% probability level. Selected bond lengths (Å) and angles (°): Ag1-C1A 1.995(3), Ag1-N6 2.295(2), Ag1-N4 2.297(2), Ag1-N2 2.316(2), C1A-O1 1.111(4), Ag1···B1 3.393, O1-C1A-Ag1 171.3(4), C1A-Ag1···B1 167.62, Ag2-C2A 1.992(3), Ag2-N8 2.287(2), Ag2-N12 2.312(2), Ag2-N10 2.324(2), C2A-O2 1.112(4), Ag2···B2 3.367, O2-C2A-Ag2 169.2(4), C2A-Ag2···B2 166.25

Tuning the electronic properties of the tris(pyrazolyl)borate skeleton (replacing both the fluorinated groups with bulky mesityl groups for example) should have increased the nucleophilicity of the ligand and brought a considerable amount of electron density to the metal centers. In order to check the last statement, ν(CO) frequencies were taken from FT-IR spectra on KBr samples: $[CH_3B(3\text{-}(Mes)Pz)_3]Cu(CO)$, $[CH_3B(3\text{-}(Mes)Pz)_3]Ag(CO)$ and $[CH_3B(3\text{-}(Mes)Pz)_3]Au(CO)$ show strong absorptions centered at 2075, 2125, and 2079 cm^{-1}, respectively. These values are - 68, - 18, and - 64 cm^{-1} red-shifted compared to 2143 cm^{-1}, the frequency for the free carbon monoxide. For comparison $[HB(3,5\text{-}(CF_3)_2Pz)_3]Cu(CO)$, $[HB(3,5\text{-}(CF_3)_2Pz)_3]Ag(CO)$ and $[HB(3,5\text{-}(CF_3)_2Pz)_3]Ag(CO)$ show absorptions centered at 2137, 2178, and 2144 cm^{-1}, respectively. Considering this trend, these new carbonyls show ***classical behavior***.

Table 4.1. X-ray structural parameters (black) versus calculated values for tris(pyrazolyl)borate complexes (blue)

Compound	M-N bond distance (Å)	B···M distance (Å)	N-B-N angle	M-C bond distance (Å)	C-O bond distance (Å)
[HB(3,5-(CF_3)Pz_3)Cu](CO)	2.052 (4) 2.068	3.075 3.070	108.30 108.67	1.808(4) 1.804	1.110 (5) 1.141
[HB(3,5-(CF_3)Pz_3)Ag](CO)	2.328 (4) 2.339	3.366 3.354	109.95 109.48	2.037(5) 2.003	1.116 (7) 1.137
[HB(3,5-(CF_3)Pz_3)Au](CO)	2.336 (5) 2.358	3.443 3.454	109.41 109.11	1.862 (9) 1.877	1.113 (11) 1.144
[CH_3B(3-(Mes)Pz_3)Cu](CO)	2.060	3.071	107.71	1.791	1.146
[CH_3B(3-(Mes)Pz_3)Ag](CO)	2.303 (2) 2.301	3.380 3.346	108.36 108.68	1.994 (3) 1.976	1.111 (4) 1.141
[CH_3B(3-(Mes)Pz_3)Au](CO)	2.324	3.438	108.13	1.867	1.150

[CH_3B(3-(Mes)Pz)$_3$]Ag(CO) shows a significantly shorter M-C distance than [HB(3,5-(CF_3)$_2$Pz)$_3$]Ag(CO), 1.994(3) versus 2.035(5) (DFT is in good agreement with the experiment predicting Δ(M-C) = - 0.027 Å) (Fig. 4.2). This is a sign of increased π-back-bonding from the metal. The Ag-C-O moiety is not linear, with an average angle of 170.3(4)°. The average C-O bond distance is 1.111(4) Å (Fig. 4.2). ESP surfaces are useful again to "visualize the charge distribution" on the molecules. The maps now look "warmer" than in the case of the other scorpionate adducts, especially in the B···M inter-nuclear region and around the M-C-O fragments (particularly in the case of Cu^{I}-CO and Au^{I}-CO, Fig. 4.3). The blue regions fall right on the 5th positions of the pyrazoles in this case. It would be very interesting to see if the addition of electron-releasing groups in those particular positions could bring about the isolation of a classical series where the ν(CO) stretching band is further shifted red in comparison to 2143 cm^{-1} (in other words, generating "more classical" carbonyls).

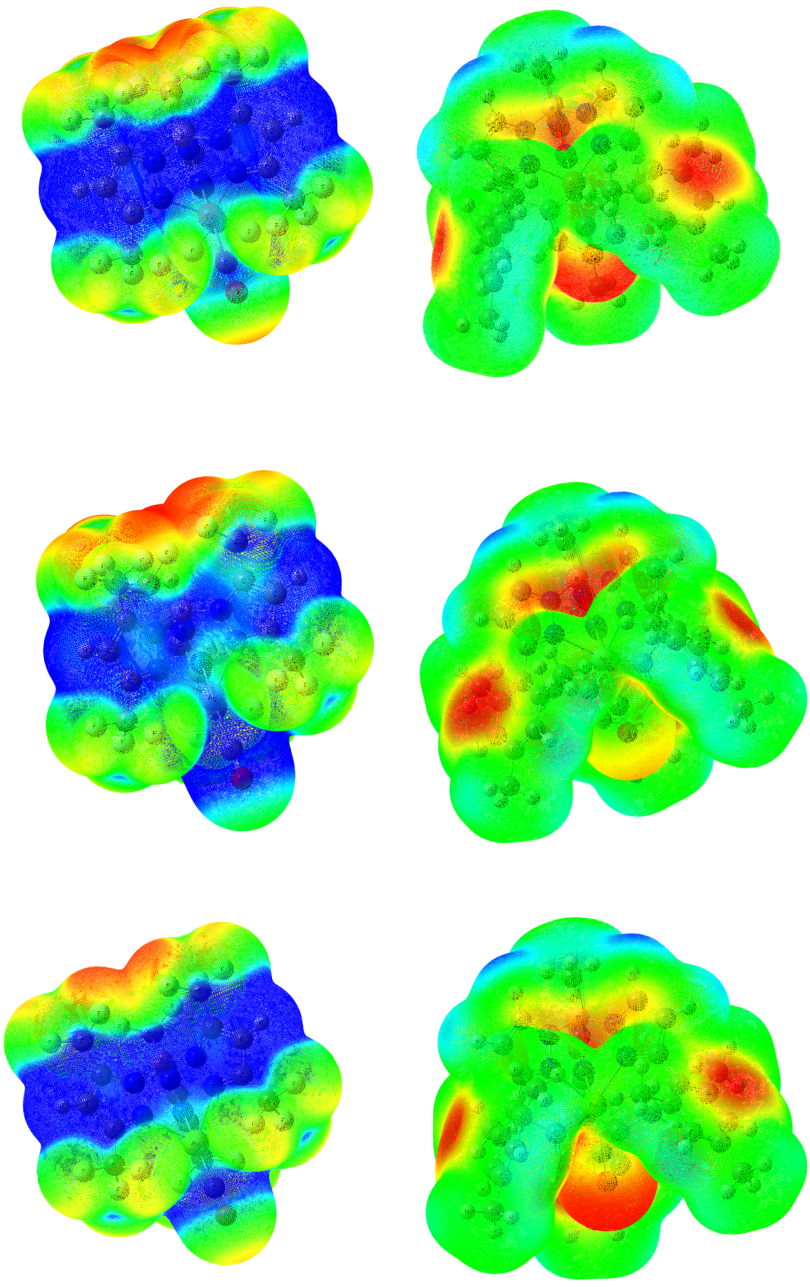

Figure 4.3. Electrostatic potential maps of [HB(3,5-(CF_3)Pz)$_3$]M(CO), left column, and [CH_3B(3-(Mes)Pz)$_3$]M(CO), right column, (M = Cu, Ag, Au, top to bottom) plotted on top of SCF density at 0.0004 hartrees

In order to gain a better understanding of the electronic structures of these compounds and to provide a reason behind this "classical" tendency, I carried out a NBO analysis on the Self Consistent Field (SCF) obtained by B3PW91/aug-cc-pVDZ-PP/6-31+G(d). Scorpionate adducts will be compared to free carbon monoxide as well as simple monocarbonyl adducts, $[M\text{-}(CO)]^+$ (M = Cu, Ag, Au). $[HB(3,5\text{-}(CF_3)_2Pz)_3]Cu(CO)$ and $[HB(3,5\text{-}(CF_3)_2Pz)_3]Au(CO)$ are the most interesting of the six compounds and so accordingly, will be discussed first; they are the only ones among the scorpionate adducts to show the presence of a localized M^I-CO orbital. The Au-C (carbon monoxide) bond is a covalent bond shared 19% by the gold atom (main contribution to the localized orbital comes from s orbital, 92%, and d orbital, 7%) and 81% by the carbon atom (63% s orbital, 37% p orbital). The Cu-C (carbon monoxide) bond is a covalent bond shared 11% by the copper atom (main contribution to the localized orbital comes from s orbital, 98%, p orbital, 1%, and d orbital, 1%) and 81% by the carbon atom (66% s orbital, 34% p orbital). In this sense, $[HB(3,5\text{-}(CF_3)_2Pz)_3]Cu(CO)$ and $[HB(3,5\text{-}(CF_3)_2Pz)_3]Au(CO)$ should be regarded as composed of two units, the $[Cu(CO)]^+$ or $[Au(CO)]^+$ fragment and the scorpionate ligand supporting them. It seems that generally, besides $[Cu(CO)]^+$, $[Ag(CO)]^+$, $[Au(CO)]^+$, $[HB(3,5\text{-}(CF_3)_2Pz)_3]Cu(CO)$, and $[HB(3,5\text{-}(CF_3)_2Pz)_3]Au(CO)$, that other carbonyls present a more electrostatic type of interaction with a clear absence of a localized covalent bond between the metal and the carbon monoxide. $[Cu(CO)]^+$, $[Ag(CO)]^+$ and $[Au(CO)]^+$ present a LN O → BD* M-C interaction—in other words, a lone pair of the oxygen is contributing to weaken the metal-carbon bond interacting with its anti-bonding orbital. This interaction is also present in $[HB(3,5\text{-}(CF_3)_2Pz)_3]Au(CO)$, but it is ~ 15 times weaker than the interaction that three lone pairs of the nitrogen donor (scorpionate) have with the metal-carbon anti-bonding orbital (formally 3 x LP N → BD* Au-C). Since BD* Au-C is 91% delocalized on the gold atom with 92% s character, we could say that the ligand is "competing" with the carbon monoxide for binding the gold atom.

Weakly-coordinating ligands “compete” in a “weak” way, which might be the reason why they are so successful in the stabilization of coinage metal carbonyl. $[Au(CO)]^+$ presents a BD* (Au-C, anti-bonding) population of 0.01 e^-, while, upon coordination of the fluorinated ligand, $[HB(3,5\text{-}(CF_3)_2Pz)_3]Au(CO)$ shows an increased BD* (Au-C) population of 0.20 e^-. For comparison, $[Cu(CO)]^+$ presents a BD* (Cu-C, anti-bonding) population of 0.00 e^-, while, upon coordination of the fluorinated ligand, $[HB(3,5\text{-}(CF_3)_2Pz)_3]Cu(CO)$ shows an increased BD* (Cu-C) population of 0.17 e^-.

As mentioned before, the other compounds presented here do not show any localized M-C orbital, therefore they cannot be regarded as totally covalent. Although a clear explanation of this phenomenon has yet to be formulated, a good reason could be that when the nucleophilicity of the ligand increases, passing from $[HB(3,5\text{-}(CF_3)_2Pz)_3]^-$ to $[CH_3B(3\text{-}(Mes)Pz)_3]^-$ (NBO charges confirm this increment of charge at the nitrogen donors, Tab. 4.2), the electron-density on the BD* M-C (anti-bonding) orbital increases as well, bringing about the dissolution of the net covalent bond between the metal and the carbon monoxide and the formation of a more “polarized” type of interaction. Tab. 4.3 below shows the π^* population at the carbon monoxide. The trend is somewhat expected, and it shows that the π^* population is generally greater for gold complexes, followed by copper and then by silver. It can also be also inferred that the increment in $\pi^*(CO)$ population almost perfectly matches the loss in population underwent by metal lone pairs (4) and (5). These lone pairs have mostly d character and represent suitable orbitals for M→CO π-back-bonding. The conclusion is that the total amount of population in the $\pi^*(CO)$ for the complexes in Tab. 4.3 comes exclusively from the metal atoms.

Table 4.2. NBO charges for tris(pyrazolyl)borato complexes. The numbers in red represent the NBO charges on non-complexed metal ions

Compound	Metal charge	C (CO)	O (CO)	N (sp^2, av.)
CO	-	+ 0.48	- 0.48	-
$[Cu(CO)]^+$	+ 0.92 **(+ 1.00)**	+ 0.38	- 0.29	-
$[Ag(CO)]^+$	+ 0.93 **(+ 1.00)**	+ 0.38	- 0.31	-
$[Au(CO)]^+$	+ 0.81 **(+ 1.00)**	+ 0.46	- 0.28	-
$[HB(3,5\text{-}(CF_3)_2Pz)_3]Cu(CO)$	+ 0.87 **(+ 1.00)**	+ 0.38	- 0.43	- 0.37
$[HB(3,5\text{-}(CF_3)_2Pz)_3]Ag(CO)$	+ 0.83 **(+ 1.00)**	+ 0.42	- 0.41	- 0.34
$[HB(3,5\text{-}(CF_3)_2Pz)_3]Au(CO)$	+ 0.79 **(+ 1.00)**	+ 0.40	- 0.42	- 0.35
$[CH_3B(3\text{-}(Mes)Pz)_3]Cu(CO)$	+ 0.90 **(+ 1.00)**	+ 0.36	- 0.46	- 0.42
$[CH_3B(3\text{-}(Mes)Pz)_3]Ag(CO)$	+ 0.84 **(+ 1.00)**	+ 0.40	- 0.44	- 0.39
$[CH_3B(3\text{-}(Mes)Pz)_3]Au(CO)$	+ 0.82 **(+ 1.00)**	+ 0.37	- 0.45	- 0.39

Table 4.3. NBO populations analysis for tris(pyrazolyl)borato complexes (in e^-)

Compound	BD M-C bonding orbital	BD * M-C anti-bonding orbital	Metal LP (6)	2 x Metal LP (4) and (5)	C lone pair	2 x π* (CO)	N (sp^2, av.)
CO	-	-	-	-	2.00	0.00	-
$[Cu(CO)]^+$	1.99	0.00	-	2 x 1.96	-	2 x 0.04	-
$[Ag(CO)]^+$	1.98	0.00	-	2 x 1.98	-	2 x 0.02	-
$[Au(CO)]^+$	1.99	0.01	-	2 x 1.92	-	2 x 0.07	-
$[HB(3,5\text{-}(CF_3)_2Pz)_3]Cu(CO)$	1.99	0.17	-	2 x 1.89	-	2 x 0.12	1.88
$[HB(3,5\text{-}(CF_3)_2Pz)_3]Ag(CO)$	-	-	0.35	2 x 1.92	1.81	2 x 0.08	1.89
$[HB(3,5\text{-}(CF_3)_2Pz)_3]Au(CO)$	1.99	0.20	-	2 x 1.85	-	2 x 0.17	1.87
$[CH_3B(3\text{-}(Mes)Pz)_3]Cu(CO)$	-	-	0.37	2 X 1.88	1.79	2 x 0.14	1.88
$[CH_3B(3\text{-}(Mes)Pz)_3]Ag(CO)$	-	-	0.36	2 x 1.90	1.80	2 x 0.11	1.88
$[CH_3B(3\text{-}(Mes)Pz)_3]Au(CO)$	-	-	0.54	2 x 1.83	1.66	2 x 0.19	1.86

Moreover, nitrogen donor atoms contribute to the LP N → π* (CO) for [CH_3B(3-(Mes)Pz)$_3$]Cu(CO), [CH_3B(3-(Mes)Pz)$_3$]Ag(CO), and [CH_3B(3-(Mes)Pz)$_3$]Au(CO), but the interactions are energetically very small if compared to the interactions brought by the metal atom, LP M → π* (CO). Energetically, the latter are 9 times more important for copper complex, 17 times for silver, and 16 times for gold than the correspondent LP N → π* (CO). Also, π systems of arene rings of the ligand [CH_3B(3-(Mes)Pz)$_3$]$^-$ do not seem to interact with the π* systems of the carbon monoxide. These three proofs together suggest the conclusion that the increased population in the π*(CO) is a direct effect of interaction with the metal only.

An important comparison to be discussed is the one between [HB(3,5-(CF_3)$_2$Pz)$_3$]Ag(CO) and [CH_3B(3-(Mes)Pz)$_3$]Ag(CO). These two complexes show exactly the same LP C population (lone pair at the carbon), 181 and 1.80 e^- respectively, but very different π*(CO) populations, 0.08 and 0.11 e^- respectively. Whatever the effect of removing electron-density from the lone pair on the carbon might be, in this case it is only the increment in π*(CO) population that weakens the C-O bond. NBO charges show a more positive Ag atom in [CH_3B(3-(Mes)Pz)$_3$]Ag(CO), + 0.84, than in [HB(3,5-(CF_3)$_2$Pz)$_3$]Ag(CO), + 0.83, but also a more negative C atom, + 0.40 vs + 0.42, and O atom, - 0.44 vs - 0.41. All [CH_3B(3-(Mes)Pz)$_3$]$^-$ complexes systematically show more positive metal atoms and more negative CO moieties than [HB(3,5-(CF_3)$_2$Pz)$_3$]$^-$ complexes. In conclusion, the mesityl ligand is able to impart more charge into the coordinated carbon monoxide via the metal atom than the fluorinated relative.

Experiments provide direct evidence of increased electron density at the silver center imparted by the electron-rich scorpionate. For instance, a telling proof is given by the systematic study of C-H activation catalyzed by tris(pyrazolyl)borate silver complexes. Rangan et al. demonstrated that electron-poor silver complexes supported by weakly-coordinating ligands, such as [HB(3,5-

$(CF_3)Pz)_3]Ag(\eta^2\text{-}C_2H_4)$ or $[CH_3B(3\text{-}(C_2F_5)Pz)_3]Ag(\eta^2\text{-}C_2H_4)$, have high selectivity toward primary C-H activation by carbenoid species generated *in situ* using precursors like EDA.[170] In Tab. 4.4 it is easy to see that the primary/tertiary C-H activation selectivity is greatly reduced when $[CH_3B(3\text{-}(Mes)Pz)_3]Ag(\eta^2\text{-}C_2H_4)$ is used as catalyst instead of $[HB(3,5\text{-}(CF_3)Pz)_3]Ag(\eta^2\text{-}C_2H_4)$ or $[CH_3B(3\text{-}(C_2F_5)Pz)_3]Ag(\eta^2\text{-}C_2H_4)$.

Table 4.4. Comparison between C-H activation on primary and tertiary carbons carried out by different Ag^I scorpionates

Catalyst	Carbonyl compound	ν(CO) cm^{-1}	Primary:tertiary C-H activation
$[HB(3,5\text{-}(CF_3)Pz)_3]Ag(\eta^2\text{-}C_2H_4)$	$[HB(3,5\text{-}(CF_3)Pz)_3]Ag(CO)$	2162 (hexane)	1:1.59
$[CH_3B(3\text{-}(C_2F_5)Pz)_3]Ag(\eta^2\text{-}C_2H_4)$	$[CH_3B(3\text{-}(C_2F_5)Pz)_3]Ag(CO)$	2152 (hexane)	1:2.33
$[CH_3B(3\text{-}(Mes)Pz)_3]Ag(\eta^2\text{-}C_2H_4)$	$[CH_3B(3\text{-}(Mes)Pz)_3]Ag(CO)$	2128 (hexane)	1:6.24

In conclusion, non-classical carbonyls of group 11 are known for copper, silver, and gold. They show very high ν(CO) frequencies and short C-O bond lengths. Copper can be tuned using ancillary ligands to give classical carbonyls, but silver and gold could not. We used a bulky electron-rich tris(pyrazolyl)borate to isolate and "protect" the first classical carbonyl of silver.[171-174] Evidence for the gold carbonyl's existence is provided by IR spectroscopy. NBO analysis provides important information on the nature of the interactions. $[HB(3,5\text{-}(CF_3)_2Pz)_3]Cu(CO)$ and $[HB(3,5\text{-}(CF_3)_2Pz)_3]Au(CO)$ show two separate units, the ligand and the fragment M-CO, where carbon monoxide is bound covalently. All the other compounds do not show any localized covalent M-C unit. $[CH_3B(3\text{-}(Mes)Pz)_3]Cu(CO)$, $[CH_3B(3\text{-}(Mes)Pz)_3]Ag(CO)$, and $[CH_3B(3\text{-}(Mes)Pz)_3]Au(CO)$ show higher π*(CO) populations compared to their fluorinated counterparts (and generally more negatively charged CO moieties), hence justifying the red-

shift in the ν(CO) stretching frequency. Their ν(CO) stretching frequencies are all below 2143 cm^{-1}. This class of compounds can be defined as the first series of “classical” carbonyls in group 11.

APPENDIX A

EXPERIMENTAL AND THEORETICAL METHODS

All manipulations were carried out under an atmosphere of dry purified argon using standard Schlenk techniques. Solvents were purchased from commercial sources, distilled and degassed by the freeze-pump-thaw method twice prior to use. Glassware was dried in the oven at 150℃ overnight. Deuterated solvents were dried over activated molecular sieves overnight and degassed with argon for 15 minutes prior to use. NMR spectra were recorded at 298 K on JEOL ECLIPSE 500 spectrometer (^{1}H, 500.16 MHz, ^{13}C, 125.77 MHz) and on a JEOL ECLIPSE 300 (^{1}H, 500.16 MHz, ^{13}C, 125.77 MHz). Both ^{1}H NMR and ^{13}C NMR signals were referenced against the solvent peak (normalized against the NMR Solvent Data Chart of Cambridge Isotope Laboratories, Inc.).

Raman spectra were recorded at 298 K on JORIBA JOBIN YVON instrument using two different laser sources, 473 nm and 633 nm. Crystals of the samples were sealed tight under argon or nitrogen (depending on their reactivity) and a quartz cuvette by means of a greased teflon cup. Different experimental settings (laser intensity, level of magnification, time of exposure, number of cycles) were used for each compound in order to obtain the best signal-to-noise ratio. UV-Vis spectra were recorded at 298 K on Agilent 8453 spectrophotometer with a quartz cell (3 mL, 1 cm path) versus a dichloromethane blank. The wavelength range used was 200 - 1000 nm.

Calculations were carried out using the G03 package revision D.02[175]. Basis sets and ECP were downloaded from Basis Set Exchange[176, 177]. Basis sets are generally sets of mathematical functions (gaussians are normally chosen for computational efficiency) describing the orbitals of the atoms. Larger basis sets (including higher angular momentum polarization and diffuse functions) normally yield to better results in computed geometries, thermodynamics and spectroscopic properties. ECP means “Electron core potential”. Electron core potentials use potential functions to replace or simulate the “core” of the atoms (generally heavy metals). Calculations using ECPs, therefore, decrease substantially the amount of computational time in comparison to full-electron basis sets, while, on the other side, they do not lose accuracy. In my case a “small core” ECP is used—in other words, only the valence and the sub-valence are not “frozen” by the ECP. “Small core” ECPs tend to be more reliable than those that “freeze” the sub-valence as well. Structures were modeled using restricted B3PW91 (Becke three parameters exchange functional + Perdew-Wang 91 correlation functional) in conjunction with aug-cc-pVTZ-PP for Cu, Ag, Au, and Pd atoms and 6-311++G(d,p) for carbon, oxygen, and hydrogen. Heavy metal core electrons (10, 28, 60) were frozen using Figgen’s fully-relativistic multiple Dirac-Fock (MDF) electron core potential. aug-cc-pVTZ-PP/6-311++G(d,p) combination uses pure d and f functions, 5D 7F[178]. Tris(pyrazolyl)borates complexes were calculated using aug-cc-pVDZ-PP/6-31+G(d) mixed basis set for computational efficiency. aug-cc-pVDZ-PP

uses pure functions, while 6-31+G(d) has been optimized using cartesian d function, 6D 7F[178]. 5D and 7F were used even in this case since the study is limited to geometry optimization and NBO analysis.

Structures were calculated with no symmetry at first and then refined using the highest point-group possible. Force constants were calculated at the beginning of the optimization and then used for successive steps. Transition states were found using Synchronous Transit-Guided Quasi-Newton (STQN) using inputs for reagents and products (QST2) as well as a good estimate for the Hessian matrix.

Acquired stationary points were characterized by Hessian analysis. Vibrations and thermo-chemical parameters were both scaled using the same scaling constant of 0.9733, obtained by least-squared linear interpolation of ν(C=C) and ν(C≡O) frequencies of eight simple ethylene and carbonyl species. Thermochemical parameters have been calculated at 298.15 K and 1 atm. Stability calculations were performed on the wavefunction of every molecule to ensure that the lower electronic state was chosen for the study.

To test the validity of the method, thermochemical data obtained on simple copper carbonyls, $M(CO)_n^+$ (with n = 1-4, M = Cu, Ag), and non-corrected for BSSE (basis set superimposition error) were compared to Armentrout's experimental results for dissociation of carbon monoxide from Cu^I and Ag^I. Metal ions were calculated both as singlets ($^1S_0$) and triplets ($^3D_3$) using O_h and C_1 (the C_1 group is necessary for breaking spatial symmetry of the orbitals). Calculations showed the ground state to be $^1S_0$ and essentially no energy difference was noticed for different symmetries, so O_h was taken. Vertical excitations have been calculated using Time-dependent DFT (BLYP) in a single point calculation starting from the structure optimized at B3PW91 level.

Table A.1. Primitives and contracted gaussians of the correlation-consistent basis sets used in this thesis

Basis set	*Primitives/contracted*
cc-pVDZ-PP	(8s7p6d1f)/[4s4p3d1f]
aug-cc-pVDZ-PP	cc-pVDZ-PP + 1s1p1d1f
cc-pVTZ-PP	(10s9p8d2f1g)/[5s5p4d2f1g]
aug-cc-pVTZ-PP	cc-pVTZ-PP + 1s1p1d1f1g

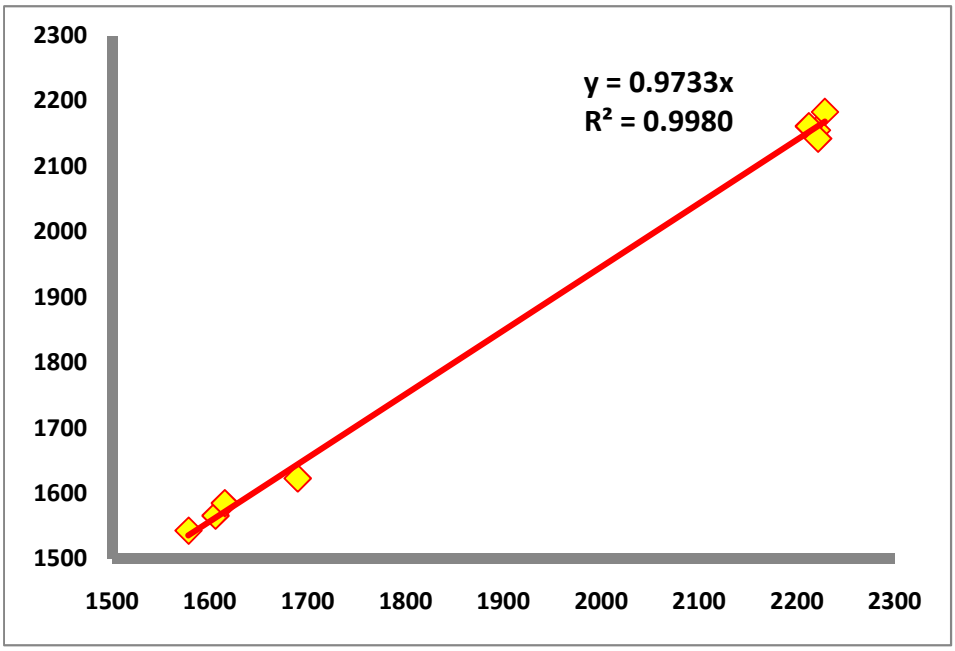

Figure A.1. Least-squares regression line of eight experimental versus calculated frequencies for the estimation of the scaling constant for frequencies and thermodynamical parameters: ν(CO) for free CO (2143 cm^{-1}), ClCuCO (2156 cm^{-1})[179], ClAgCO (2184 cm^{-1})[179], ClAuCO (2162 cm^{-1})[179] and ν(C=C) for free C_2H_4 (1623 cm^{-1}), $[Cu(C_2H_4)_3]^+$ (1566 cm^{-1}), $[Ag(C_2H_4)_3]^+$ (1584 cm^{-1}), $[Au(C_2H_4)_3]^+$ (1543 cm^{-1})

(1) $[Ag(C_2H_4)_3][SbF_6]$: $AgSbF_6$ 98% (0.250 g, 0.71 mmol) was placed in a flask with magnetic stir bar. Dichloromethane (10 mL) saturated with ethylene were added to the

mixture at room temperature. The mixture was stirred for about 3 hours under ethylene atmosphere ($AgSbF_6$ dissolved completely). Ethylene was gently bubbled into the mixture (3 x 5 min.) during this period to maintain an ethylene rich solution. The solution was concentrated under reduced pressure to about 3 mL of dichloromethane, and then dried using a stream of ethylene. X-ray quality colorless crystals can be obtained from a CH_2Cl_2/Hexafluorobenzene (1:1) solution at -20°C. This compound is quite sensitive to moisture and tends to decompose leaving a silver mirror on the walls of the flask. ^1H NMR (CD_2Cl_2, 298 K, ppm): δ 5.83 (s, C***H₂***=C***H₂***). ^{13}C {^1H} NMR (CD_2Cl_2, 298 K, ppm): δ 116.9 (s, ***C***H_2=***C***H_2). Raman (solid, 298K, cm^{-1}): 3161 (w), 3089 (w), 3007 (s), 1584 (s), 1324 (s), 986 (w), 645 (s), 570 (w), 276 (m), 249 (m).

(2) [Cu(C₂H₄)₃][SbF₆]: CuBr (0.150 g, 1.0 mmol) and $AgSbF_6$ 98% (0.367 g, 1.0 mmol) were placed in a flask with magnetic stir bar. Dichloromethane (10 mL) saturated with ethylene were added to the mixture at room temperature. The mixture was stirred for about 3 hours under an ethylene atmosphere ($AgSbF_6$ dissolved completely). Ethylene was gently bubbled into the mixture (3 x 5 min.) during this period to maintain an ethylene rich solution. The resulting greenish precipitate (AgBr) was removed by filtration using a Celite bed. The pale yellow solution was concentrated under reduced pressure to about 3 mL of dichloromethane. This supersaturated solution was placed under an ethylene atmosphere and cooled to -20 °C to obtain colorless crystals. NMR and Raman spectra were collected on crystals dried under an ethylene stream. This compound is quite sensitive to moisture and air and, upon exposure, tends to decompose into a copper colored film, followed by blue-green and then black specks (this process can be observed under the microscope). A Raman spectrum of this compound was obtained with great difficulty and long period of exposure of the sample to the laser were avoided. However, a solution of these crystals in dichloromethane, sealed in a NMR tube under argon and stored at 4 °C, is quite stable for about 10 days (both visually and based on the NMR). ^1H NMR (CD_2Cl_2, 298 K): δ 5.44 (s, C***H₂***=C***H₂***). ^{13}C {^1H} NMR (CD_2Cl_2, 298 K): δ 109.6 (s, ***C***H_2=***C***H_2). Raman (solid, 298K, cm^{-1}): 3089 (w), 3004 (m), 1566 (m), 1307 (s), 1003 (w), 645 (m), 569 (m), 331 (w), 276 (w).

(3) [Au(C₂H₄)₃][SbF₆]: AuCl (0.100 g, 0.51 mmol) and $AgSbF_6$ 98% (0.146 g, 0.42 mmol) were placed in a flask with magnetic stir bar. Dichloromethane (10 mL) saturated with ethylene were added to the mixture at room temperature. The mixture was stirred for

about 3 hours under an ethylene atmosphere ($AgSb_6$ dissolved completely). Ethylene was gently bubbled into the mixture (3 x 5 min.) during this period to maintain an ethylene rich solution. The resulting grey precipitate (AgCl) was removed by filtration using a Celite bed. The solution was concentrated under reduced pressure to about 3 mL of dichloromethane. This supersaturated solution was placed under an ethylene atmosphere and cooled to -20 ℃ to obtain colorless crystals. NMR and Raman spectra were collected on crystals dried under an ethylene stream. This compound is extremely sensitive to moisture, air and light and, upon exposure, it immediately turns black. A Raman spectrum of this compound was obtained with great difficulty, within 10 seconds from the initial exposure to the laser (1s). However, a solution of these crystals in dichloromethane, sealed in a NMR tube under argon and stored at 4℃, appears to be quite stable for about 10 days (both visually and based on the NMR), provided that the light is also excluded. After several days, a small amount of black precipitate is observed on the bottom of the NMR tube, but its presence does not affect the quality of the NMR spectrum. X-ray quality colorless crystals can be obtained from a CH_2Cl_2 solution at -20 ℃. ^{1}H NMR (CD_2Cl_2, 298 K): δ 4.94 (s, C***H*****$_2$**=C***H*****$_2$**). ^{13}C {^{1}H} NMR (CD_2Cl_2, 298 K): δ 92.7 (s, ***C***H_2=***C***H_2). Raman (solid, 298K, cm^{-1}): 3161 (w), 3100 (w), 3004 (m), 1543 (m), 1284 (s), 1017 (w), 648 (m), 379 (m), 307 (w,), 279 (w).

(4) **$[Ag(C_7H_{10})_3][SbF_6]$**: $AgSb_6$ 98% (0.400 g, 1.14 mmol) is placed in a flask with magnetic stir bar. Norbornene C_7H_{10} (0.500 g, 5.3 mmol) and 30 mL of dry/degassed dichloromethane are mixed together at room temperature in another flask. The norbornene solution is transferred to the flask containing the silver salt. The reaction is immediate. The reaction flask is covered with aluminum foil to protect it from the light and the mixture is stirred overnight under a nitrogen atmosphere and then filtered on a Celite bed. The filtrate is placed in the freezer at - 20 ℃ for couple of days. During this time, crystals of compound form at the bottom of the flask. They are separated by filtration and the filtrate is concentrated under reduced pressure to ~ 2 mL and placed back in the freezer. A second batch of crystals can be obtained in this way (overall yield, 0.336 g, 46%). X-ray quality colorless crystals can be obtained from dilute CH_2Cl_2 solution at -20℃. This compound appears to be stable in paratone oil, but it slightly turns tan if left exposed at the air/light at room temperature. It is best stored at low temperature in a Dry-box freezer -20℃ in nitrogen atmosphere. ^{1}H NMR (CD_2Cl_2, 298 K): δ 0.84 (m, 1H), 1.01 (m, 2H), 1.18 (m, 1H), 1.77 (m, 2H), 3.20 (s, 2H), 6.42 (s, 2H,

C***H***=C***H***). ^{13}C {^{1}H} NMR (CD_2Cl_2, 298 K): δ 23.6, 43.7, 48.5, 132.6 (s, ***C***H=***C***H). Raman (solid, 298K, cm^{-1}): 1507 cm^{-1} (C=C stretching band). Elemental analysis: calculated, C, 40.29%, H, 4.83%, found, C, 40.27%, H, 4.85%. M.P.: dec > 120 ℃, melt with decomposition.

(5) **$[Cu(C_7H_{10})_3][SbF_6]$**: $[Ag(C_7H_{10})_3][SbF_6]$ (0.200 g, 0.32 mmol) and CuBr (0.069 g, 0.48 mmol) are placed in a flask with magnetic stir bar. Dichloromethane (50 mL) is added at room temperature. The reaction flask is covered with aluminum foil to protect it from the light. The mixture is stirred for three hours under a nitrogen atmosphere. The resulting greenish precipitate (presumably AgBr plus excess of CuBr) is removed by filtering through a Celite bed. The yellowish solution is placed in the freezer at -20 ℃. Crystalline compound (0.120 g) is precipitated from this mixture after about 5 days (yield 65%). X-ray quality colorless crystals can be obtained from dilute CH_2Cl_2/hexafluorobenzene (50%:50%) solution at -20℃. This compound appears to be most stable among the Au, Ag and Cu norbornene adducts described here. However, it is best stored under nitrogen, in a low temperature freezer. ^{1}H NMR (CD_2Cl_2, 298 K): δ 0.53 (d, 1H), 1.12 (s, 3H), 1.77 (d, 2H), 3.23 (s, 2H), 5.77 (s, 2H, C***H***=C***H***). ^{13}C {^{1}H} NMR (CD_2Cl_2, 298 K): δ 24.7, 44.2, 45.9, 122.1 (s, ***C***H=***C***H). Raman (solid, 298K, cm^{-1}): 1491 cm^{-1} (C=C stretching band). Elemental analysis: calculated, C, 43.36%, H, 5.20%, found, C, 44.05%, H, 5.59%. M.P.: dec > 128 ℃, dec .

(6) **$[Au(C_7H_{10})_3][SbF_6]$**: AgSbF6 98% (0.140 g, 0.40 mmol) and norbornene (0.175 g, 1.8 mmol) are placed in a flask with magnetic stir bar. Dichloromethane (20 mL) is added at room temperature and stirred for a few minutes to obtain a clear solution. AuCl(0.115 g, 0.48 mmol) and norbornene (0.068 g, 0.7 mmol) are placed in a separate flask and dichloromethane (20 mL) is added and the mixture is stirred for a few minutes (10 minutes) to get a clear solution. The $AgSbF_6$/norbornene solution is then cooled to - 30 ℃ using dry ice-acetone bath and treated with AuCl /norbornene solution. The resulting mixture was protected from light (using aluminum foil) and stirred for 2 hours at - 30 ℃ and additional 3 hours at about 0 ℃. The mixture was filtered through a Celite bed to remove the resulting grey precipitate and the filtrate is collected and concentrated under reduced pressure to about 5 mL. The compound precipitate as a white solid. The supernatant is removed and the precipitate is dried under vacuum to obtain 0.115 g of white solid (yield 41%). Additional product can be obtained from the supernatant if

necessary, since it contains $[Au(C_7H_{10})_3][SbF_6]$ based on ^1H NMR data. ^1H NMR (CD_2Cl_2, 298 K): δ 0.49 (m, 1H), 0.78 (m, 1H), 1.15 (m, 2H), 1.88 (m, 2H), 3.30 (s, 2H), 5.53 (s, 2H, C***H***=C***H***). ^{13}C {^1H} NMR (CD_2Cl_2, 298 K): δ 25.2, 43.8, 44.1, 112.6 (br, ***C***H=***C***H). ^1H NMR (CD_2Cl_2, 273 K): δ 0.34 (m, 1H), 0.70 (m, 1H), 1.17 (m, 2H), 1.86 (m, 2H), 3.28 (s, 2H), 5.38 (s, 2H, C***H***=C***H***). ^{13}C {^1H} NMR (CD_2Cl_2, 298 K): δ 25.2, 43.2, 43.4, 109.2 (br, ***C***H=***C***H). Elemental analysis: calculated, C, 35.27%, H, 4.23%, found, C, 35.37%, H, 4.32%. The solubility of the compound drops significantly upon cooling, which presents difficulties when collecting ^{13}C NMR at low temperature (even below -20 ℃). X-ray quality colorless crystals can be obtained from a dichloromethane/hexafluorobenzene (50%:50%) solution at - 20 ℃. Solid samples slowly turn slightly pink (at least at the surface) if left exposed at light/air at room temperature. It is best stored under nitrogen, protected from light in a low temperature freezer. One of our first attempt to synthesize $[Au(C_7H_{10})_3][SbF_6]$ shows that it can be also made using $[Ag(C_7H_{10})_3][SbF_6]$ and AuCl but the reaction is not clean. For example, a mixture of $[Ag(C_7H_{10})_3][SbF_6]$ (0.200 g, 0.32 mmol) and AuCl (0.115 g, 0.48 mmol) in dichloromethane (30 mL) at room temperature also gives $[Au(C_7H_{10})_3][SbF_6]$ in low yield along with some decomposition products. M.P.: dec > 65 ℃, dec.

(7) **$\{[Ag(C_{12}H_{18})][SbF_6]\}_n$**: 2.161 g of $AgSbF_6$ (98% purity, 6.16 mmol) and 1.000 g of (E,E,E)-1,5,9-cyclododecatriene (6.16 mmol) are placed in a 25 mL flask with a magnetic stir bar. Dichloromethane (20 mL) is added to this mixture at room temperature. A white solid precipitates immediately. The mixture is stirred overnight and then the supernatant liquid is removed by syringe. The precipitate is washed with 2 x 10 mL of dichloromethane to give $[Ag(ttt\text{-cdt})(SbF_6)]_n$ as a white powder in quantitative yield. It is not soluble in chlorinated solvents (perhaps has a polymeric structure), but dissolves well in acetone. It is not overly sensitive to light either. ^1H NMR (C_3D_6O, 298 K, ppm): δ 2.04, 2.05 (d, 12 H, overlapping with deuterated solvent), 5.03 (s, C*H*=C*H*). ^{13}C {^1H} NMR (C_3D_6O, 298 K, ppm): δ 33.0 (s, CH_2), 36.5 (s, CH_2), 131.2 (s, *C*H=*C*H). Elemental analysis: calc., C, 28.49 %, H, 3.59 %; found, C, 27.89 %, H, 3.71 %. M.P.: dec > 160 ℃.

(8) **$[Cu(C_{12}H_{18})][SbF_6]$**: 0.500 g of $[Ag(ttt\text{-cdt})(SbF_6)]_n$ (0.99 mmol) and 0.163 g of CuCl (90%, 1.48 mmol) were placed in a 50 mL flask with a magnetic stir bar. Dichloromethane (40 mL) was added to the mixture at room temperature. The mixture

was stirred for about 24 hours and filtered over a bed of Celite. The filtrate was collected and the solvent was removed under vacuum to give [Cu(*ttt*-cdt)($FSbF_5$)] in essentially quantitative yield. X-ray quality colorless crystals can be obtained from a CH_2Cl_2/hexafluorobenzene (1:1) solution at -20℃. This compound does not show any decomposition when exposed to air at room temperature. It can be stored in a vial without any precautions. However, solutions of [Cu(*ttt*-cdt)($FSbF_5$)] in chlorinated solvents, wet acetone and THF tend to decompose over time giving a deep green-bluish solution. ^{1}H NMR (CD_2Cl_2, 298 K, ppm): δ 2.42 (m, 6H), 2.60 (d, 6H), 5.87 (s, C*H*=C*H*). ^{13}C {^{1}H} NMR (CD_2Cl_2, 298 K, ppm): δ 36.4 (s, CH_2), 131.1 (s, *C*H=*C*H). Raman (solid, 298K, notable bands, cm^{-1}): 1581 (s, C=C). IR (Nujol, 298K, cm^{-1}): 1582 (vw, C=C). Elemental analysis: calc., C, 31.23 %, H, 3.93 %; found, C, 31.27 %, H, 3.84 %. M.P.: dec > 220 ℃

(9) [Cu($C_{12}H_{18}$)(CO)][SbF_6]: 0.500 g of [Cu(*ttt*-cdt)($FSbF_5$)] (1.08 mol) were dissolved in 5 mL of dichloromethane at room temperature. Carbon monoxide was gently bubbled into the solution for about 15 mins. The solution was concentrated under reduced pressure to a point where about 1 mL of solvent was left in the flask. Then the remaining solvent was evaporated under a carbon monoxide stream to give the carbonyl compound [Cu(*ttt*-cdt)(CO)][SbF_6]. ^{1}H NMR (CD_2Cl_2, 298 K, ppm): δ 2.38 (m, 6H), 2.57 (d, 6H), 5.86 (s, C*H*=C*H*). ^{13}C {^{1}H} NMR (CD_2Cl_2, 298 K, ppm): δ 36.2 (s, CH_2), 130.4, *C*H=*C*H). Raman (solid, 298K, notable bands, cm^{-1}): 2160 (s, C≡O), 1601 (s, C=C). IR (Nujol, 298K, cm^{-1}): 2160 (s, CO), 1602 (vw, C=C). M.P.: dec > 220 ℃, no appreciable transition is seeing for the loss of the coordinated CO.

(10) [CH_3B(3-(Mes)Pz)$_3$]Cu(η^2-C_2H_4): 0.400 g of [CH_3B(3-(Mes)Pz)$_3$]Tl[180] (0.51 mmol) and 0.171 g of [$Cu(SO_3CF_3)]_2.C_6H_6$ 90% (0.31 mmol) are put in a 50 mL flask, equipped with stirbar, and dissolved in 10 mL of dichloromethane, saturated with ethylene. The reaction is left stirring for 30 minutes. During this time, the saturation of the solution is maintained bubbling ethylene twice for 5 minutes every 15. The solvent is removed under vacuum and the compound is extracted with 20 mL of hexane saturated with ethylene. The extraction works at its best during a period of 3 hours. The precipitate is then filtered off. The solution is pumped dry under vacuum to give 0.280 g of whitish compound (yield 82%). A suitable crystal for X-ray diffraction can be obtained from a hexane solution at -20℃. This compound is stable and does not require particular care.

It can be stored in a dessiccator without decomposition. ^{1}H NMR ($CDCl_3$, 298 K): ^{1}H NMR ($CDCl_3$, 298 K): δ 1.10 (s, 3H, CH_3B), 1.87 (s, 18H, *o*-C***H***$_3$), 2.22 (s, 9H, *p*-C***H***$_3$), 2.61 (s, C***H***$_2$=C***H***$_2$), 5.97 (d, 3H, $^{3}J_{HH}$ = 1.9 Hz, C4***H***), 6.78 (s, 6H, *m*-C***H***), 7.74 (d, 3H, $^{3}J_{HH}$ = 1.9 Hz, C5***H***).

(11) [CH_3B(3-(Mes)Pz)$_3$]Ag(η^2-C_2H_4): 0.400 g of [CH_3B(3-(Mes)Pz)$_3$]Tl (0.51 mmol) and 0.157 g of Ag(SO_3CF_3) (0.66 mmol) are put in a 50 mL flask, equipped with stirbar, and dissolved in 10 mL of dichloromethane, saturated with ethylene. The reaction is left stirring for 30 minutes. During this time, the saturation of the solution is maintained bubbling ethylene twice for 5 minutes every 15. The solvent is removed under vacuum and the compound is extracted with 20 mL of hexane saturated with ethylene. The extraction works at its best during a period of 3 hours. The precipitate is then filtered off. The solution is pumped dry under vacuum. When only a small quantity of solvent (tipically 1 mL) is left in the flask, ethylene is bubbled again into solution. At this point the liquid left can either be removed by vacuum or in stream of ethylene to give 0.209 g of white compound (yield 57%). A suitable crystal for X-ray diffraction can be obtained from a hexane solution at -20 ℃. This compound is stable and does not require particular care. It can be stored without decomposition. ^{1}H NMR ($CDCl_3$, 298 K): δ 1.13 (s, 3H, CH_3B), 1.86 (s, 18H, *o*-C***H***$_3$), 2.21 (s, 9H, *p*-C***H***$_3$), 3.42 (s, C***H***$_2$=C***H***$_2$), 6.00 (d, 3H, $^{3}J_{HH}$ = 2.0 Hz, C4***H***), 6.77 (s, 6H, *m*-C***H***), 7.78 (d, 3H, $^{3}J_{HH}$ = 2.0 Hz, C5***H***). ^{13}C {^{1}H} NMR ($CDCl_3$, 298 K, ppm): δ 5.0, 20.6, 21.1, 95.4 (br, ***C***H_2=***C***H_2), 103.6, 127.7, 132.9, 133.1, 137.1, 138.0, 150.3. ^{1}H NMR (C_6D_{12}, 298 K): δ 1.13 (s, 3H, CH_3B), 1.86 (s, 18H, *o*-C***H***$_3$), 2.18 (s, 9H, *p*-C***H***$_3$), 3.40 (s, C***H***$_2$=C***H***$_2$), 5.89 (d, 3H, $^{3}J_{HH}$ = 2.0 Hz, C4***H***), 6.69 (s, 6H, *m*-C***H***), 7.72 (d, 3H, $^{3}J_{HH}$ = 2.0 Hz, C5***H***). Elemental analysis: calc., C, 65.29 %, H, 6.46 %, N, 11.71 %; found, C, 65.11 %, H, 6.35 %, N, 11.72 %. M.P.: ≥ 101 ℃ dec. [CH_3B(3-(Mes)Pz)$_3$]Ag(η^2-C_2H_4) crystallizes in the Trigonal crystal system and *R*3c space group. The structure was solved using Direct methods. The molecule sits on a three-fold rotation axis containing B and Ag. Unfortunately, this makes the ethylene moiety disordered equally over three sites. Hydrogen atoms of the ethylene unit could not be located cleanly from the difference map. The B-CH_3 hydrogen atoms were located and included. Other hydrogens, including those on C_2H_4, were placed at the calculated positions and refined using a riding model. All non-hydrogen atoms were refined anisotropically. $C_{39}H_{46}N_6AgB$, Rhombohedral, Space group *R*3c; 100K; a=b=12.0079(5) Å, c = 43.861(2) Å, V = 5477.0(4) Å^3, Z = 6, ρ(calc.) = 1.305 Mg/m^3;

R1, wR2 ($I > 2\sigma(I)$) = 0.0176, wR2 = 0.0452; GOF = 1.074.

(12) $[CH_3B(3\text{-}(Mes)Pz)_3]Cu(CO)$: 0.400 g of $[CH_3B(3\text{-}(Mes)Pz)_3]Tl$ (0.51 mmol) and 0.171 g of $[Cu(SO_3CF_3)]_2.C_6H_6$ 90% (0.31 mmol) are put in a 50 mL flask, equipped with stirbar, and dissolved in 10 mL of dichloromethane, saturated with carbon monoxide. The reaction is left stirring for 30 minutes. During this time, the saturation of the solution is maintained bubbling carbon monoxide twice for 5 minutes every 15. The solvent is removed under vacuum and the compound is extracted with 20 mL of hexane saturated with carbon monoxide. The extraction works at its best during a period of 3 hours. The precipitate is then filtered off. The solution is pumped dry under vacuum to give 0.272 g of whitish compound (yield 81%). A suitable crystal for X-ray diffraction can be obtained from a hexane solution at -20℃. This compound is stable and does not require particular care. It can be stored at room temperature at the air without decomposition. ^1H NMR (CD_2Cl_3, 298 K): δ 1.08 (s, 3H, CH_3B), 1.88 (s, 18H, *o*-C***H***$_3$), 2.24 (s, 9H, *p*-C***H***$_3$), 6.07 (d, 3H, $^3J_{HH}$ = 2.3 Hz, C4***H***), 6.81 (s, 6H, *m*-C***H***), 7.76 ppm (d, 3H, $^3J_{HH}$ = 2.3 Hz, C5***H***). ^{13}C {^1H} NMR (CD_2Cl_3, 298 K, ppm): δ 20.8, 21.3, 105.1, 128.2, 131.6, 133.0, 137.9, 138.0, 151.2. FT-IR, ν(CO) cm^{-1}: 2075 cm^{-1} (KBr pellets, resolution 2 cm^{-1}). Elemental analysis: calc., C, 67.80 %, H, 6.29 %, N, 12.48 %; found, C, 67.33 %, H, 5.96 %, N, 12.10 %.

(13) $[CH_3B(3\text{-}(Mes)Pz)_3]Ag(CO)$: 0.100 g of $[CH_3B(3\text{-}(Mes)Pz)_3]Ag(\eta^2\text{-}C_2H_4)$ () are put in a 25 mL flask, equipped with stirbar, and dissolved in 5 mL of hexane. The reaction is left stirring for one hour. During this time, the carbon monoxide is bubbled every 5 minutes in the solution as a reagent and a carrier to purge non-coordinated ethylene out. The solvent is removed under vacuum until about 1 mL is left in the flask. At that point the solution is dried in a stream of carbon monoxide to give a white solid in quantitative yield. A suitable crystal for X-ray diffraction can be obtained from a hexane solution at –20 ℃. This compound is stable. It can be stored without decomposition, even though an inert atmosphere might be indicated. However it tends to evolve carbon monoxide from diluted solutions when dried in vacuum. ^1H NMR (C_6D_{12}, 298 K): δ 1.11 (s, 3H, CH_3B), 1.86 (s, 18H, *o*-C***H***$_3$), 2.15 (s, 9H, *p*-C***H***$_3$), 5.91 (d, 3H, $^3J_{HH}$ = 2.0 Hz, C4***H***), 6.69 (s, 6H, *m*-C***H***), 7.70 ppm (d, 3H, $^3J_{HH}$ = 2.0 Hz, C5***H***). ^{13}C {^1H} NMR ($CDCl_3$, 298 K, ppm): δ 5.0, 20.6, 21.1, 95.4 (br, ***C***H_2=***C***H_2), 103.6, 127.7, 132.9, 133.1, 137.1, 138.0, 150.3. FT-IR, ν(CO) cm^{-1}: 2125 cm^{-1} (KBr pellets, ^{13}CO satellite observed at 2079 cm^{-1},

Resolution 1 cm^{-1}); 2128 cm^{-1} (Hexane, Resolution 2 cm^{-1}); 2126 cm^{-1} (Nujol mull, Resolution 2 cm^{-1}); 2129 cm^{-1} (CH_2Cl_2, Resolution 2 cm^{-1}) Elemental analysis: calc., C, 63.61 %, H, 5.90 %, N, 11.71 %; found, C, 63.17 %, H, 6.08 %, N, 11.40 %. M.P.: ≥ 105 ℃ dec. $[CH_3B(3\text{-}(Mes)Pz)_3]Ag(CO)$ crystallizes in *P2₁/n* space group. The structure was solved using Direct methods. There are two chemically similar but crystallographically different molecules in the asymmetric unit. All non-hydrogen atoms were refined anisotropically. All hydrogens atoms were placed at the calculated positions and refined using a riding model. $C_{38}H_{42}N_6AgBO$, Monoclinic, Space group *P2₁/n*; 198K; a = 24.2090(17) Å, b = 11.2923(8) Å, c = 23.8553(19) Å, β = 100.8030(10)°, V = 7211.5(9) $Å^3$, Z = 8, ρ(calc.) = 1.322 Mg/m^3; R1, wR2 ($I > 2\sigma(I)$) = 0.0402, wR2 = 0.0907; GOF = 1.023.

(14) {$CH_3B[3\text{-}(Mes)Pz]_3Au(CO)$}: equimolar amounts of $[CH_3B(3\text{-}(Mes)Pz)_3]Ag(CO)$ and AuCl were put in a flask and 20 mL of hexane were added at low temperature (~ - 50 ℃). The reaction was protected from light. When the reaction reached room temperature, it was allowed to stir for another hour and then the yellowish solid was filtred on Celite bed. The filtrate was put in the freezer at – 20 ℃ and after some days some crystals were formed. Unfortunately we were not able to collect a good diffraction, but FT-IR on the crushed crystal in KBr showed the presence of a sharp band at 2079 cm^{-1}.

APPENDIX B

NMR AND RAMAN SPECTRA

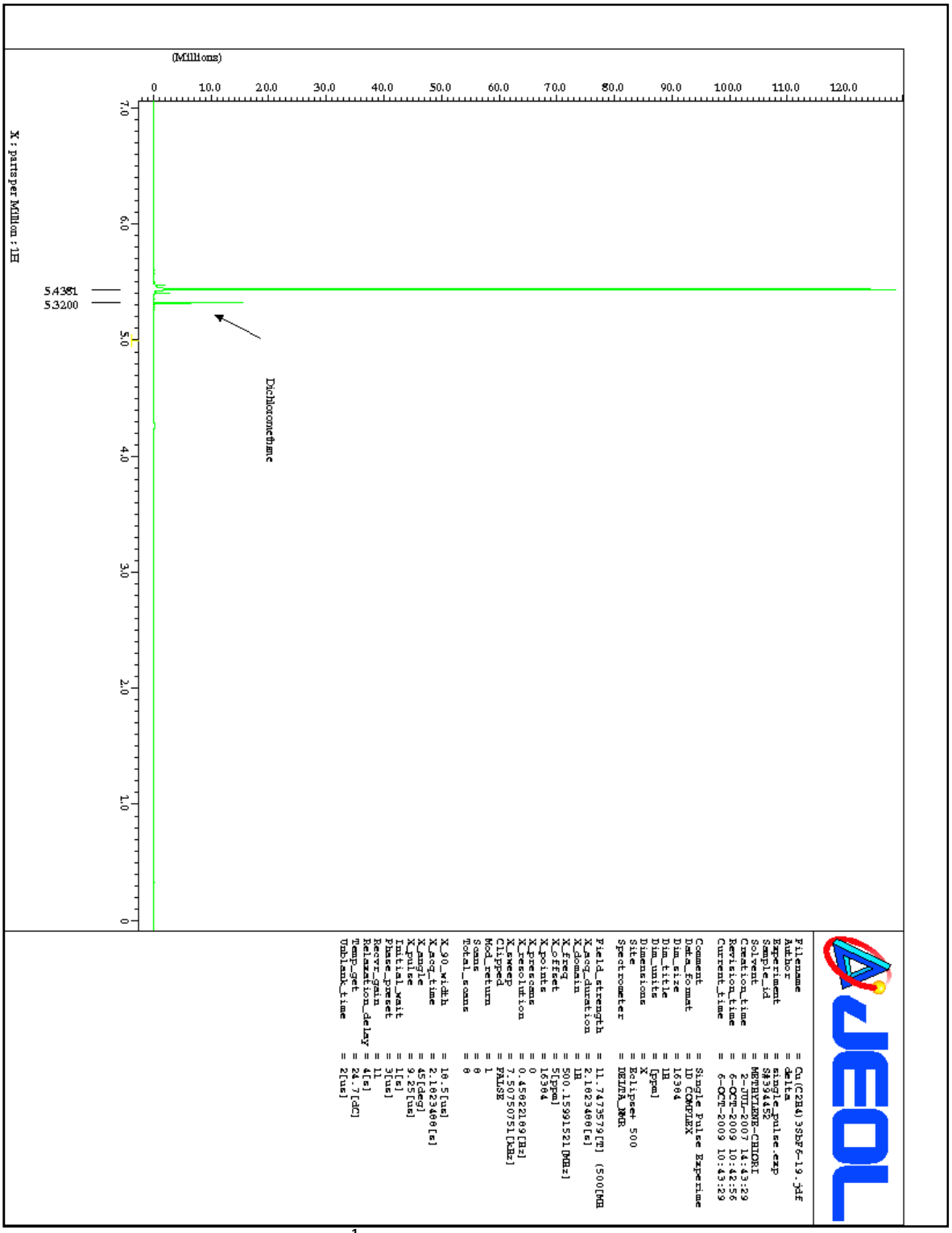

Figure B.1. ^{1}H NMR spectrum of $[Cu(C_2H_4)_3][SbF_6]$

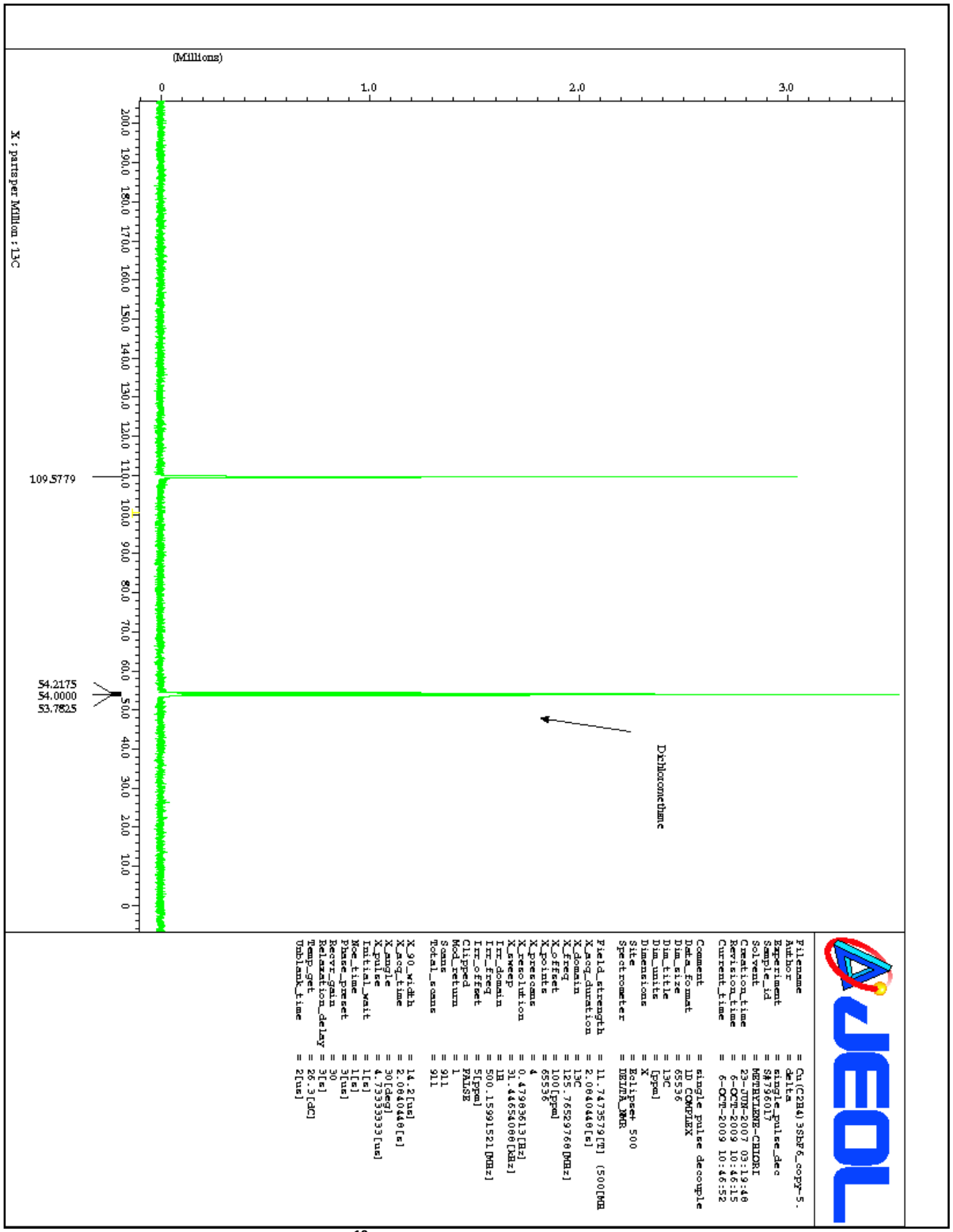

Figure B.2. ^{13}C NMR spectrum of $[Cu(C_2H_4)_3][SbF_6]$

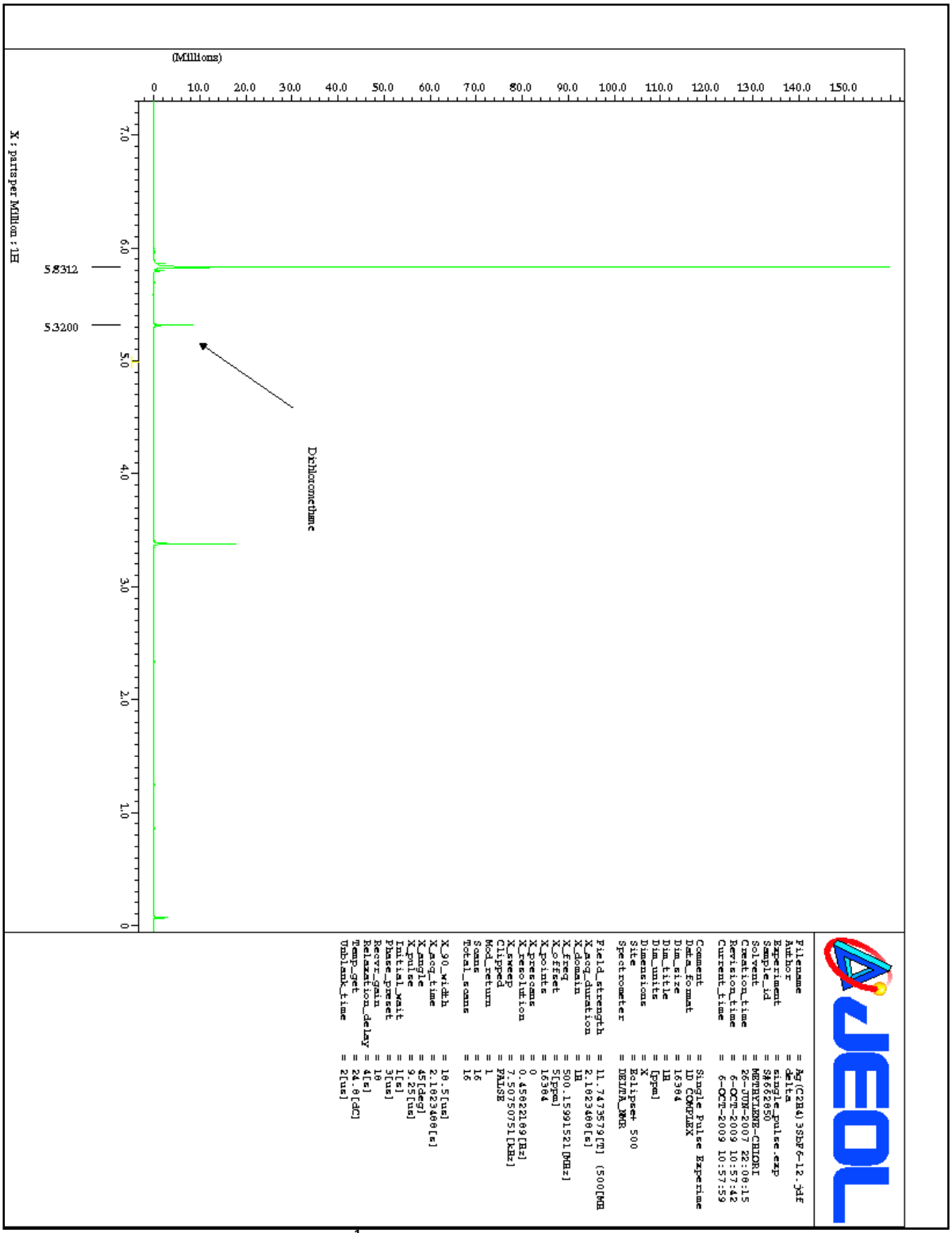

Figure B.3. ^{1}H NMR spectrum of $[Ag(C_2H_4)_3][SbF_6]$

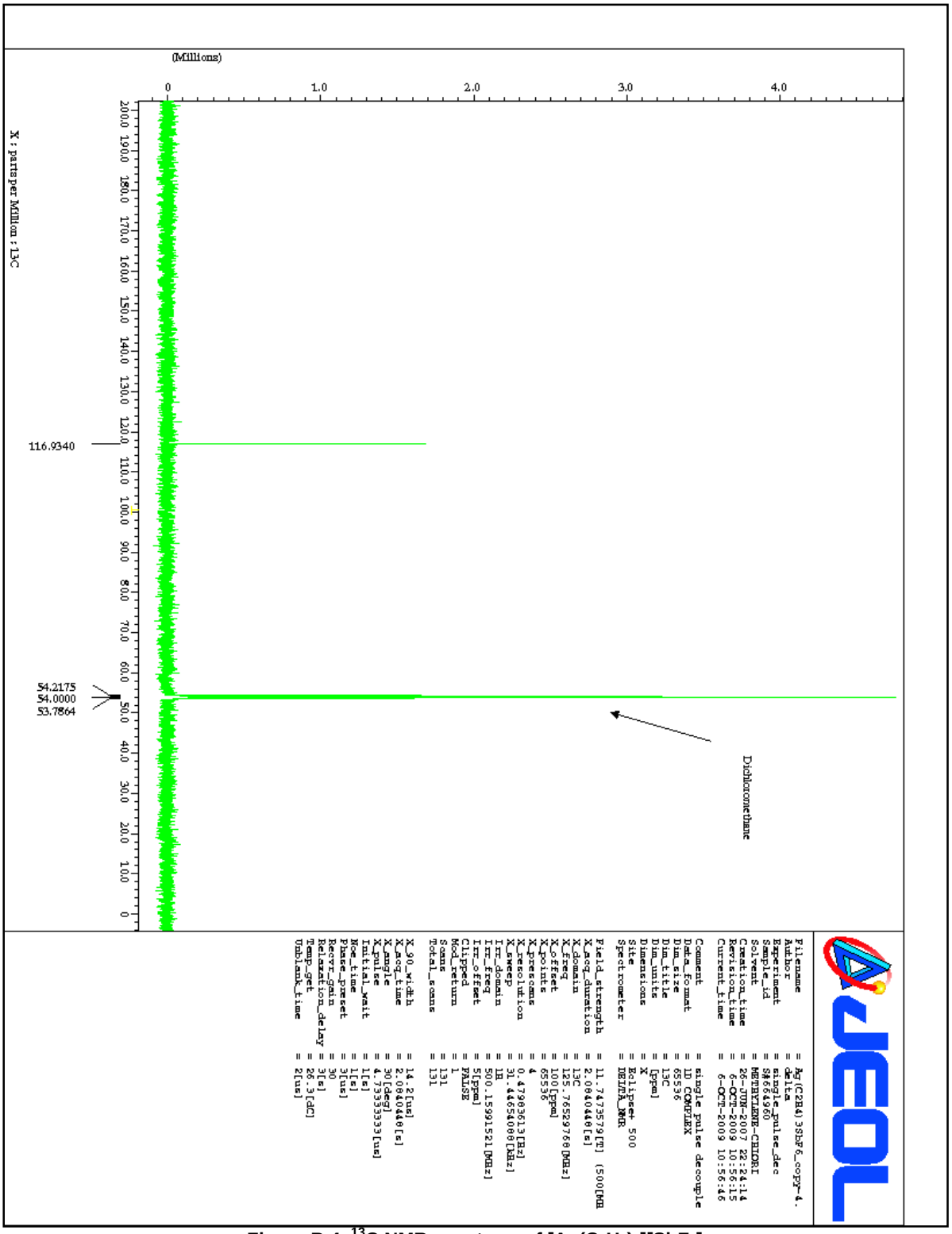

Figure B.4. ^{13}C NMR spectrum of $[Ag(C_2H_4)_3][SbF_6]$

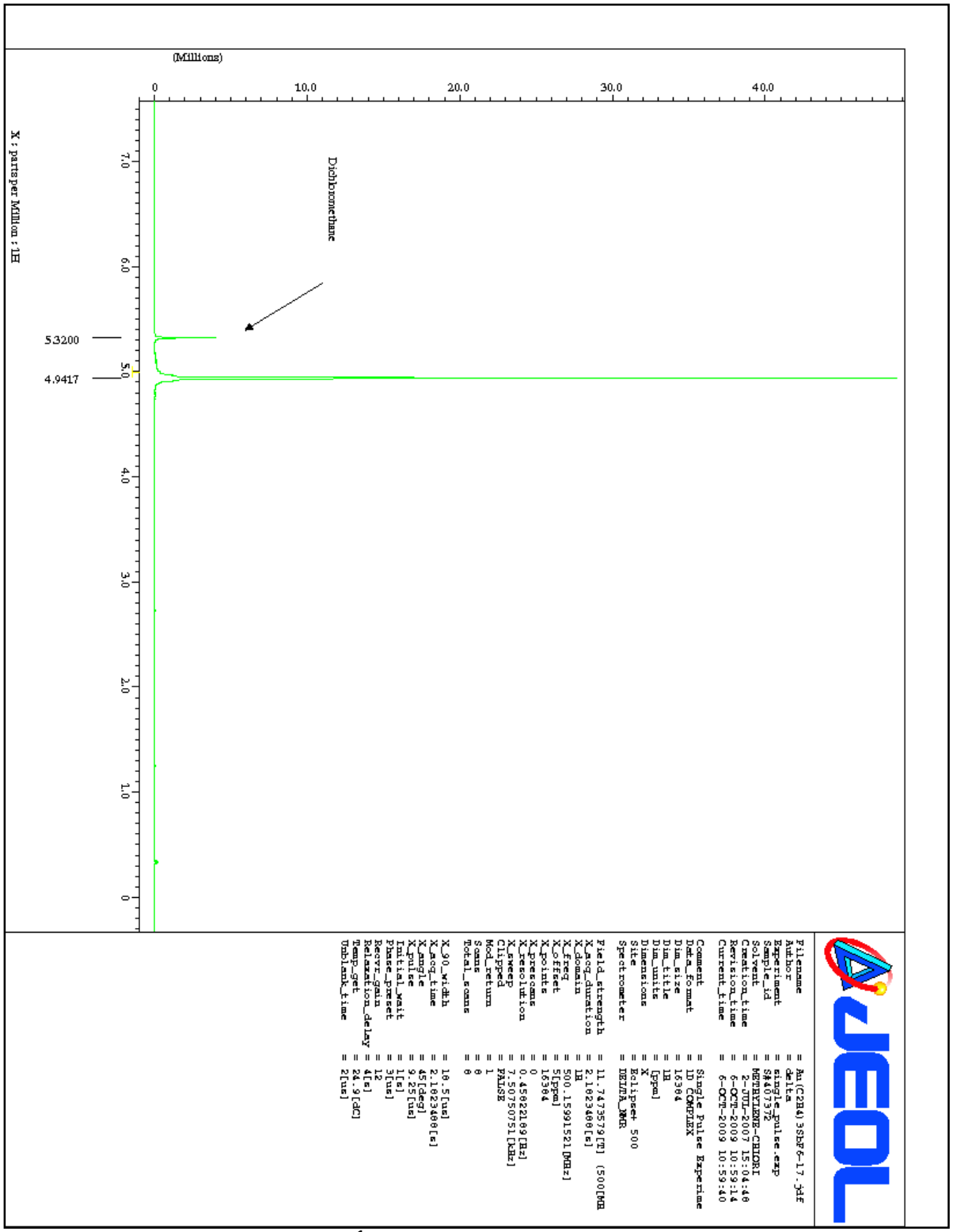

Figure B.5. ^{1}H NMR spectrum of $[Au(C_2H_4)_3][SbF_6]$

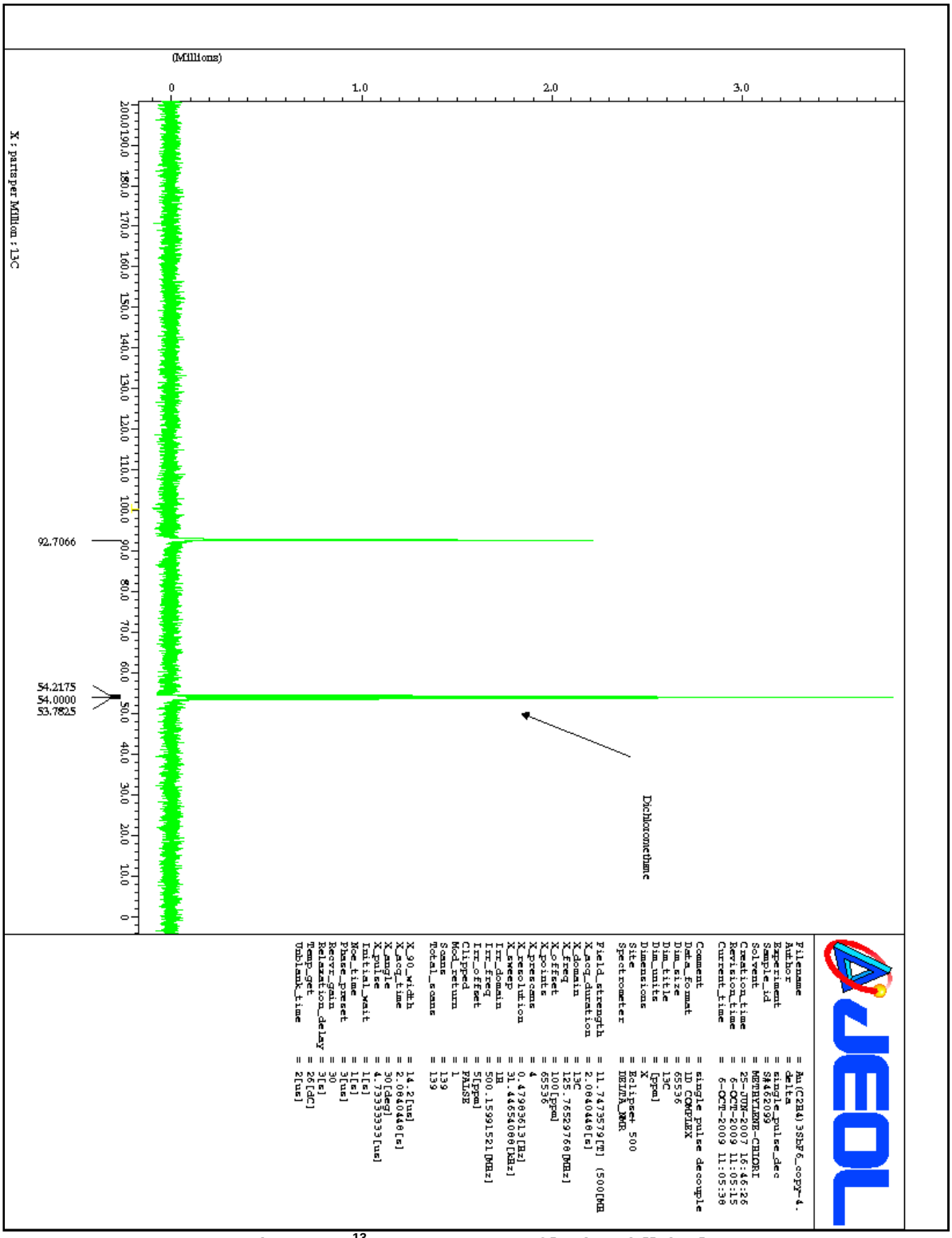

Figure B.6. ^{13}C NMR spectrum of $[Au(C_2H_4)_3][SbF_6]$

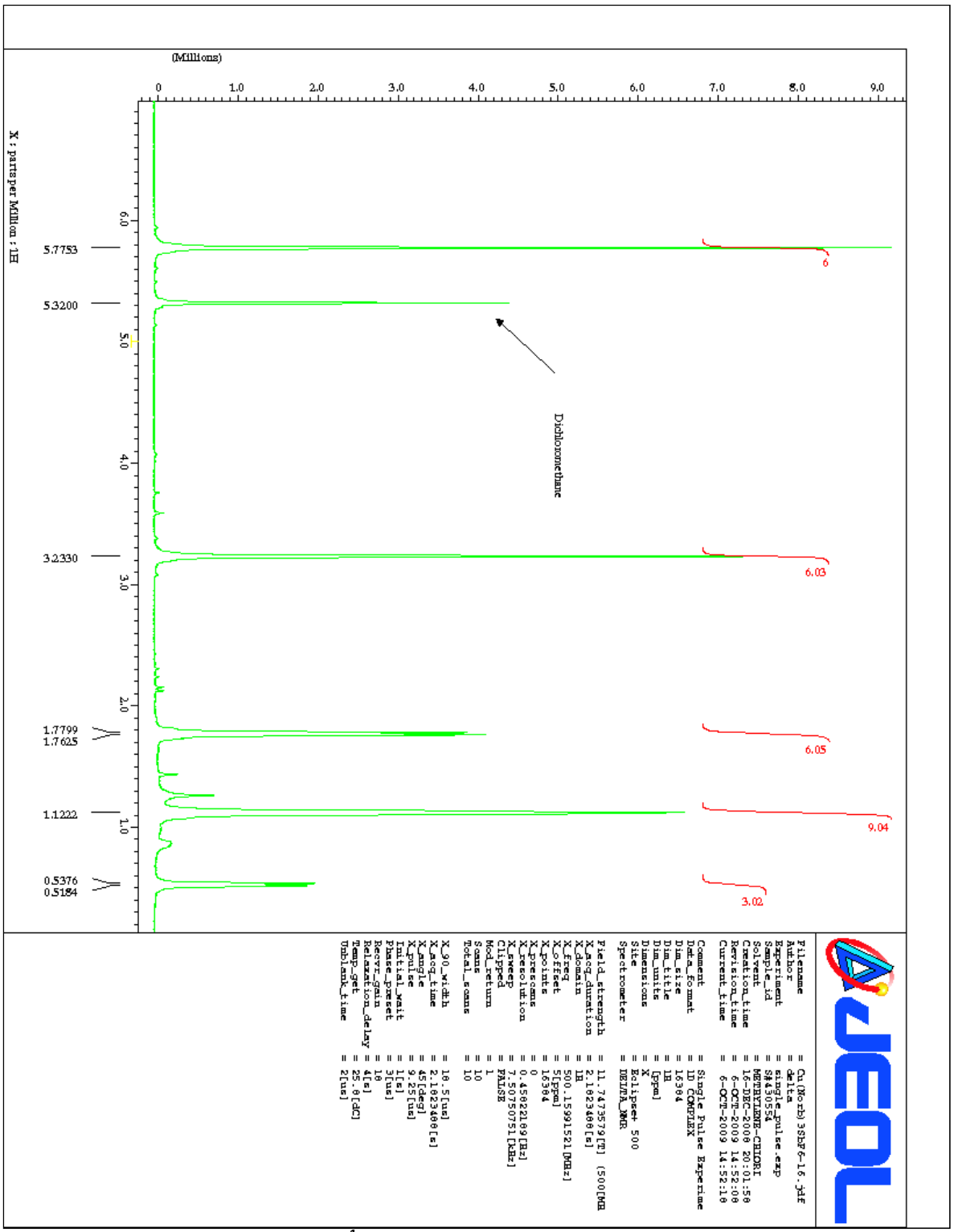

Figure B.7. ^{1}H NMR spectrum of $[Cu(C_7H_{10})_3][SbF_6]$

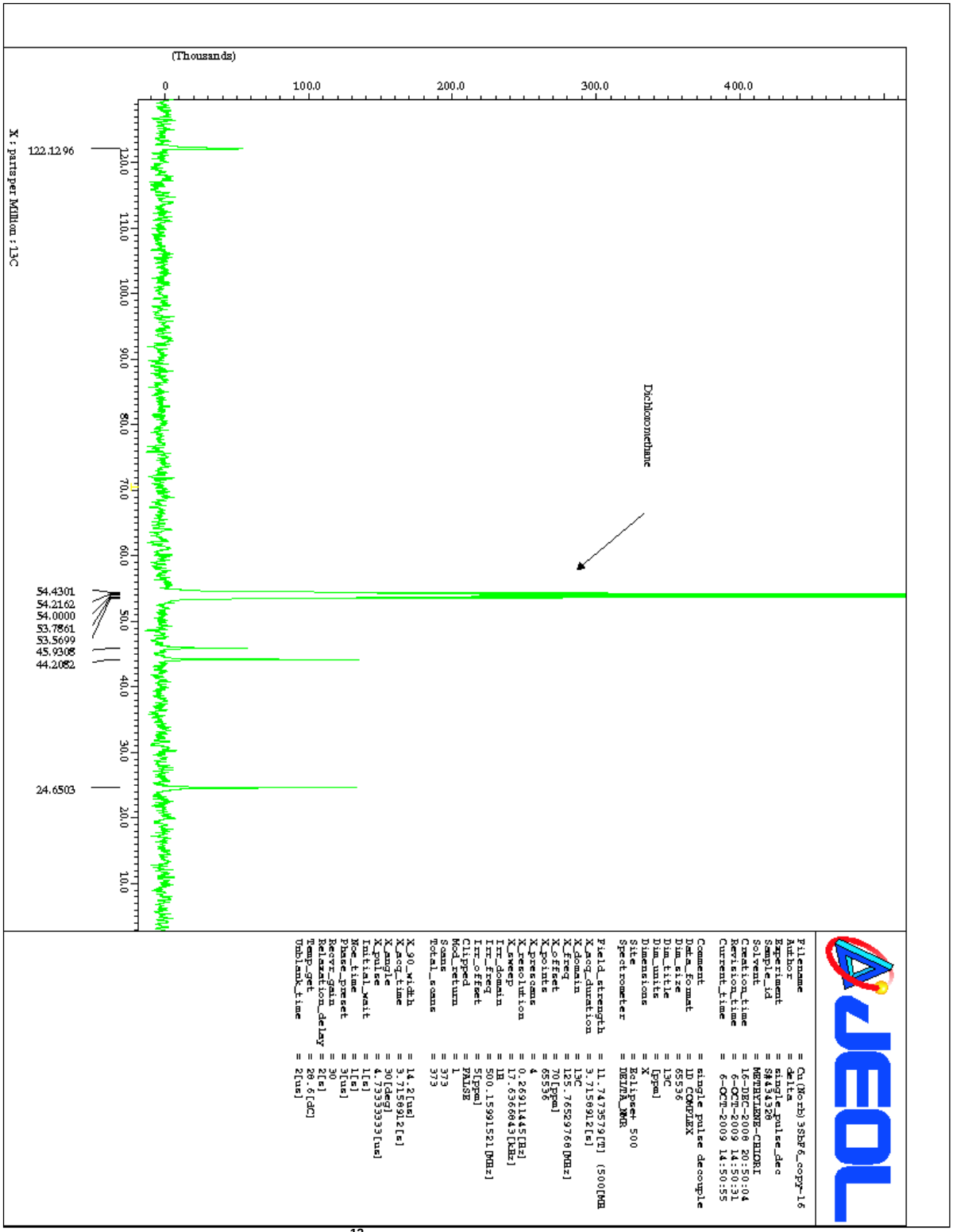

Figure B.8. ^{13}C NMR spectrum of $[Cu(C_7H_{10})_3][SbF_6]$

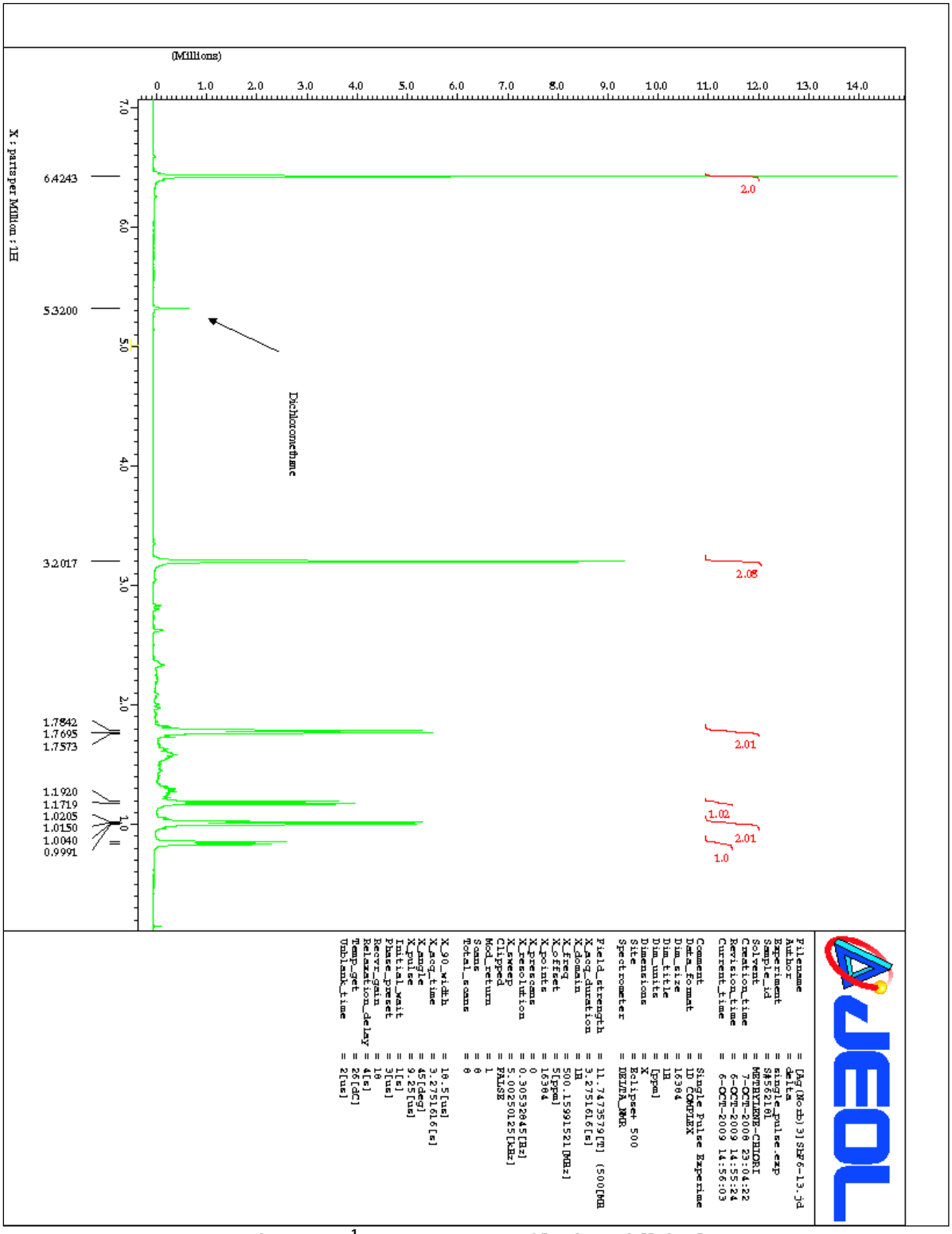

Figure B.9. ^{1}H NMR spectrum of $[Ag(C_7H_{10})_3][SbF_6]$

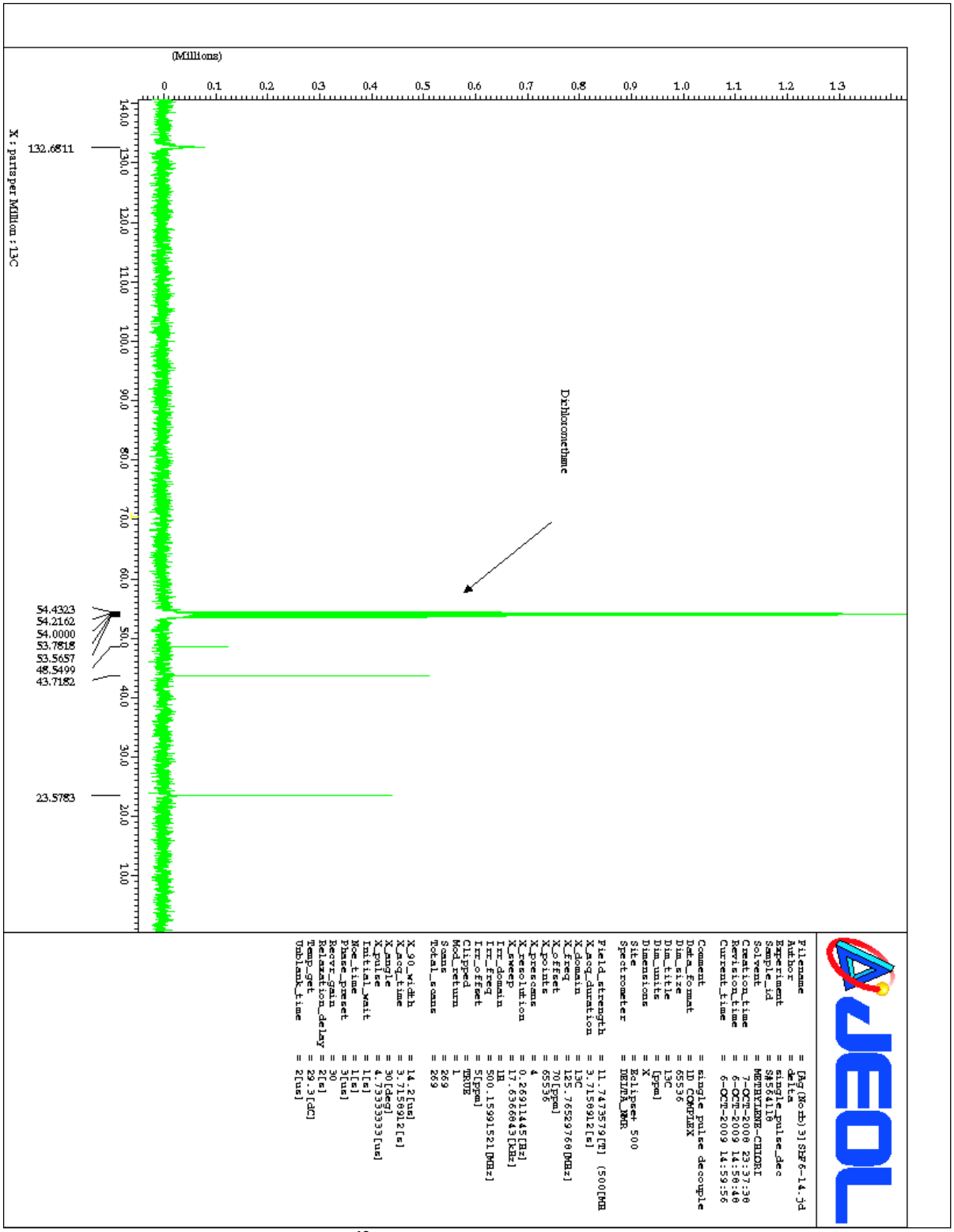

Figure B.10. ^{13}C NMR spectrum of $[Ag(C_7H_{10})_3][SbF_6]$

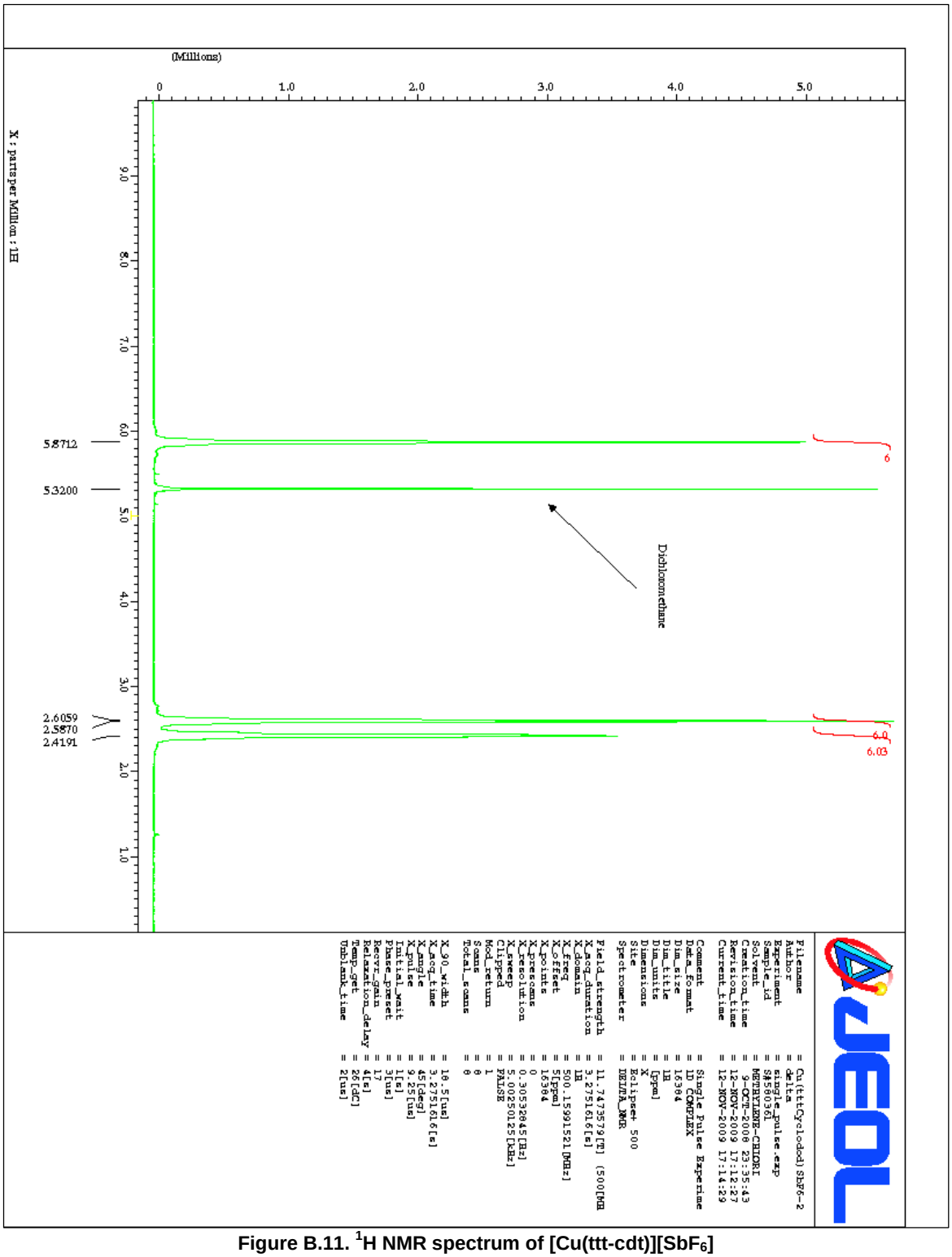

Figure B.11. ^{1}H NMR spectrum of [Cu(ttt-cdt)][SbF$_6$]

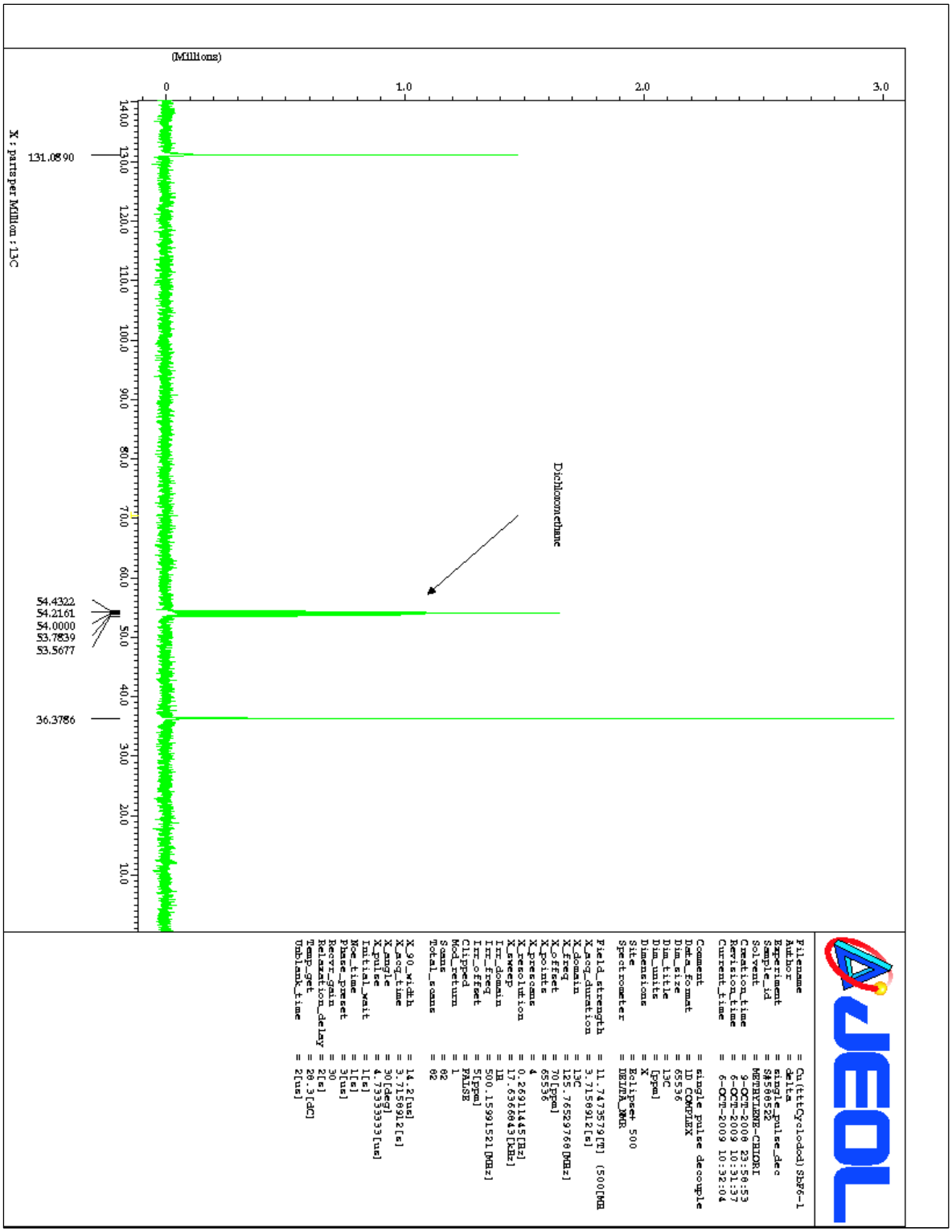

Figure B.12. ^{13}C NMR spectrum of [Cu(ttt-cdt)][SbF_6]

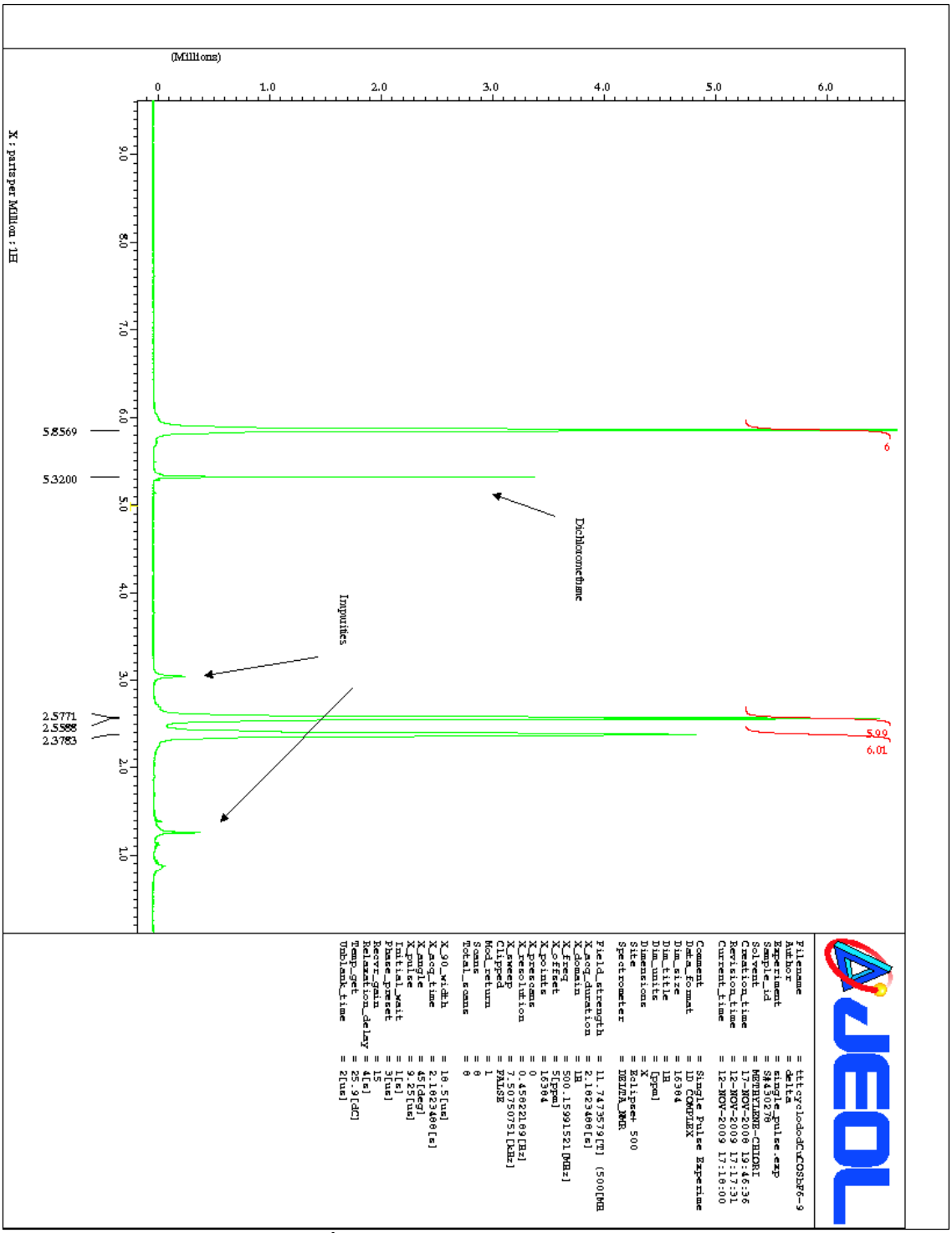

Figure B.13. ^{1}H NMR spectrum of [Cu(ttt-cdt)(CO)][SbF_6]

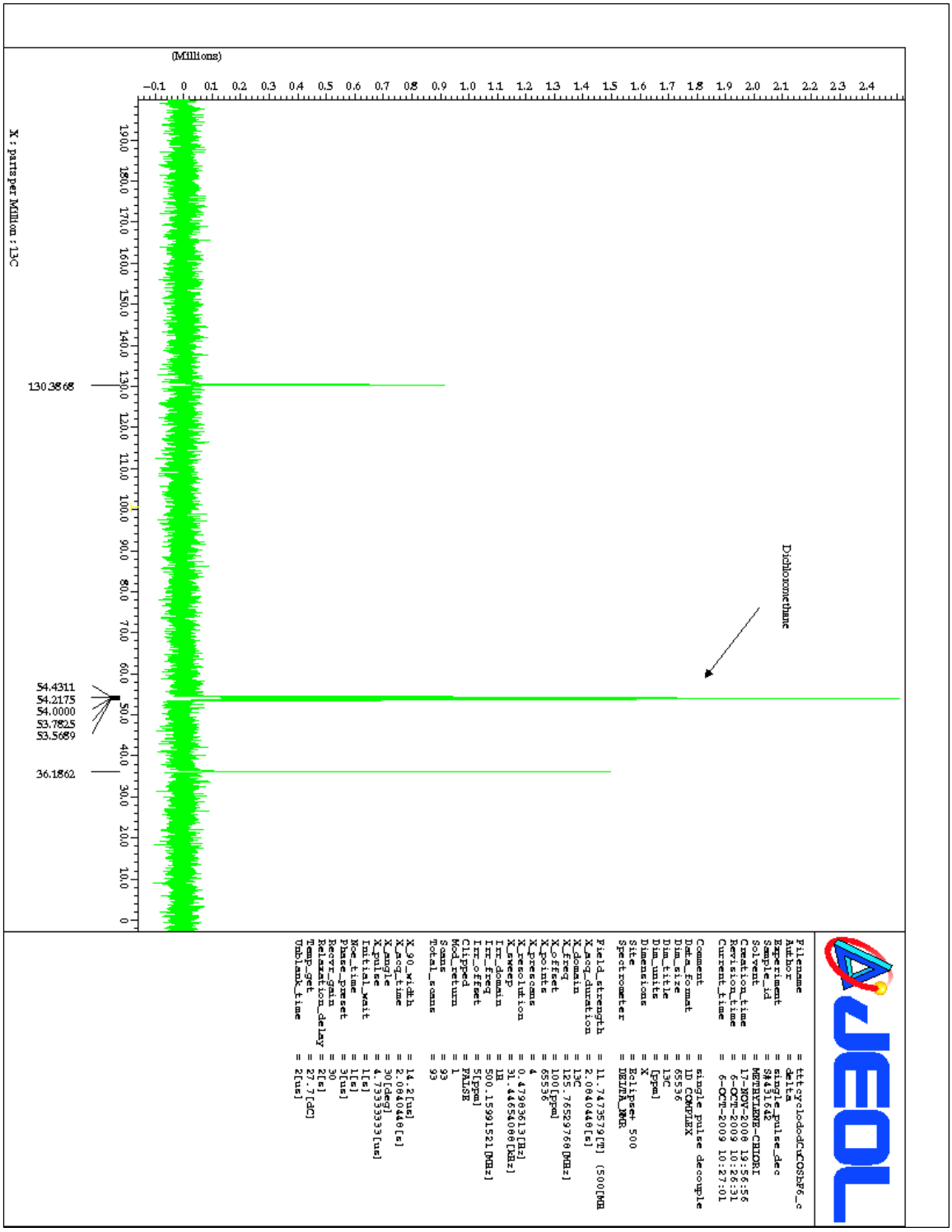

Figure B.14. ^{13}C NMR spectrum of [Cu(ttt-cdt)(CO)][SbF$_6$]

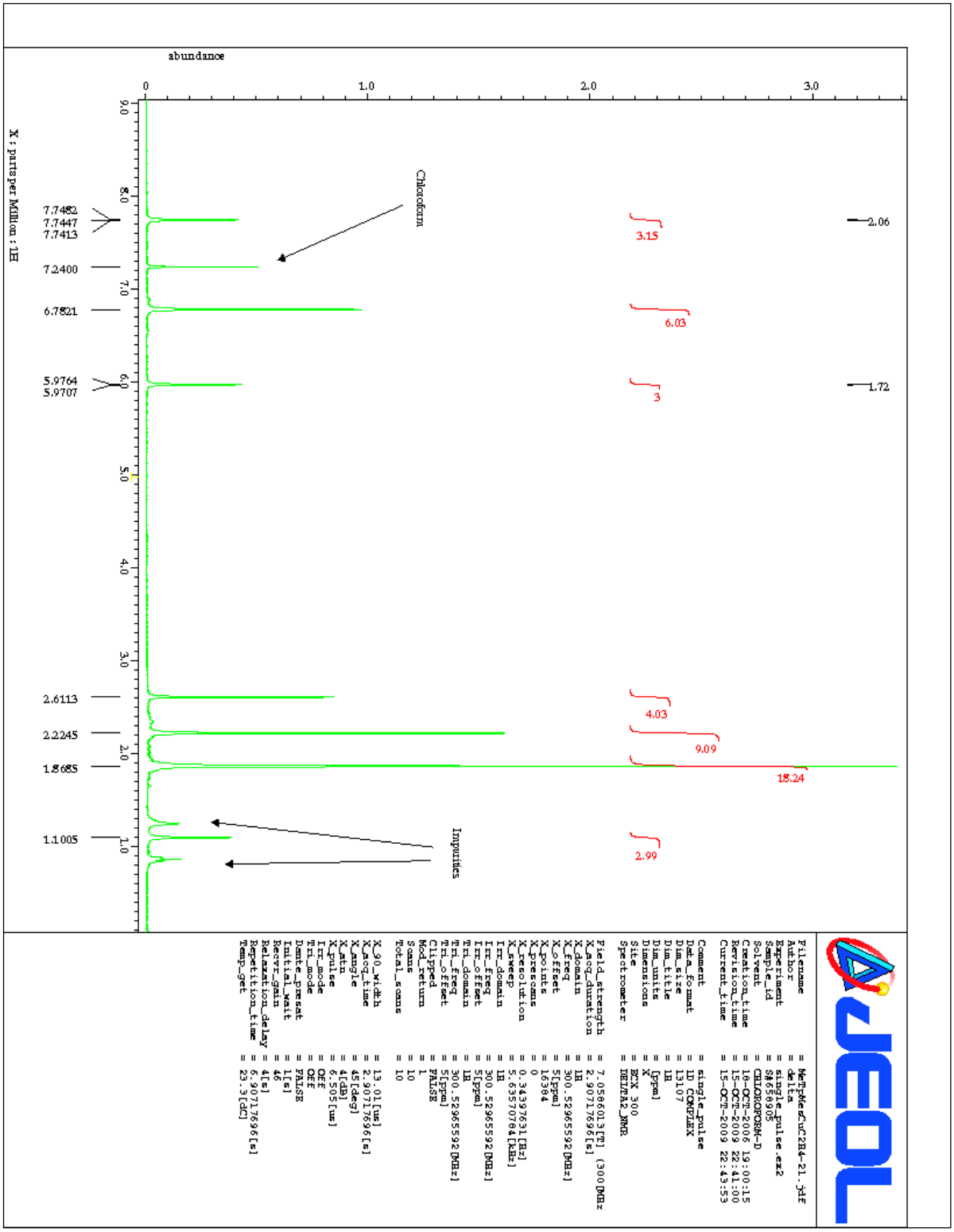

Figure B.15. ^{1}H NMR spectrum of $[CH_3B(3\text{-}(Mes)Pz)_3]Cu(\eta^2\text{-}C_2H_4)$

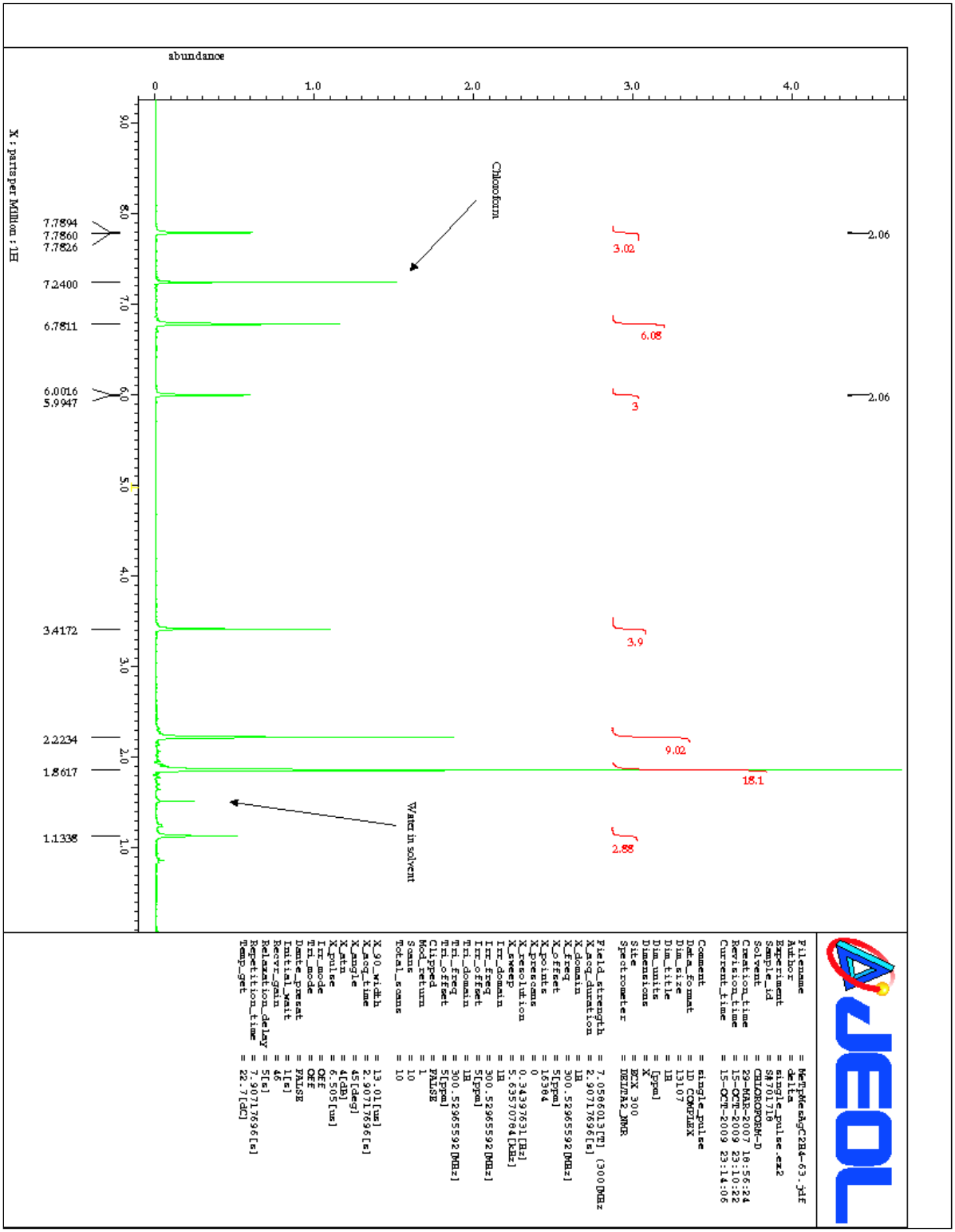

Figure B.16. ^{1}H NMR spectrum of $[CH_3B(3\text{-}(Mes)Pz)_3]Ag(\eta^2\text{-}C_2H_4)$

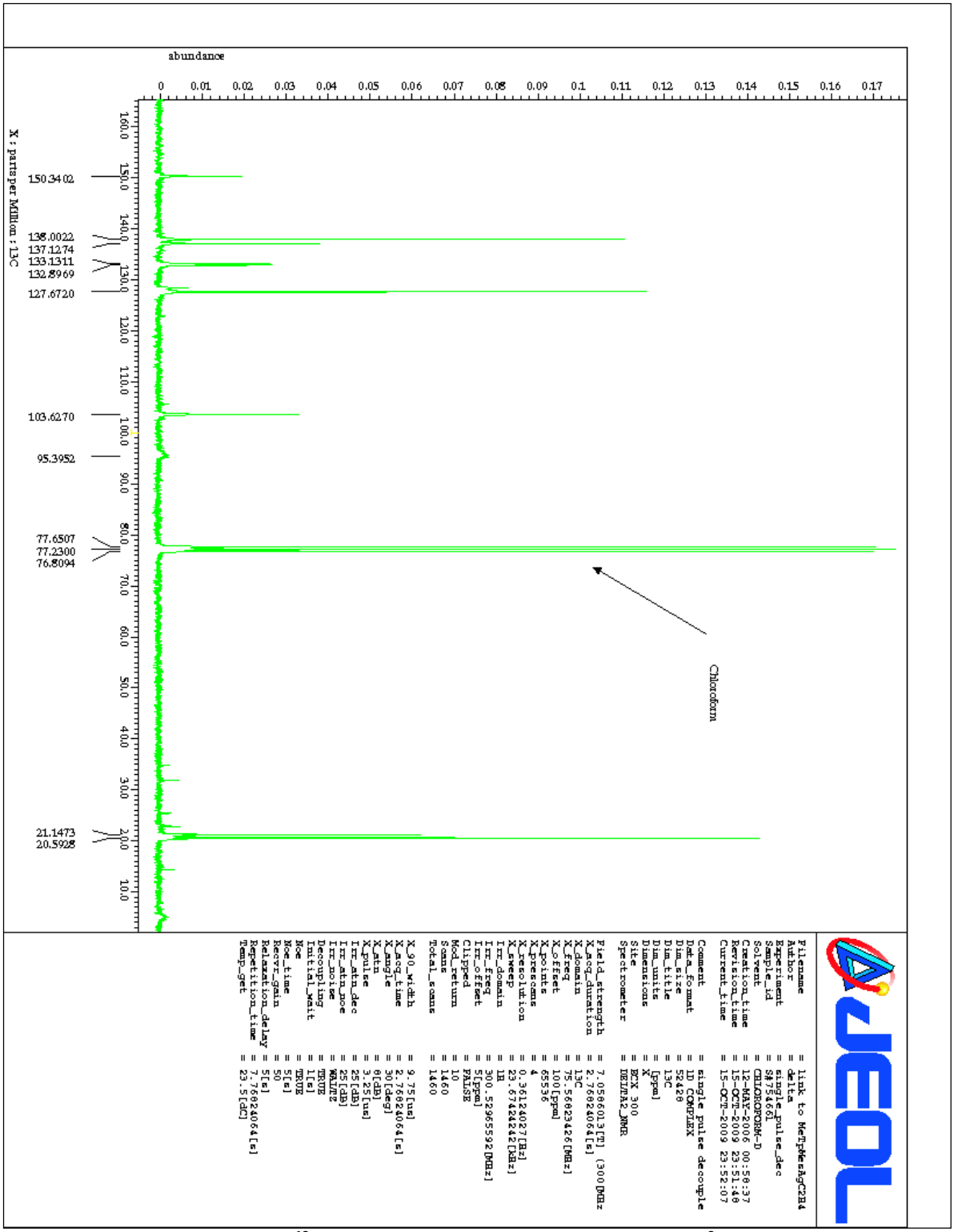

Figure B.17. ^{13}C NMR spectrum of $[CH_3B(3\text{-}(Mes)Pz)_3]Ag(\eta^2\text{-}C_2H_4)$

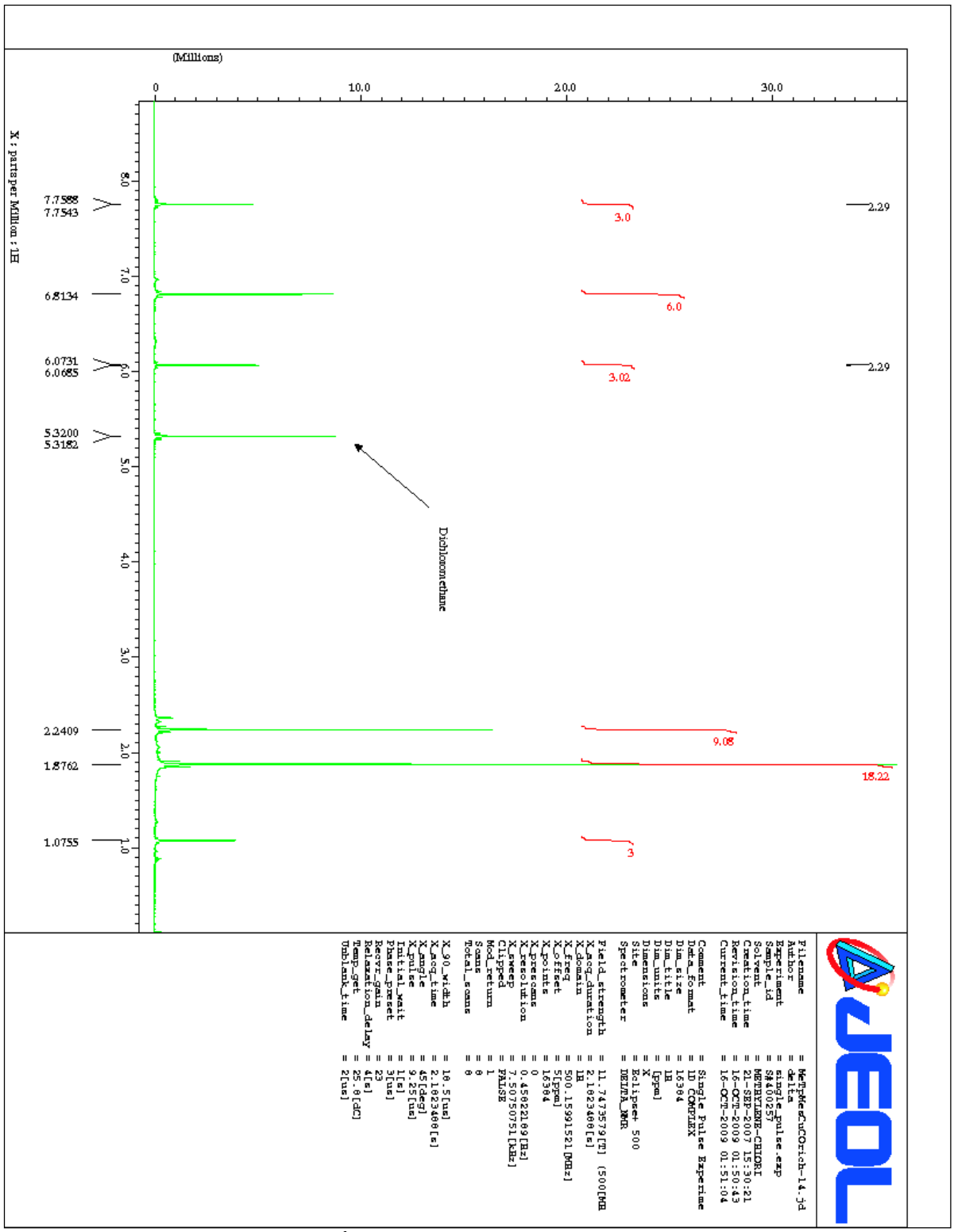

Figure B.18. ^{1}H NMR spectrum of $[CH_3B(3\text{-}(Mes)Pz)_3]Cu(CO)$

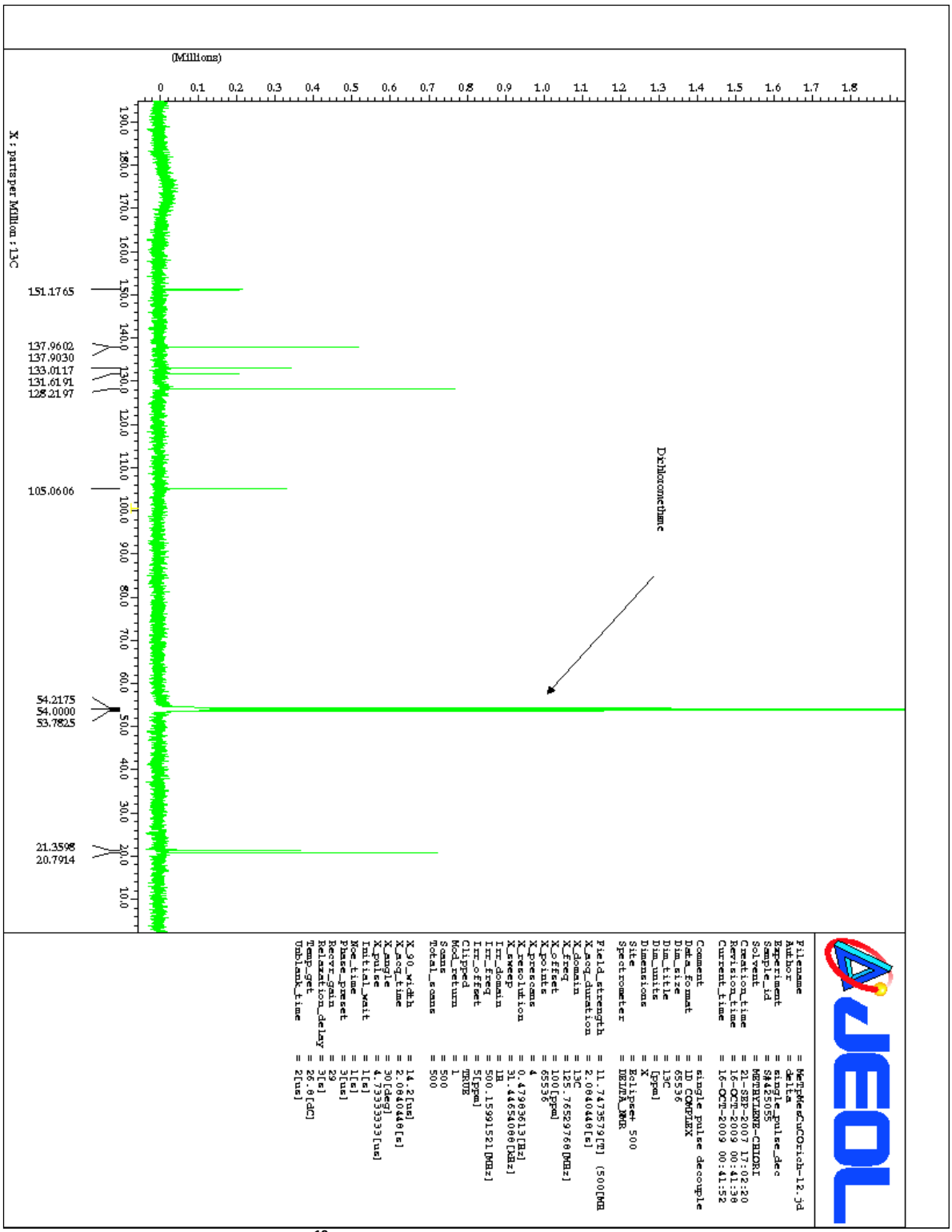

Figure B.19. ^{13}C NMR spectrum of $[CH_3B(3\text{-}(Mes)Pz)_3]Cu(CO)$

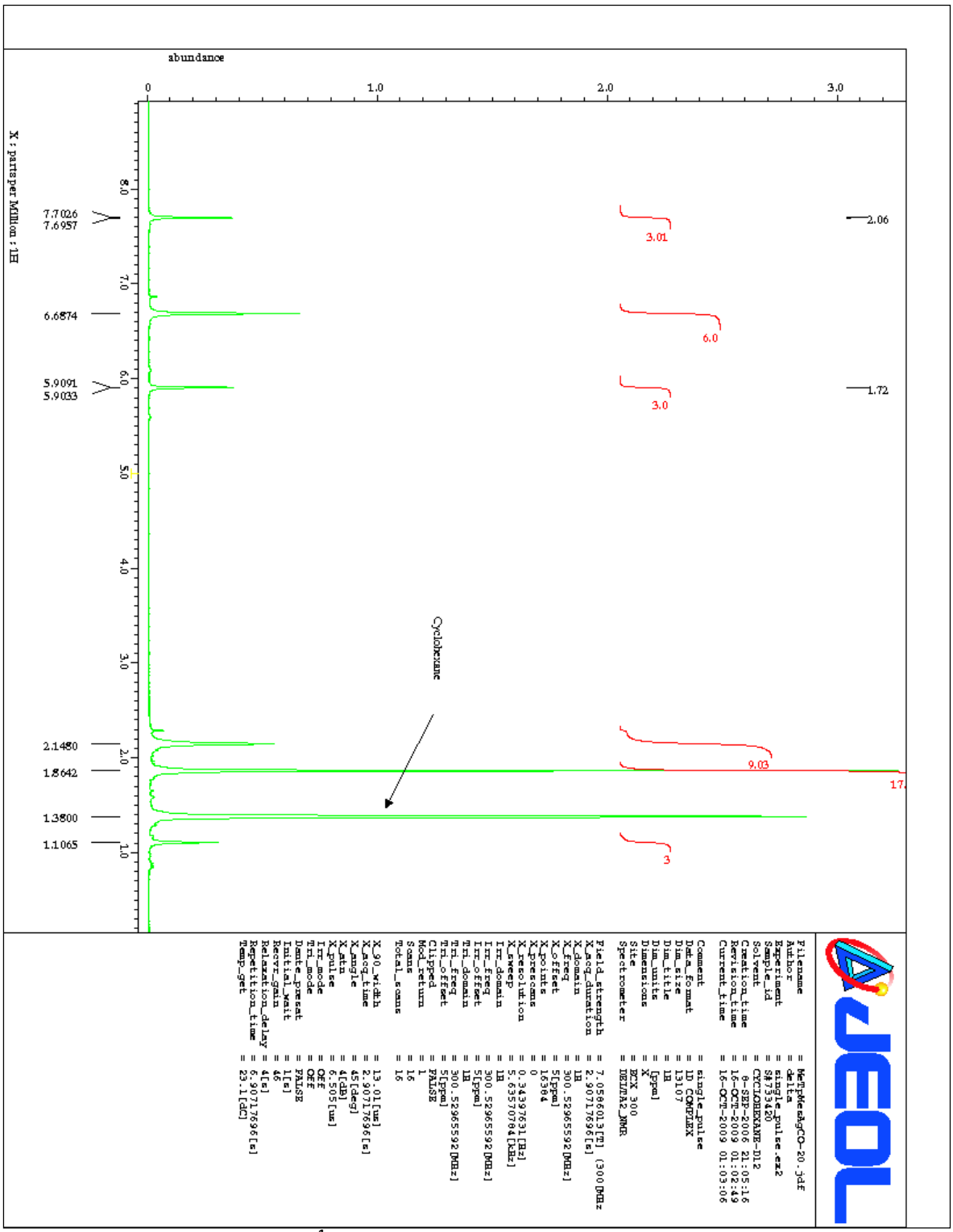

Figure B.20. ^{1}H NMR spectrum of $[CH_3B(3\text{-}(Mes)Pz)_3]Ag(CO)$

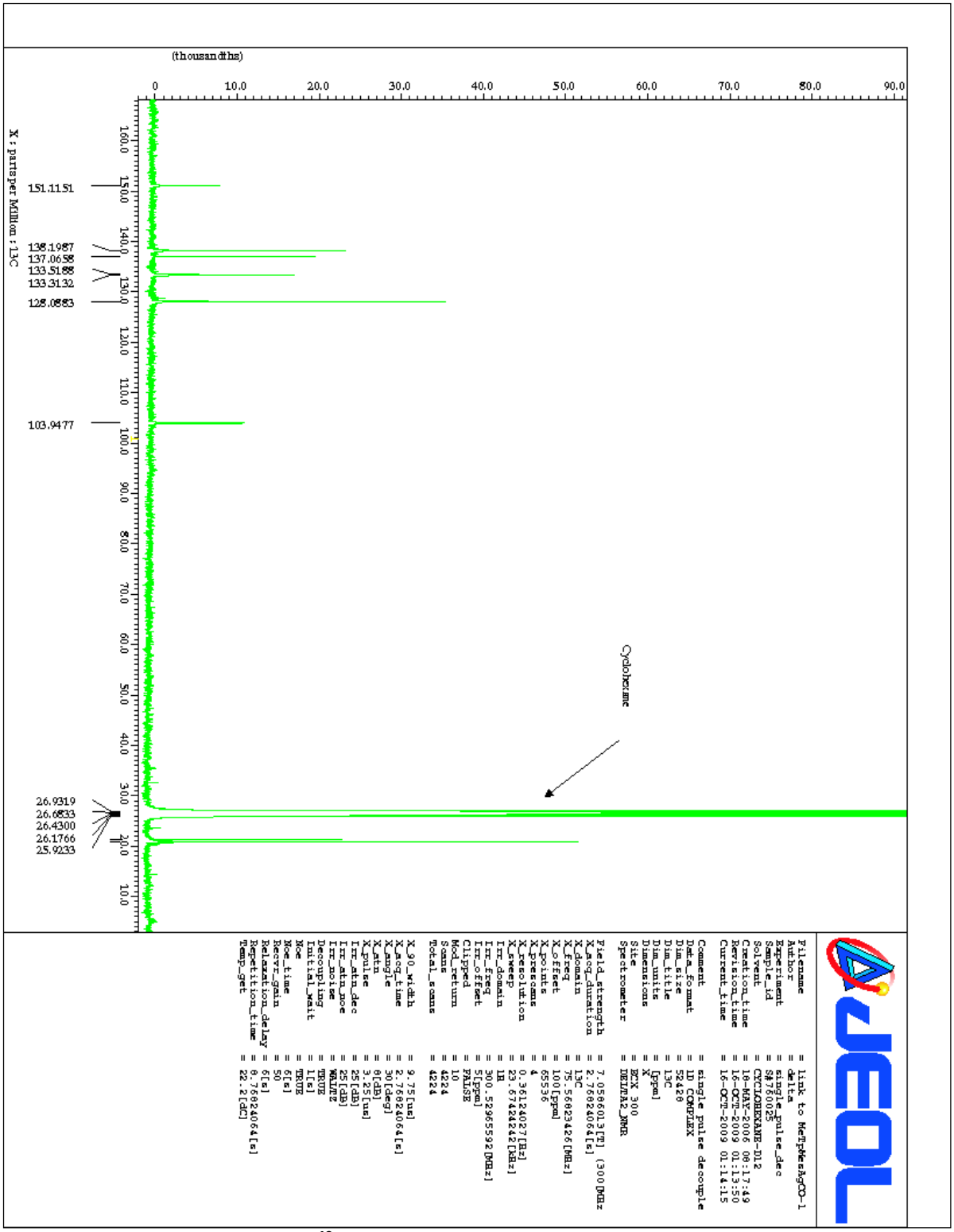

Figure B.21. ^{13}C NMR spectrum of [$CH_3B(3\text{-}(Mes)Pz)_3$]Ag(CO)

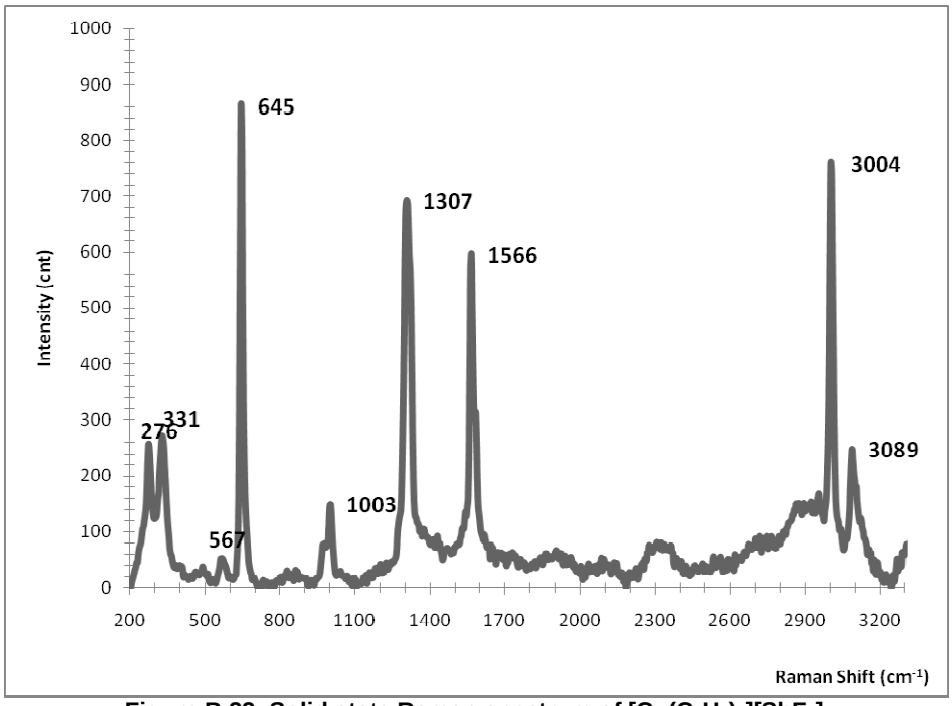

Figure B.22. Solid state Raman spectrum of $[Cu(C_2H_4)_3][SbF_6]$

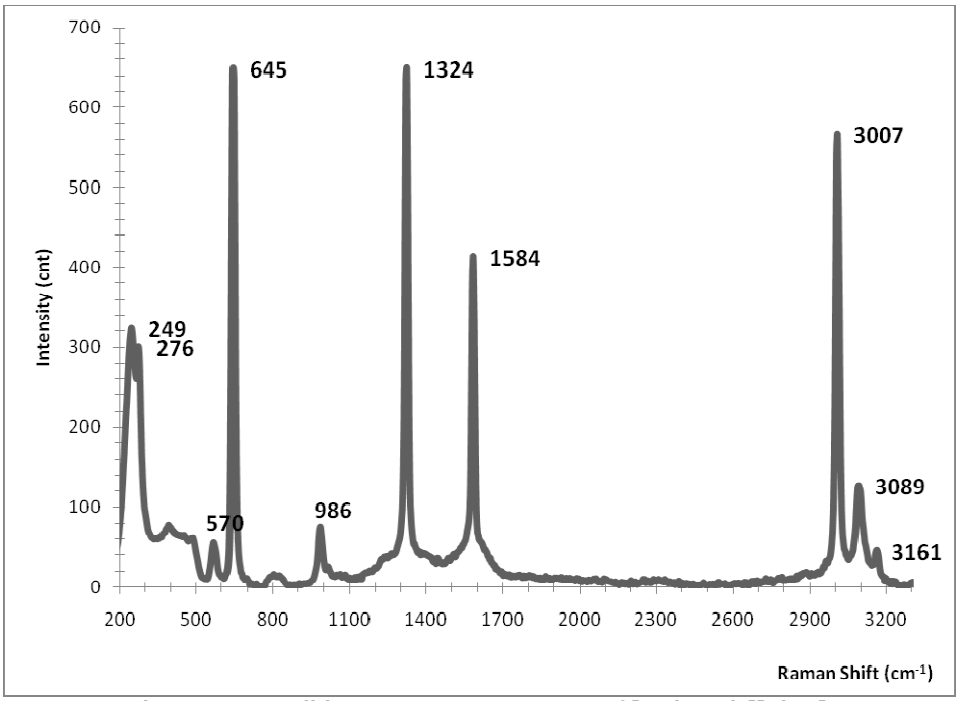

Figure B.23. Solid state Raman spectrum of $[Ag(C_2H_4)_3][SbF_6]$

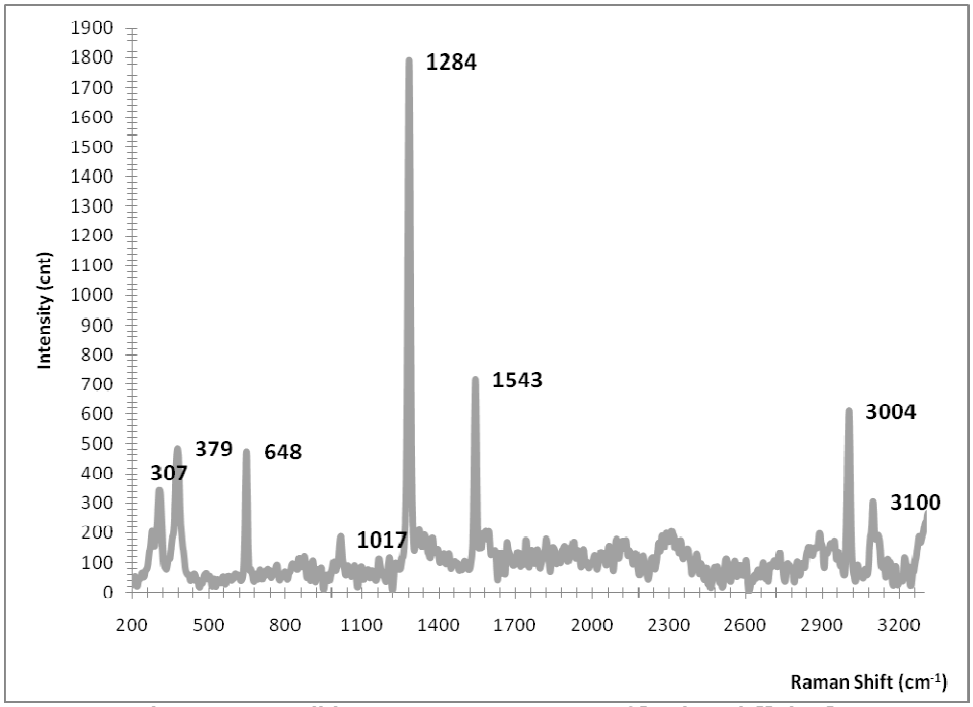

Figure B.24. Solid state Raman spectrum of $[Au(C_2H_4)_3][SbF_6]$

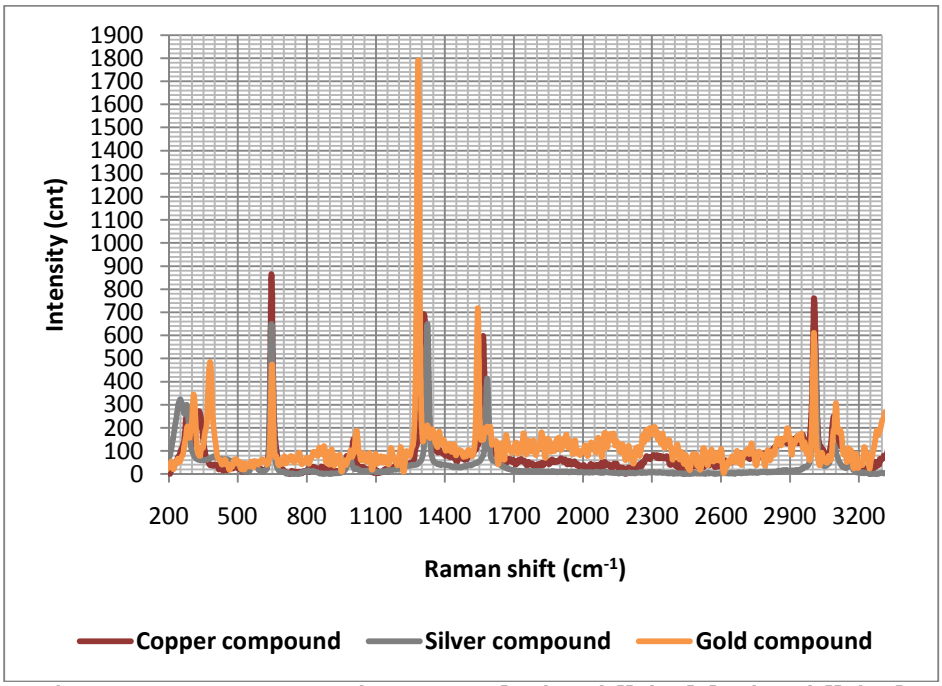

Figure B.25. Raman comparison among $[Cu(C_2H_4)_3][SbF_6]$, $[Ag(C_2H_4)_3][SbF_6]$ and $[Au(C_2H_4)_3][SbF_6]$

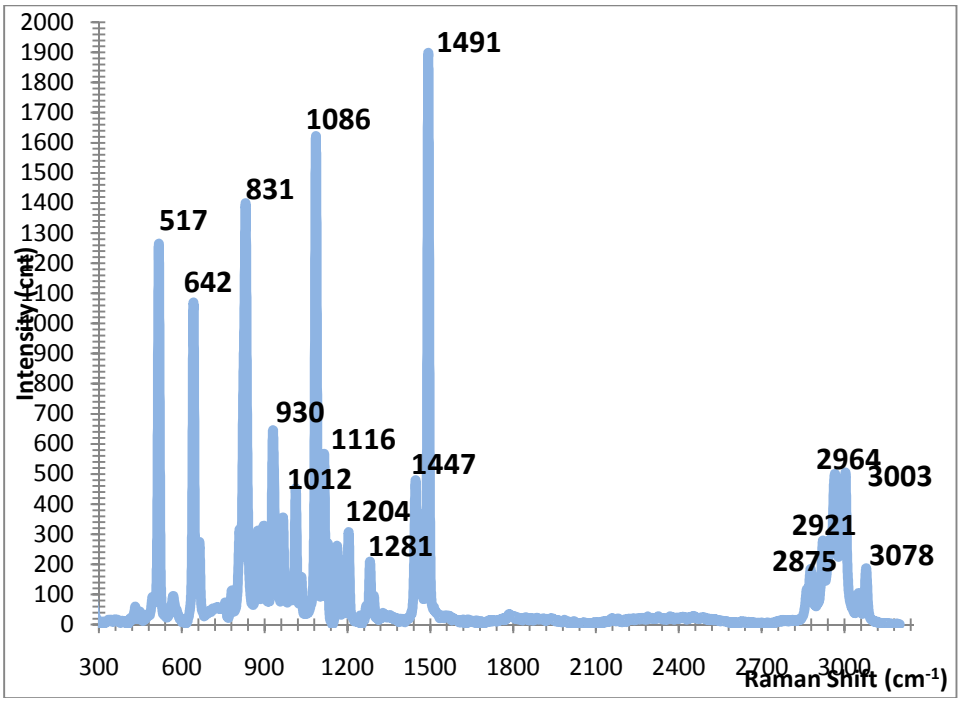

Figure B.26. Solid state Raman spectrum of $[Cu(C_7H_{10})_3][SbF_6]$

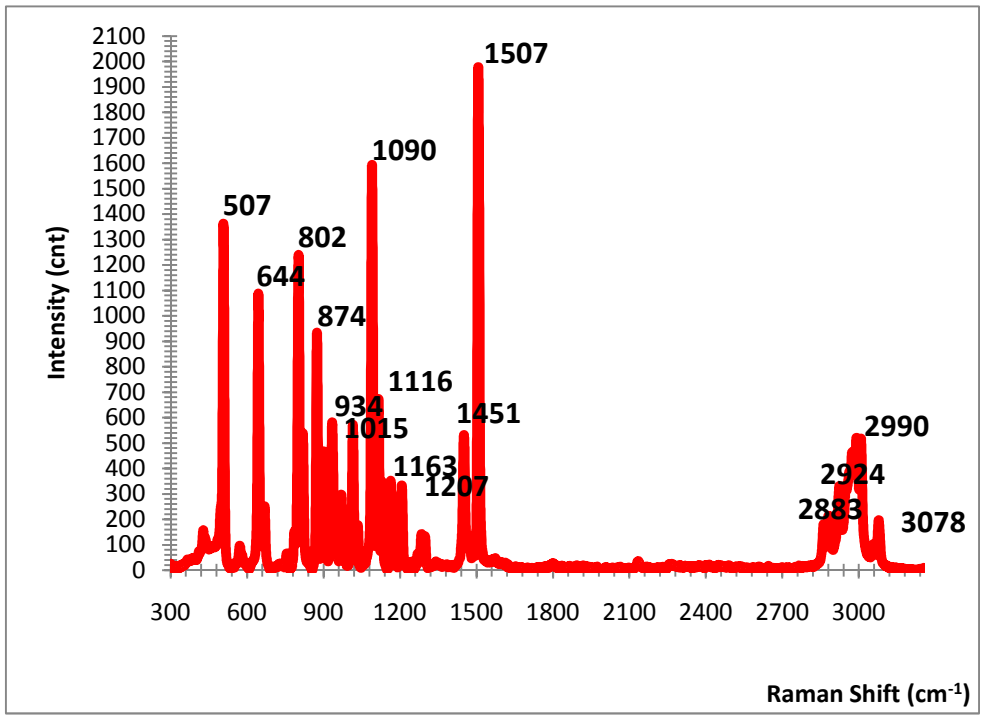

Figure B.27. Solid state Raman spectrum of $[Ag(C_7H_{10})_3][SbF_6]$

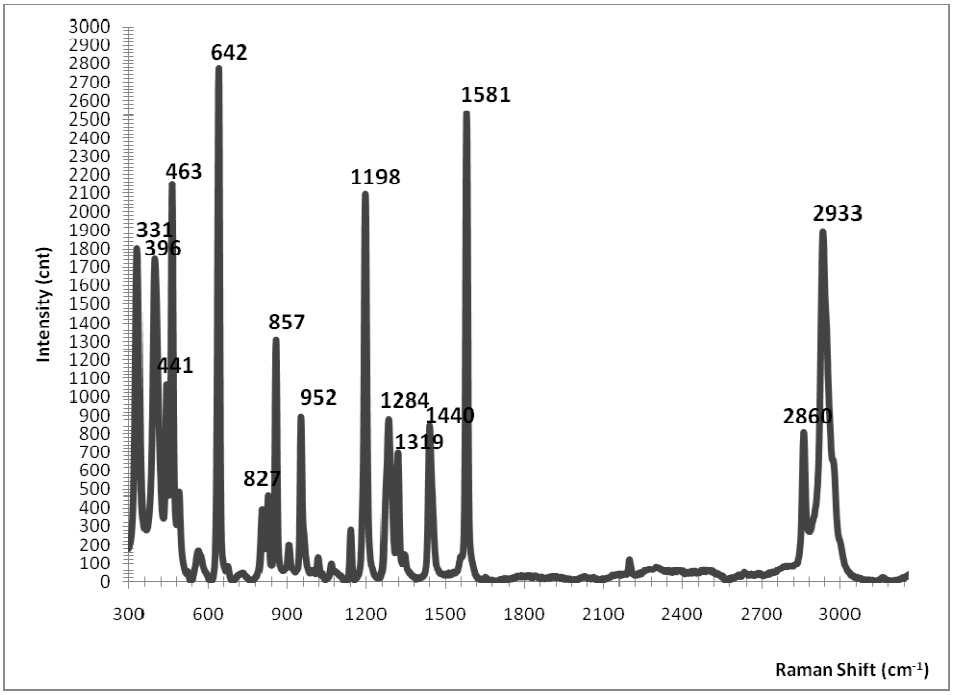

Figure B.28. Solid state Raman spectrum of [Cu(ttt-cdt)][SbF_6]

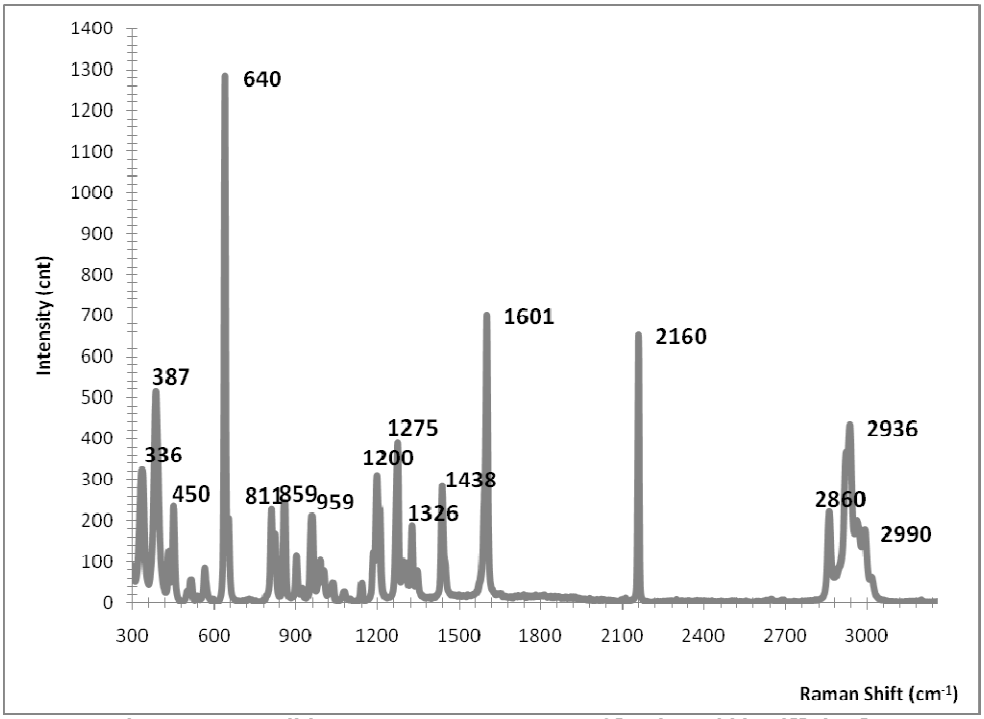

Figure B.29. Solid state Raman spectrum of [Cu(ttt-cdt)(CO)][SbF_6]

APPENDIX C

CARTESIAN COORDINATES TABLES OF SELECTED COMPOUNDS

$Cu(C_2H_4)_3^+$ cartesian coordinates

[B3PW91/aug-cc-pVTZ-PP for Cu and 6-311++G(d,p) for C, H]

Center Number	Atomic Number	Atomic Type	Coordinates (Angstroms) X	Y	Z
1	6	0	0.680321	2.063037	0.000000
2	1	0	1.239436	2.177136	0.923354
3	1	0	1.239436	2.177136	-0.923354
4	6	0	-0.680321	2.063037	0.000000
5	1	0	-1.239436	2.177136	-0.923354
6	1	0	-1.239436	2.177136	0.923354
7	6	0	-2.126803	-0.442343	0.000000
8	1	0	-2.505173	-0.015185	0.923354
9	1	0	-2.505173	-0.015185	-0.923354
10	6	0	-1.446482	-1.620694	0.000000
11	1	0	-1.265737	-2.161951	-0.923354
12	1	0	-1.265737	-2.161951	0.923354
13	6	0	2.126803	-0.442343	0.000000
14	1	0	2.505173	-0.015185	-0.923354
15	1	0	2.505173	-0.015185	0.923354
16	6	0	1.446482	-1.620694	0.000000
17	1	0	1.265737	-2.161951	0.923354
18	1	0	1.265737	-2.161951	-0.923354
19	29	0	0.000000	0.000000	0.000000

$Ag(C_2H_4)_3^+$ cartesian coordinates

[B3PW91/aug-cc-pVTZ-PP for Ag and 6-311++G(d,p) for C, H]

Center Number	Atomic Number	Atomic Type	Coordinates (Angstroms) X	Y	Z
1	6	0	0.678270	2.283261	0.000000
2	1	0	1.240170	2.374533	0.924772
3	1	0	1.240170	2.374533	-0.924772
4	6	0	-0.678270	2.283261	0.000000
5	1	0	-1.240170	2.374533	-0.924772
6	1	0	-1.240170	2.374533	0.924772
7	6	0	-2.316497	-0.554231	0.000000
8	1	0	-2.676491	-0.113248	0.924772
9	1	0	-2.676491	-0.113248	-0.924772
10	6	0	-1.638227	-1.729030	0.000000
11	1	0	-1.436321	-2.261285	-0.924772
12	1	0	-1.436321	-2.261285	0.924772
13	6	0	2.316497	-0.554231	0.000000
14	1	0	2.676491	-0.113248	-0.924772
15	1	0	2.676491	-0.113248	0.924772
16	6	0	1.638227	-1.729030	0.000000
17	1	0	1.436321	-2.261285	0.924772
18	1	0	1.436321	-2.261285	-0.924772
19	47	0	0.000000	0.000000	0.000000

$Au(C_2H_4)_3^+$ cartesian coordinates

[B3PW91/aug-cc-pVTZ-PP for Au and 6-311++G(d,p) for C, H]

Center Number	Atomic Number	Atomic Type	Coordinates (Angstroms) X	Y	Z
1	79	0	0.000000	0.000000	0.000000
2	6	0	-0.688551	2.177177	0.000000
3	1	0	-1.242768	2.315062	0.922687
4	1	0	-1.242768	2.315062	-0.922687
5	6	0	0.688551	2.177177	0.000000
6	1	0	1.242768	2.315062	-0.922687
7	1	0	1.242768	2.315062	0.922687
8	6	0	2.229766	-0.492286	0.000000
9	1	0	2.626287	-0.081262	0.922687
10	1	0	2.626287	-0.081262	-0.922687
11	6	0	1.541215	-1.684891	0.000000
12	1	0	1.383519	-2.233800	-0.922687
13	1	0	1.383519	-2.233800	0.922687
14	6	0	-2.229766	-0.492286	0.000000
15	1	0	-2.626287	-0.081262	-0.922687
16	1	0	-2.626287	-0.081262	0.922687
17	6	0	-1.541215	-1.684891	0.000000
18	1	0	-1.383519	-2.233800	0.922687
19	1	0	-1.383519	-2.233800	-0.922687

$Cu(C_7H_{10})_3^+$ cartesian coordinates

[B3PW91/aug-cc-pVTZ-PP for Cu and 6-311++G(d,p) for C, H]

Center Number	Atomic Number	Forces (Hartrees/Bohr) X	Y	Z
1	29	0.000009132	0.000017875	-0.000167195
2	6	0.000041003	0.000052400	0.000531756
3	1	-0.000076261	0.000011021	0.000028118
4	6	0.000279226	0.000104638	-0.000238174
5	1	-0.000037689	-0.000016181	-0.000051378
6	6	-0.000081588	0.000002593	0.000573641
7	1	0.000024906	-0.000075946	0.000027074
8	6	-0.000220951	0.000188206	-0.000223588
9	1	0.000029844	-0.000025380	-0.000043422
10	6	-0.000055460	-0.000271618	-0.000233709
11	1	0.000004418	0.000037180	-0.000044657
12	6	-0.000008778	-0.000093267	0.000527707
13	1	0.000051386	0.000058649	0.000025909
14	6	0.000145878	-0.000125560	0.000106165
15	1	-0.000018374	0.000003198	-0.000001384
16	6	0.000091135	0.000025581	-0.000338892
17	1	-0.000007338	0.000008095	-0.000012014
18	6	-0.000167555	-0.000061212	0.000100854
19	1	0.000018658	0.000022639	0.000001775
20	6	-0.000023416	-0.000106845	-0.000307587

21	1	0.000002964	0.000008685	-0.000014351
22	6	0.000021931	0.000204183	0.000074527
23	1	0.000014321	-0.000036252	0.000012750
24	6	-0.000056381	0.000081925	-0.000314378
25	1	0.000005613	0.000011551	-0.000015960
26	6	0.000013467	0.000000443	0.000048675
27	6	-0.000012263	-0.000014214	-0.000004413
28	6	-0.000058643	0.000030056	-0.000046452
29	6	0.000010067	0.000011371	0.000051173
30	6	0.000024431	0.000007427	-0.000006996
31	6	-0.000003031	-0.000064983	-0.000034032
32	1	0.000004065	-0.000004244	-0.000005691
33	1	0.000003113	-0.000000294	0.000000323
34	1	0.000012880	0.000001651	-0.000000296
35	1	-0.000001949	0.000002061	0.000005327
36	1	-0.000008321	0.000007048	0.000005532
37	1	-0.000001704	-0.000005676	-0.000002710
38	1	-0.000005918	0.000009578	0.000000367
39	1	-0.000001479	-0.000001729	0.000005039
40	1	-0.000001648	0.000002420	-0.000000093
41	1	0.000002655	0.000002959	-0.000005958
42	1	0.000023394	-0.000071383	0.000007479
43	1	0.000007051	0.000002126	-0.000002931
44	6	-0.000028340	-0.000012209	0.000038699
45	6	-0.000007940	0.000019945	-0.000018072
46	1	-0.000002287	-0.000003806	0.000002129
47	1	-0.000009839	0.000000831	-0.000008286
48	1	0.000000647	-0.000012477	0.000000438
49	1	0.000002078	0.000001220	0.000005932
50	6	0.000039819	0.000023378	-0.000048141
51	1	0.000014721	0.000037151	0.000014373
52	1	-0.000001651	0.000005193	-0.000005001

$Ag(C_7H_{10})_3^+$ cartesian coordinates

[B3PW91/aug-cc-pVTZ-PP for Ag and 6-311++G(d,p) for C, H]

Center Number	Atomic Number	Atomic Type	Coordinates (Angstroms) X	Y	Z
1	47	0	0.000000	0.000000	0.658586
2	6	0	-2.024452	-1.293692	0.975149
3	1	0	-1.834940	-1.649452	1.983929
4	6	0	-2.433945	-0.028029	0.652874
5	1	0	-2.623096	0.768816	1.364073
6	6	0	-0.108145	2.400073	0.975149
7	1	0	-0.510997	2.413831	1.983929
8	6	0	1.192699	2.121873	0.652874
9	1	0	1.977362	1.887260	1.364073
10	6	0	1.241246	-2.093844	0.652874
11	1	0	0.645734	-2.656076	1.364073
12	6	0	2.132596	-1.106380	0.975149
13	1	0	2.345937	-0.764379	1.983929

14	6	0	1.444214	2.706527	-0.721088
15	1	0	2.305003	2.322226	-1.265954
16	6	0	-0.698901	3.173675	-0.184198
17	1	0	-1.785572	3.215049	-0.240277
18	6	0	-3.066028	-0.102538	-0.721088
19	1	0	-3.163608	0.835078	-1.265954
20	6	0	-2.399032	-2.192104	-0.184198
21	1	0	-1.891528	-3.153876	-0.240277
22	6	0	1.621815	-2.603989	-0.721088
23	1	0	0.858605	-3.157304	-1.265954
24	6	0	3.097934	-0.981571	-0.184198
25	1	0	3.677101	-0.061174	-0.240277
26	6	0	1.471442	4.250047	-0.467589
27	6	0	0.000000	4.570511	-0.097476
28	6	0	0.059402	2.562266	-1.372897
29	6	0	2.944928	-3.399329	-0.467589
30	6	0	3.958179	-2.285256	-0.097476
31	6	0	2.189286	-1.332577	-1.372897
32	1	0	2.181483	4.527077	0.314070
33	1	0	1.775153	4.763477	-1.382914
34	1	0	-0.106048	5.023490	0.890137
35	1	0	-0.455639	5.251021	-0.820582
36	1	0	-0.222177	1.523395	-1.578478
37	1	0	-0.041876	3.146296	-2.290498
38	1	0	4.403494	-2.419905	0.890137
39	1	0	4.775337	-2.230915	-0.820582
40	1	0	3.237716	-3.919066	-1.382914
41	1	0	2.829822	-4.152759	0.314070
42	1	0	1.430387	-0.569286	-1.578478
43	1	0	2.745710	-1.536882	-2.290498
44	6	0	-4.416370	-0.850718	-0.467589
45	6	0	-3.958179	-2.285256	-0.097476
46	1	0	-5.012869	-0.844411	-1.382914
47	1	0	-5.011305	-0.374318	0.314070
48	1	0	-4.297446	-2.603585	0.890137
49	1	0	-4.319698	-3.020106	-0.820582
50	6	0	-2.248688	-1.229689	-1.372897
51	1	0	-1.208210	-0.954109	-1.578478
52	1	0	-2.703834	-1.609413	-2.290498

$Au(C_7H_{10})_3^+$ cartesian coordinates

[B3PW91/aug-cc-pVTZ-PP for Au and 6-311++G(d,p) for C, H]

Center Number	Atomic Number	Atomic Type	Coordinates (Angstroms) X	Y	Z
1	6	0	-1.881323	-1.335815	0.804449
2	1	0	-1.735841	-1.791516	1.779164
3	6	0	-2.320668	-0.030266	0.617051
4	1	0	-2.571827	0.648120	1.424885
5	6	0	-0.216188	2.297181	0.804449
6	1	0	-0.683577	2.399040	1.779164

7	6	0	1.134123	2.024891	0.617051
8	1	0	1.847202	1.903208	1.424885
9	6	0	1.186545	-1.994625	0.617051
10	1	0	0.724626	-2.551327	1.424885
11	6	0	2.097511	-0.961366	0.804449
12	1	0	2.419418	-0.607525	1.779164
13	6	0	1.512591	2.619172	-0.725350
14	1	0	2.426318	2.245567	-1.184004
15	6	0	-0.679030	3.072063	-0.411740
16	1	0	-1.753320	3.110765	-0.583389
17	6	0	-3.024565	0.000357	-0.725350
18	1	0	-3.157877	0.978469	-1.184004
19	6	0	-2.320969	-2.124089	-0.411740
20	1	0	-1.817341	-3.073802	-0.583389
21	6	0	1.511974	-2.619529	-0.725350
22	1	0	0.731559	-3.224036	-1.184004
23	6	0	3.000000	-0.947974	-0.411740
24	1	0	3.570661	-0.036963	-0.583389
25	6	0	1.504871	4.157213	-0.451664
26	6	0	0.000000	4.467792	-0.233853
27	6	0	0.203836	2.475101	-1.517412
28	6	0	2.847817	-3.381863	-0.451664
29	6	0	3.869221	-2.233896	-0.233853
30	6	0	2.041582	-1.414078	-1.517412
31	1	0	2.127570	4.429541	0.403127
32	1	0	1.900225	4.683454	-1.323674
33	1	0	-0.210259	4.909318	0.742565
34	1	0	-0.380599	5.156571	-0.991659
35	1	0	-0.049564	1.439760	-1.764072
36	1	0	0.197332	3.071211	-2.432603
37	1	0	4.356724	-2.272569	0.742565
38	1	0	4.656021	-2.248677	-0.991659
39	1	0	3.105878	-3.987370	-1.323674
40	1	0	2.772310	-4.057300	0.403127
41	1	0	1.271650	-0.676956	-1.764072
42	1	0	2.561081	-1.706500	-2.432603
43	6	0	-4.352688	-0.775350	-0.451664
44	6	0	-3.869221	-2.233896	-0.233853
45	1	0	-5.006102	-0.696084	-1.323674
46	1	0	-4.899880	-0.372240	0.403127
47	1	0	-4.146465	-2.636749	0.742565
48	1	0	-4.275422	-2.907894	-0.991659
49	6	0	-2.245419	-1.061023	-1.517412
50	1	0	-1.222087	-0.762803	-1.764072
51	1	0	-2.758413	-1.364712	-2.432603
52	79	0	0.000000	0.000000	0.586359

$Cu(C_{12}H_{18})^{+}$ cartesian coordinates

[B3PW91/aug-cc-pVTZ-PP for Cu and 6-311++G(d,p) for C, H]

Center Number	Atomic Number	Atomic Type	Coordinates (Angstroms) X	Y	Z

Center Number	Atomic Number	Atomic Type	Coordinates (Angstroms) X	Y	Z
1	6	0	-2.089437	0.059106	0.359189
2	6	0	-2.450558	1.421220	-0.194877
3	6	0	-1.380770	2.473282	0.190390
4	6	0	-0.025002	2.088213	-0.362527
5	6	0	1.095906	1.779952	0.359189
6	6	0	2.456091	1.411635	-0.194877
7	1	0	-2.129523	-0.032875	1.448284
8	1	0	-3.424882	1.731242	0.197408
9	1	0	-2.547299	1.369524	-1.284471
10	1	0	-1.673832	3.452381	-0.203127
11	1	0	-1.328215	2.570130	1.279917
12	1	0	0.066618	2.121492	-1.451887
13	1	0	1.036292	1.860659	1.448284
14	1	0	3.211740	2.100414	0.197408
15	1	0	2.459692	1.521264	-1.284471
16	6	0	-1.795944	-1.065758	-0.362527
17	6	0	2.832310	-0.040859	0.190390
18	6	0	-1.451540	-2.432423	0.190390
19	1	0	-1.870575	-1.003054	-1.451887
20	6	0	1.820946	-1.022454	-0.362527
21	1	0	3.826766	-0.276609	-0.203127
22	1	0	2.889905	-0.134797	1.279917
23	6	0	-0.005534	-2.832855	-0.194877
24	1	0	-2.152933	-3.175772	-0.203127
25	1	0	-1.561690	-2.435332	1.279917
26	6	0	0.993531	-1.839059	0.359189
27	1	0	1.803957	-1.118439	-1.451887
28	1	0	0.213141	-3.831656	0.197408
29	1	0	0.087607	-2.890788	-1.284471
30	1	0	1.093232	-1.827784	1.448284
31	29	0	0.000000	0.000000	0.003916

$[Cu(C_{12}H_{18})(CO)]^{+}$ cartesian coordinates

[B3PW91/aug-cc-pVTZ-PP for Cu and 6-311++G(d,p) for C, H, O]

Center Number	Atomic Number	Atomic Type	Coordinates (Angstroms) X	Y	Z
1	6	0	-0.000787	0.001609	-0.000907
2	6	0	0.001693	0.001867	1.504594
3	6	0	1.445467	0.001292	2.054688
4	6	0	2.275523	1.156216	1.539567
5	6	0	3.110653	1.055816	0.472718
6	6	0	4.029314	2.115531	-0.074647
7	1	0	0.595509	-0.786162	-0.464870
8	1	0	-0.564524	0.855024	1.892519
9	1	0	-0.508584	-0.901306	1.861389
10	1	0	1.929677	-0.939345	1.772282
11	1	0	1.416307	0.025919	3.147216
12	1	0	2.263533	2.080816	2.116879
13	1	0	3.207380	0.073432	0.006909

14	1	0	3.829163	3.082952	0.397583
15	1	0	5.064572	1.852798	0.175592
16	6	0	-0.742282	0.785227	-0.826629
17	6	0	3.904443	2.214893	-1.611404
18	6	0	1.642127	1.488096	-2.472328
19	6	0	2.487926	2.474043	-2.074555
20	6	0	-0.724239	0.652558	-2.333368
21	1	0	-1.457440	1.483748	-0.391963
22	1	0	4.258624	1.278477	-2.054903
23	1	0	4.563294	3.006741	-1.977415
24	6	0	0.246573	1.642002	-3.015726
25	1	0	2.038327	0.471270	-2.494768
26	1	0	2.174622	3.513116	-2.176957
27	1	0	-0.429973	-0.368508	-2.597645
28	1	0	-1.731955	0.803332	-2.729411
29	1	0	-0.101819	2.673751	-2.901343
30	1	0	0.258972	1.432919	-4.092544
31	29	0	1.173342	1.899248	-0.307839
32	6	0	0.516734	3.579308	0.266177
33	8	0	0.125697	4.579851	0.608027

REFERENCES

1. N.N. Greewood, A. E., Chimica degli Elementi; Piccin, Padova, **1984**

2. Pyykko, P., *Abstracts of Papers, 226th ACS National Meeting, New York, NY, United States, September 7-11,* ***2*****003**

3. Pyykko, P., *Angew. Chem., Int. Ed.* **2002,** 41, (19), 3573-3578

4. Pyykko, P.; Stoll, H., *Chem. Modell.* **2000,** 1, 239-305

5. Pyykko, P., *Science* **2000,** 290, (5489), 64-65

6. Doll, K.; Pyykko, P.; Stoll, H., *J. Chem. Phys.* **1998,** 109, (6), 2339-2345

7. Pyykko, P.; Mendizabal, F., *Chem.--Eur. J.* **1997,** 3, (9), 1458-1465

8. Pyykko, P.; Runeberg, N.; Mendizabal, F., *Chem.--Eur. J.* **1997,** 3, (9), 1451-1457

9. Pyykko, P.; Seth, M., *Theor. Chem. Acc.* **1997,** 96, (2), 92-104

10. Pyykko, P., *Eff. Relativ. At., Mol., Solid State, [Proc. Meet.]* **1991**, 1-13

11. Pyykko, P.; Zhao, Y., *Chem. Phys. Lett.* **1991,** 177, (1), 103-6

12. Pyykko, P.; Zhao, Y., *Angew. Chem.* **1991,** 103, (5), 622-3 (See also Angew Chem , Int Ed Engl , 1991, 30(5), 604-5)

13. Pyykko, P., *Chem. Rev.* **1988,** 88, (3), 563-94

14. Pyykko, P.; Goerling, A.; Roesch, N., *Mol. Phys.* **1987,** 61, (1), 195-205

15. Pyykko, P.; *[Proceedings of a Symposium; 1982; Abo, Finland. In: Int. J. Quantum Chem, 1983; 25(1)]*. 1983; p 276 pp

16. Pyykko, P., *Kem. - Kemi* **1981,** 8, (7-8), 498-500

17. Pyykko, P.; Desclaux, J. P., *C. R. Seances Acad. Sci., Ser. 2* **1981,** 292, (23), 1513-15

18. Pyykko, P., *Arkhimedes* **1979,** 31, (1), 15-22

19. Pyykko, P.; Desclaux, J. P., *Acc. Chem. Res.* **1979,** 12, (8), 276-81

20. Pyykko, P., *Adv. Quantum Chem.* **1978,** 11, 353-409

21. Pyykko, P., *Chem Soc Rev* **2008,** 37, (9), 1967-97

22. F.A. Cotton, G. W., C.A. Murillo, M. Bochmann, Advanced Inorganic Chemistry; John Wiley & Sons, Inc., New York, **1999**

23. Dias, H. V. R.; Wang, Z., *Inorg. Chem.* **2000,** 39, (16), 3724-3727

24. Blumenthal, I., *J. R. Soc. Med.* **2001,** 94, (6), 270-272

25. Crabtree, R. H., The Organometallic Chemistry of the Transition Metals; John Wiley & Sons, Inc., New York, **2001**,

26. C. Elschenbroich, A. S., Organometallics: A Concise Introduction; VCH, Weinheim, **1992**

27. Mond, L.; Langer, C.; Quincke, F., *J. Chem. Soc., Trans.* **1890,** 57, 749-753
28. Prockop, L. D.; Chichkova, R. I., *J. Neurol. Sci.* **2007,** 262, (1-2), 122-130
29. Wu, L.; Wang, R., *Pharmacol. Rev.* **2005,** 57, (4), 585-630
30. J.E. Huheey, E. A. K., R.L. Keiter, Chimica Inorganica. **1999**
31. Strauss, S. H., Copper(I) and silver(I) carbonyls. *Dalton Trans.* **2000**, (1), 1-6
32. Lupinetti, A. J.; Frenking, G.; Strauss, S. H., *Angew. Chem., Int. Ed.* **1998,** 37, (15), 2113-2116
33. Goldman, A. S.; Krogh-Jespersen, K., *J. Am. Chem. Soc.* **1996,** 118, (48), 12159-12166
34. Capracotta, M. D.; Sullivan, R. M.; Martin, J. D., *J. Am. Chem. Soc.* **2006,** 128, (41), 13463-13473
35. Hurlburt, P. K.; Rack, J. J.; Luck, J. S.; Dec, S. F.; Webb, J. D.; Anderson, O. P.; Strauss, S. H., *J. Am. Chem. Soc.* **1994,** 116, (22), 10003-14
36. Dias, H. V. R.; Jin, W., *Inorg. Chem.* **1996,** 35, (12), 3687-3694
37. Dias, H. V. R.; Jin, W., *J. Am. Chem. Soc.* **1995,** 117, (45), 11381-2
38. Ivanova, S. M.; Ivanov, S. V.; Miller, b. S. M.; Anderson, O. P.; Solntsev, K. A.; Strauss, S. H., *Inorg. Chem.* **1999,** 38, (17), 3756-3757
39. Willner, H.; Schaebs, J.; Hwang, G.; Mistry, F.; Jones, R.; Trotter, J.; Aubke, F., *J. Am. Chem. Soc.* **1992,** 114, (23), 8972-80
40. Hwang, G.; Wang, C.; Aubke, F.; Willner, H.; Bodenbinder, M., *Can. J. Chem.* **1993,** 71, (9), 1532-6
41. Bodenbinder, M.; Balzer-Joellenbeck, G.; Willner, H.; Batchelor, R. J.; Einstein, F. W. B.; Wang, C.; Aubke, F., *Inorg. Chem.* **1996,** 35, (1), 82-92
42. Aubke, F., *J. Fluorine Chem.* **1995,** 72, (2), 195-201
43. Willner, H.; Bodenbinder, M.; Wang, C.; Aubke, F., *J. Chem. Soc., Chem. Commun.* **1994**, (10), 1189-90
44. Jonas, V.; Thiel, W., *J. Chem. Soc., Dalton Trans.* **1999**, (21), 3783-3790
45. Schroeder, D.; Hrusak, J.; Hertwig, R. H.; Koch, W.; Schwerdtfeger, P.; Schwarz, H., *Organometallics* **1995,** 14, (1), 312-16
46. Lupinetti, A. J.; Jonas, V.; Thiel, W.; Strauss, S. H.; Frenking, G., *Chem.--Eur. J.* **1999,** 5, (9), 2573-2583
47. Mogi, K.; Sakai, Y.; Sonoda, T.; Xu, Q.; Souma, Y., *J. Phys. Chem. **2003,*** 107, (19), 3812-3821
48. Veldkamp, A.; Frenking, G., *Organometallics* **1993,** 12, (11), 4613-22
49. Meyer, F.; Chen, Y.-M.; Armentrout, P. B., *J. Am. Chem. Soc.* **1995,** 117, (14), 4071-81

50. Barnes, L. A.; Rosi, M.; Bauschlicher, C. W., Jr., *J. Chem. Phys.* **1990,** 93, (1), 609-24

51. K.P.C. Vollhardt, N. E. Schore., Organic chemistry Structure and Function; W.H. Freeman and Company, New York **2003**

52. Barrows, S. E.; Eberlein, T. H., *J. Chem. Educ.* **2005,** 82, (9), 1329-1333

53. J. Clayden, N. G., S. Warren, P. Wothers, Organic Chemistry. **2001**

54. O'Brien, C. J.; Tellez, J. L.; Nixon, Z. S.; Kang, L. J.; Carter, A. L.; Kunkel, S. R.; Przeworski, K. C.; Chass, G. A., *Angew. Chem., Int. Ed.* **2009,** 48, (37), 6836-6839

55. Black, M.; Mais, R. H. B.; Owston, P. G., *Acta Crystallogr., Sect. B* **1969,** 25, (9), 1753-9

56.Jarvis, J. A. J.; Kilbourn, B. T.; Owston, P. G., *Acta Crystallogr., Sect. B* **1971,** 27, (2), 366-72

57. Wunderlich, J. A.; Mellor, D. P., *Acta Crystallogr.* **1954,** 7, 130

58. Salomon, R. G.; Kochi, J. K., *J. Organometal. Chem.* **1972,** 43, (1), C7-C10

59. Solomon, R. G.; Kochi, J. K., *J. Chem. Soc., Chem. Commun.* **1972**, (9), 559-60

60. Lewandos, G. S.; Gregston, D. K.; Nelson, F. R., *J. Organomet. Chem.* **1976,** 118, (3), 363-74

61. Solodar, J.; Petrovich, J. P., *Inorg. Chem.* **1971,** 10, (2), 395-7

62. Fischer, K.; Jonas, K.; Misbach, P.; Stabba, R.; Wilke, G., *Angew. Chem., Int. Ed. Engl.* **1974,** 12, (12), 943-53

63. Fischer, K.; Jonas, K.; Wilke, G., *Angew. Chem.* **1973,** 85, (14), 620-1

64. Pitzer, R. M.; Schaefer, H. F., III, *J. Am. Chem. Soc.* **1979,** 101, (24), 7176-83

65. Green, M.; Howard, J. A. K.; Spencer, J. L.; Stone, F. G. A.,. *J. Chem. Soc., Chem. Commun.* **1975**, (11), 449-51

66. Green, M.; Howard, J. A. K.; Spencer, J. L.; Stone, F. G. A., *J. Chem. Soc., Dalton Trans.* **1977**, (3), 271-7

67. Krossing, I.; Reisinger, A., *Angew. Chem., Int. Ed.* **2003,** 42, (46), 5725-5728

68. Santiso-Quinones, G.; Reisinger, A.; Slattery, J.; Krossing, I., C*hem. Commun.* **2007**, (47), 5046-5048

69. Hertwig, R. H.; Koch, W.; Schroeder, D.; Schwarz, H.; Hrusak, J.; Schwerdtfeger, P., *J. Phys. Chem.* **1996,** 100, (30), 12253-12260

70. Kim, C. K.; Lee, K. A.; Kim, C. K.; Lee, B.-S.; Lee, H. W., *Chem. Phys. Lett.* **2004,** 391, (4-6), 321-324

71. Kaneti, J.; de Smet, L. C. P. M.; Boom, R.; Zuilhof, H.; Sudhoelter, E. J. R., *J. Phys. Chem. A* **2002,** 106, (46), 11197-11204

72. Nechaev, M. S.; Rayon, V. M.; Frenking, G., *J. Phys. Chem.* **2004,** 108, (15), 3134-3142.

73. Alexander, B. D.; Dines, T. J., *J. Phys. Chem.* **2004,** 108, (1), 146-156
74. Luna, A.; Mo, O.; Yanez, M.; Morizur, J. P.; Leclerc, E.; Desmazieres, B.; Haldys, V.; Chamot-Rooke, J.; Tortajada, J., *Int. J. Mass Spectrom.* **2003,** 228, (2-3), 359-371
75. Klippenstein, S. J.; Yang, C. N., *Int. J. Mass Spectrom.* **2000,** 201, (1-3), 253-267
76. Schroeder, D.; Wesendrup, R.; Hertwig, R. H.; Dargel, T. K.; Grauel, H.; Koch, W.; Bender, B. R.; Schwarz, H., *Organometallics* **2000,** 19, (13), 2608-2615
77. Boehme, M.; Wagener, T.; Frenking, G., *J. Organomet. Chem.* **1996,** 520, (1-2), 31-43
78. Fournier, R., *Int. J. Quantum Chem.* **1994,** 52, (4), 973-85
79. Schroeder, D.; Schwarz, H., *Angew. Chem.* **1993,** 105, (10), 1493-5 (See also Angew Chem , Int Ed Engl , 1193, 32(10), 1420-22)
80. Sodupe, M.; Bauschlicher, C. W., Jr.; Langhoff, S. R.; Partridge, H., *J. Phys. Chem.* **1992,** 96, (13), 5670
81. Sodupe, M.; Bauschlicher, C. W., Jr.; Langhoff, S. R.; Partridge, H., *J. Phys. Chem.* **1992,** 96, (5), 2118-22
82. Nicolas, G.; Spiegelmann, F., *J. Am. Chem. Soc.* **1990,** 112, (14), 5410-19
83. Budzelaar, P. H. M.; Timmermans, P. J. J. A.; Mackor, A.; Baerends, E. J., *J. Organomet. Chem.* **1987,** 331, (3), 397-407
84. Merchan, M.; Gonzalez-Luque, R.; Nebot-Gil, I.; Tomas, F., *Chem. Phys. Lett.* **1984,** 112, (5), 412-16
85. Kelber, J. A.; Harrah, L. A.; Jennison, D. R., *J. Organomet. Chem.* **1980,** 199, (2), 281-91.
86. Ziegler, T.; Rauk, A., *Inorg. Chem.* **1979,** 18, (6), 1558-65
87. Barnett, N. J.; Slipchenko, L. V.; Gordon, M. S., *J. Phys. Chem. A* **2009,** 113, (26), 7474-7481
88. Tian, Z.; Tang, Z., *Rapid Commun. Mass Spectrom.* **2005,** 19, (20), 2893-2904
89. Manard, M. J.; Kemper, P. R.; Bowers, M. T., *Int. J. Mass Spectrom.* **2005,** 241, (2-3), 109-117
90. Damyanova, B.; Momtchilova, S.; Bakalova, S.; Zuilhof, H.; Christie, W. W.; Kaneti, J., *THEOCHEM* **2002,** 589-590, 239-249
91. Ma, N. L., *Chem. Phys. Lett.* **1998,** 297, (3,4), 230-238
92. Guo, B. C.; Castleman, A. W., Jr., *Chem. Phys. Lett.* **1991,** 181, (1), 16-20
93. Cohen, D.; Basch, H., *J. Am. Chem. Soc.* **1983,** 105, (23), 6980-2
94. Kasai, P. H.; McLeod, D., Jr.; Watanabe, T., *J. Am. Chem. Soc.* **1980,** 102, (1), 179-90
95. Kasai, P. H.; McLeod, D., Jr., *J. Am. Chem. Soc.* **1975,** 97, (22), 6602-3
96. Sakaki, S., *Theor. Chim. Acta* **1973,** 30, (2), 159-67

97. Powell, D. B.; Scott, J. G. V.; Sheppard, N., *Spectrochim. Acta, Part A* **1972,** 28, (2), 327-35.
98. Basch, H., *J. Chem. Phys.* **1972,** 56, (1), 441-50
99. Stringer, K. L.; Citir, M.; Metz, R. B., *J. Phys. Chem. A* **2004,** 108, (34), 6996-7002
100.Schroeder, D.; Schwarz, H.; Hrusak, J.; Pyykkoe, P., *Inorg. Chem.* **1998,** 37, (4), 624-632
101.Hrusak, J.; Hertwig, R. H.; Schroeder, D.; Schwerdtfeger, P.; Koch, W.; Schwarz, H., *Organometallics* **1995,** 14, (3), 1284-91
102. Kasai, P. H., *J. Am. Chem. Soc.* **1983,** 105, (22), 6704-10
103. Dias, H. V. R.; Fianchini, M.; Cundari, T. R.; Campana, C. F., *Angew. Chem., Int. Ed.* **2008,** 47, (3), 556-559
104.Tai, H.-C.; Krossing, I.; Seth, M.; Deubel, D. V.,. *Organometallics* **2004,** 23, (10), 2343-2349
105. Deubel, D. V., *J. Am. Chem. Soc.* **2002,** 124, (41), 12312-12318
106. Mardashev, Y. S.; Roev, L. M., *Dokl. Akad. Nauk B. SSR* **1974,** 18, (8), 722-4
107. Sievers, M. R.; Jarvis, L. M.; Armentrout, P. B., *J. Am. Chem. Soc.* **1998,** 120, (8), 1891-1899
108. Himmel, D.; Trapp, N.; Krossing, I.; Altmannshofer, S.; Herz, V.; Eickerling, G.; Scherer, W., *Angew. Chem., Int. Ed.* **2008,** 47, (41), 7798-7801
109. Jiang, D.-e.; Dai, S., *J. Phys. Chem. B* **2008,** 112, (33), 10202-10206
110. Fianchini, M.; Dai, H.; Dias, H. V. R., *Chem. Commun.* **2009**, (42), 6373-6375
111. Hooper, T. N.; Green, M.; McGrady, J. E.; Patel, J. R.; Russell, C. A., *Chem. Commun.* **2009**, (26), 3877-3879
112. Ohwada, T., *Chem. Rev.* **1999,** 99, (5), 1337-1375
113. Huber, H.; Ozin, G. A.; Power, W. J., *J. Am. Chem. Soc.* **1976,** 98, (21), 6508-11
114. Mink, J.; Gal, M.; Goggin, P. L.; Spencer, J. L., *J. Mol. Struct.* **1986,** 142, 467-72
115. Csaszar, P.; Goggin, P. L.; Mink, J.; Spencer, J. L., *J. Organomet. Chem.* **1989,** 379, (3), 337-49
116. Herges, R.; Papafilippopoulos, A., *Angew. Chem., Int. Ed.* **2001,** 40, (24), 4671-4674
117. Fianchini, M.; Dias, H. V. R., *Abstracts of Papers, 236th ACS National Meeting, Philadelphia, PA, United States, August 17-21,* **2008**
118. Lautens, M.; Klute, W.; Tam, W., *Chem. Rev.* **1996,** 96, (1), 49-92
119. Anet, F. A. L.; Rawdah, T. N., *J. Am. Chem. Soc.* **1978,** 100, (16), 5003-7 and ref. therein
120. Pettinari, C., Scorpionates II: Chelating Borate Ligands; Imperial College Press, London **2008**
121. Trofimenko, S., Scorpionates The Coordination Chemistry of Polypyrazolylborate Ligands; Imperial College Press, London **1999**

122. Dias, H. V. R.; Browning, R. G.; Richey, S. A.; Lovely, C. J., *Organometallics* **2005,** 24, (23), 5784

123. Dias, H. V. R.; Browning, R. G.; Richey, S. A.; Lovely, C. J., *Organometallics* **2004,** 23, (6), 1200-1202

124. Lovely, C. J.; Browning, R. G.; Polach, S. A.; Dias, H. V. R., *Abstracts of Papers, 225th ACS National Meeting, New Orleans, LA, United States, March 23-27,* **2003**

125. Diaz-Requejo, M. M.; Perez, P. J., *Chem. Rev.* **2008,** 108, (8), 3379-3394

126. Gomez-Emeterio, B. P.; Urbano, J.; Diaz-Requejo, M. M.; Perez, P. J., *Organometallics* **2008,** 27, (16), 4126-4130

127. Perez, P. J.; Diaz-Requejo, M. M., *N-Heterocycl. Carbenes Synth.* **2006**, 257-274

128. Dias, H. V. R.; Browning, R. G.; Polach, S. A.; Diyabalanage, H. V. K.; Lovely, C. J., *J. Am. Chem. Soc.* **2003,** 125, (31), 9270-9271

129. Urbano, J.; Braga, A. A. C.; Maseras, F.; Alvarez, E.; Diaz-Requejo, M. M.; Perez, P. J., *Organometallics* **2009,** 28, (20), 5968-5981

130. Dias, H. V. R.; Lu, H.-L.; Kim, H.-J.; Polach, S. A.; Goh, T. K. H. H.; Browning, R. G.; Lovely, C. J., *Organometallics* **2002,** 21, (7), 1466-1473

131. Cano, I.; Nicasio, M. C.; Perez, P. J., *Dalton Trans.* **2009**, (4), 730-734

132. Mairena, M. A.; Diaz-Requejo, M. M.; Belderrain, T. R.; Nicasio, M. C.; Trofimenko, S.; Perez, P. J., *Organometallics* **2004,** 23, (2), 253-256

133. Mar Diaz-Requejo, M.; Perez, P. J., *J. Organomet. Chem.* **2001,** 617-618, 110-118.

134. Diaz-Requejo, M. M.; Perez, P. J.; Brookhart, M.; Templeton, J. L., *Organometallics* **1997,** 16, (20), 4399-4402

135. Perez, P. J.; Brookhart, M.; Templeton, J. L., *Organometallics* **1993,** 12, (2), 261-2

136. Cano, I.; Nicasio, M. C.; Perez Pedro, J., *Dalton Trans* **2009**, (4), 730-4

137. Caballero, A.; Sabater, M.; Morilla, M. E.; Nicasio, M. C.; Belderrain, T. R.; Diaz-Requejo, M. M.; Perez, P. J., *Inorg. Chim. Acta* **2009,** 362, (12), 4599-4602

138. Fructos, M. R.; Diaz-Requejo, M. M.; Perez, P. J., *Chem. Commun.* **2009**, (34), 5153-5155.

139. Haldon, E.; Alvarez, E.; Nicasio, M. C.; Perez, P. J., *Organometallics* **2009,** 28, (13), 3815-3821

140. Caballero, A.; Prieto, A.; Diaz-Requejo, M. M.; Perez, P. J., *Eur. J. Inorg. Chem.* **2009**, (9), 1137-1144

141. Prieto, A.; Fructos, M. R.; Diaz-Requejo, M. M.; Perez, P. J.; Perez-Galan, P.; Delpont, N.; Echavarren, A. M., *Tetrahedron* **2009,** 65, (9), 1790-1793

142. Lenders, B.; Klaeui, W., *Chem. Ber.* **1990,** 123, (12), 2233-40

143. Dias, H. V. R.; Lu, H.-L., *Inorg. Chem.* **1995,** 34, (21), 5380-2
144. Chiong, H. A.; Daugulis, O., *Organometallics* **2006,** 25, (17), 4054-4057
145. Fowler, P. W.; Mizoguchi, N.; Bean, D. E.; Havenith, R. W. A., *Chem.--Eur. J.* **2009,** 15, (28), 6964-6972
146. Cuesta, I. G.; Sanchez De Meras, A.; Pelloni, S.; Lazzeretti, P., *J. Comput. Chem.* **2009,** 30, (4), 551-564
147. Bast, R.; Juselius, J.; Saue, T., *Chem. Phys.* **2009,** 356, (1-3), 187-194
148. Pelloni, S.; Lazzeretti, P., *Chem. Phys.* **2009,** 356, (1-3), 153-163
149. Mitchell, R. H.; Zhang, R.; Berg, D. J.; Twamley, B.; Williams, R. V., *J. Am. Chem. Soc.* **2009,** 131, (1), 189-199
150. Soncini, A.; Teale, A. M.; Helgaker, T.; De Proft, F.; Tozer, D. J., *J. Chem. Phys.* **2008,** 129, (7), 074101/1-074101/15
151. Iwamoto, H.; Fukazawa, Y., *Heterocycles* **2008,** 75, (7), 1711-1723
152. Periyasamy, G.; Burton, N. A.; Hillier, I. H.; Thomas, J. M. H., *J. Phys. Chem. A* **2008,** 112, (26), 5960-5972
153. Yoon, S.-Y.; Lai, Y.-H., *Tetrahedron Lett.* **2008,** 49, (27), 4282-4285
154. Pelloni, S.; Lazzeretti, P., *J. Chem. Phys.* **2008,** 128, (19), 194305/1-194305/10
155. Pelloni, S.; Lazzeretti, P., *J. Phys. Chem.* **2008,** 112, (23), 5175-5186
156. Kato, T., *Chem. Phys. Res. J.* **2007,** 1, (1), 60-96
157. Monaco, G.; Zanasi, R., *AIP Conf. Proc.* **2007,** 963, 1302-1305
158. Soncini, A.; Fowler, P. W., *Chem. Phys. Lett.* **2007,** 450, (4-6), 431-436
159. Kato, T.; Yamabe, T., *Synth. Met.* **2007,** 157, (21), 793-806
160. Kanno, M.; Hoki, K.; Kono, H.; Fujimura, Y., *J. Chem. Phys.* **2007,** 127, (20), 204314/1-204314/9
161. Nakamura, Y.; Aratani, N.; Osuka, A., *Chem.--Asian J.* **2007,** 2, (7), 860-866
162. Lazzeretti, P., *Prog. Nucl. Magn. Reson. Spectrosc.* **2000,** 36, (1), 1-88
163. Ma, Z.; Halling, M. D.; Solum, M. S.; Harper, J. K.; Orendt, A. M.; Facelli, J. C.; Pugmire, R. J.; Grant, D. M.; Amick, A. W.; Scott, L. T., *Phys. Chem.* **2007,** 111, (10), 2020-2027
164. Steiner, E.; Fowler, P. W.; Soncini, A.; Jenneskens, L. W., *Faraday Discuss.* **2007,** 135, 309-323
165. Hajgato, B.; Deleuze, M. S.; Ohno, K., *Chem.--Eur. J.* **2006,** 12, (22), 5757-5769
166. Steiner, E.; Fowler, P. W., *Org. Biomol. Chem.* **2006,** 4, (12), 2473-2476
167. Soncini, A.; Viglione, R. G.; Zanasi, R.; Fowler, P. W.; Jenneskens, L. W.,. *C. R. Chim.* **2006,** 9, (7-8), 1085-1093

168. Havenith, R. W. A., *J. Org. Chem.* **2006,** 71, (9), 3559-3563
169. Facelli, J. C., *Magn. Reson. Chem.* **2006,** 44, (3), 401-408
170. Rangan, K.; Fianchini, M.; Singh, S.; Rasika Dias, H. V., *Inorg. Chim. Acta* **2009,** 362, (12), 4347-4352
171. Fianchini, M.; Dias, H. V. R., *Abstracts of Papers, 236th ACS National Meeting, Philadelphia, PA, United States, August 17-21,* **2008**
172. Dias, H. V. R.; Fianchini, *Comments Inorg. Chem.* **2007,** 28, (1-2), 73-92
173. Dias, H. V. R.; Fianchini, M., Silver(I) *Abstracts of Papers, 233rd ACS National Meeting, Chicago, IL, United States, March 25-29,* **2007**
174. Dias, H. V. R.; Fianchini, M., *Angew Chem Int Ed Engl* **2007,** 46, (13), 2188-91
175. Gaussian 03, R. D.; M. J. Frisch, G. W. T., H. B. Schlegel, G. E. Scuseria, ; M. A. Robb, J. R. C., J. A. Montgomery, Jr., T. Vreven, ; K. N. Kudin, J. C. B., J. M. Millam, S. S. Iyengar, J. Tomasi, ; V. Barone, B. M., M. Cossi, G. Scalmani, N. Rega, ; G. A. Petersson, H. N., M. Hada, M. Ehara, K. Toyota, ; R. Fukuda, J. H., M. Ishida, T. Nakajima, Y. Honda, O. Kitao, ; H. Nakai, M. K., X. Li, J. E. Knox, H. P. Hratchian, J. B. Cross, ; V. Bakken, C. A., J. Jaramillo, R. Gomperts, R. E. Stratmann, ; O. Yazyev, A. J. A., R. Cammi, C. Pomelli, J. W. Ochterski, ; P. Y. Ayala, K. M., G. A. Voth, P. Salvador, J. J. Dannenberg, ; V. G. Zakrzewski, S. D., A. D. Daniels, M. C. Strain, ; O. Farkas, D. K. M., A. D. Rabuck, K. Raghavachari, ; J. B. Foresman, J. V. O., Q. Cui, A. G. Baboul, S. Clifford, ; J. Cioslowski, B. B. S., G. Liu, A. Liashenko, P. Piskorz, ; I. Komaromi, R. L. M., D. J. Fox, T. Keith, M. A. Al-Laham, ; C. Y. Peng, A. N., M. Challacombe, P. M. W. Gill, ; B. Johnson, W. C., M. W. Wong, C. Gonzalez, and J. A. Pople, ; Gaussian, I., Wallingford CT, 2004
176. Feller, D., *J. Comput. Chem.* **1996,** 17, (13), 1571-1586
177. Schuchardt, K. L.; Didier, B. T.; Elsethagen, T.; Sun, L.; Gurumoorthi, V.; Chase, J.; Li, J.; Windus, T. L., *J. Chem. Inf. Model.* **2007,** 47, (3), 1045-1052
178. Peterson, K. A.; Puzzarini, C., *Theor. Chem. Acc.* **2005,** 114, (4-5), 283-296
179. Walker, N. R.; Gerry, M. C. L., *Inorg. Chem.* **2002,** 41, (5), 1236-1244
180. Dias, H. V. R.; Wang, X., *Polyhedron* **2004,** 23, (16), 2533-2539

BIOGRAPHICAL INFORMATION

Mauro Fianchini was born the 19th of June 1979 in Camerino (MC), Italy. After completing his high school studies in July of 1998, he attended chemistry lectures at the Department of Chemistry, University of Camerino. In February of 2004, he received his master's degree in inorganic chemistry discussing a thesis on pyrazole-based ligands under the supervision of Prof. Claudio Pettinari. In Spring of 2002, he was a visiting scholar at the University of Seville (Spain) where he had the chance to attend advanced inorganic/organometallic chemistry courses, as well as to appreciate and learn the Spanish language and culture. In Fall of 2009 he completed his Ph.D. work at the University of Texas at Arlington with work on the chemistry of group 11 metals with small molecules like carbon monoxide and ethylene, under the supervision of Prof. H.V. Rasika Dias.

His work has culminated in the publication of several papers in highly rated international journals including Angewandte Chemie, Chemical Communications, Inorganic Chemistry, Dalton Transaction and Journal of the Material Chemistry. Most of these articles have been selected as "hot articles" or appeared on section covers. During his academic career, he participated as a speaker at important congresses such as the American Chemical Society National Meeting in Chicago, 2007, and Philadelphia, 2008.

He won several fellowships and awards, such as the Excellence Fellowship and the Dean's Fellowship at the University of Camerino (Italy), the prestigious Dean's Excellence Scholarship, the Award as Outstanding Researcher 2007, and the first prize at ACES competition in 2009 at the University of Texas at Arlington (USA).

He is a firm believer that, though very difficult and perhaps "asymptotical", a chemist should embrace chemistry "at 360° degrees", learning to understand and use concepts of many chemical disciplines, from pure theory to applied synthesis. In his spare time, he loves to read and study computational/theoretical chemistry, visit friends, practice sports like soccer and martial arts, ride motorbikes, watch movies and play videogames. He has always been an avid reader of the history of the ancient world, with a particular emphasis on the period of the late Republican/Imperial Roman civilization.